UNIVERSITÀ DEGLI STUDI DI PAVIA

Dipartimento di Biologia e Biotecnologie

"L. SPALLANZANI"

Identification and characterization of new signaling pathways altered in Cockayne syndrome

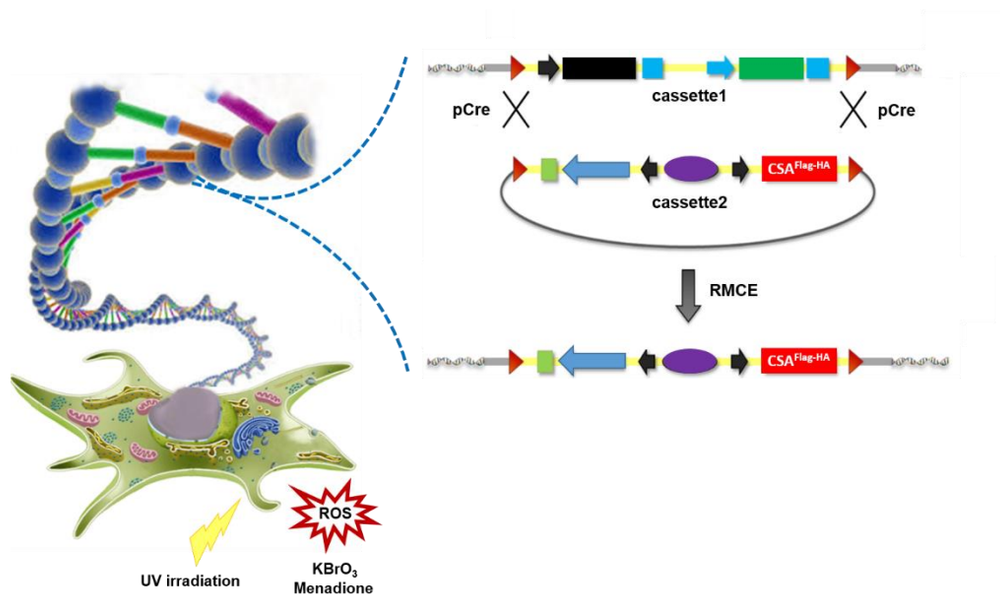

Martina Uggè

Dottorato di ricerca in

Genetica, Biologia Molecolare e Cellulare

XXIX Ciclo (2013-2016)

UNIVERSITÀ DEGLI STUDI DI PAVIA

Dipartimento di Biologia e Biotecnologie

"L. SPALLANZANI"

Identification and characterization of new signaling pathways altered in Cockayne syndrome

Martina Uggè

Supervised by Dr. Donata Orioli

Dottorato di Ricerca in Genetica, Biologia Molecolare e Cellulare

XXIX Ciclo – A.A. 2013-2016

Table of contents

Abstract

Cockayne syndrome (CS) is a rare autosomal recessive disorder characterized by progressive growth failure, neurological dysfunction and segmental premature aging. These alterations are due to mutations in the *CSA* or *CSB* genes, which are involved in transcription-coupled nucleotide excision repair (TC-NER), the mechanism devoted to the removal of UV-induced DNA damage blocking the progression of the transcription machinery in actively transcribed DNA strand.
The lack of a clear genotype-phenotype relationship and the broad range in type and severity of the CS clinical symptoms cannot be simply explained by the persistency of UV-induced DNA damage. These lines of evidence suggested that CSA and CSB might have additional roles outside TC-NER. The structure of CSA, a 44 kDa protein containing seven WD repeat domains, acts as a scaffold for protein-protein interactions. The finding that distinct *CSA* mutations provide different levels of cellular sensitivity to UV irradiation or oxidative stress has suggested that CSA might accomplish its other functions by interacting with different protein partners/complexes. To gain further insight into the various cellular activities engaging CSA and to identify novel CSA-binding proteins, we generated by the Recombinase-Mediated Cassette Exchange (RMCE) technique a panel of isogenic cell lines stably expressing the wild type or mutated forms of CSA, fused *in frame* with the Flag and HA epitope tags ($CSA^{Flag\text{-}HA}$). All the analyzed *CSA* mutations were unable to fully complement the UV-sensitive phenotype of CSA-defective cells and conferred sensitivity to the oxidant agent menadione. These isogenic cell lines were then used to evaluate the effects of specific point mutations on *CSA* transcript, protein stability and their consequences on the CSA protein interactions pattern. We demonstrated that specific mutations impair the stability of the protein without altering the stability of the transcript and, in some cases, affect the CSA subcellular localization.
Previous analysis performed in our laboratory identified thirty-six novel CSA interacting proteins. This work of thesis has been focused on two novel CSA interactors, namely CCT3 and CCT8, and demonstrated that their binding to CSA is affected by CSA mutations as well as by the action of specific cellular stressing agents. CCT3 and CCT8 are two subunits of the TRiC/CCT complex, a chaperonin oligomer involved in the folding of newly synthesized or unfolded proteins. Therefore, we investigated the functional role of CSA interaction with the TRiC/CCT complex by silencing experiments. We demonstrated that in primary fibroblasts from a healthy donor, the silencing of *CCT3* affects the RNA recovery synthesis (RRS) after UV-induced DNA damage, thus demonstrating that TRiC/CCT silencing partially impairs the cellular DNA repair capacity.

In addition, this research study has also been focused on the identification of novel disease gene for CS. In particular, we concentrated our attention to an Italian patient (CS11/9_PV) who was recently reported to our laboratory and showed the clinical features of the severe form of CS. Primary dermal fibroblasts from the CS11/9_PV patient showed cellular features typical of TC-NER alterations, but no inactivating mutations were found in CS genes, either *CSA* or *CSB*. To identify the molecular defect associated to this CS case, we started a collaboration with Prof. Tomoo Ogi (Nagoya University, Japan), who performed whole exome sequencing of all the CS11/9_PV family members. From this analysis we identified a small number of putative causative genes and, for two of them, demonstrated that they encode proteins interacting with CSA. To investigate the possible involvement of these genes in CS pathogenesis, we knocked down their expression by RNA interference in primary fibroblasts from healthy donors and performed RRS analysis after UV-induced DNA damage. We demonstrate that silencing of one of these candidate genes decreases the RRS level ability after UV irradiation, thus strongly supporting the notion that it may be involved in CS etiopathogenesis.

Overall, this study contributes to shed light on the molecular defects underlying CS phenotype by: i) demonstrating the essential role of TRiC/CCT complex for the stability and functionality of the CSA protein; ii) the identification of putative novel CS causative genes.

Acknoledgements

I would like to express my special gratitude to my supervisor Dr. Donata Orioli for being a mentor for me, for the continuous support of my Ph.D study, for her patience, motivation and knowledge.
Special thanks go also to Manuela Lanzafame, who guided me through these years with passion, proficiency and friendship.
I am also grateful to Prof. Tomoo Ogi and Prof. Luca Bini for the tremendous contribution they gave to my work in terms of data and expertise, and for accepting to be my external referees.
My personal and scientific growth would not have been the same without the efforts and the affection of Dr. Tiziana Nardo.
I would like to thank all the lab members for their feedback, cooperation and of course friendship.

Grazie mamma e papà: in ogni mio traguardo, in ogni mio successo c'è la vostra impronta inconfondibile.
Anita e Bart: tutti i giorni, per tre anni, sempre insieme. Ci siamo aiutati, divertiti, guardati le spalle a vicenda e non vi dimenticherò mai.

Abbreviations

aa	amino acids
AR	androgen receptor
ATP	adenosine triphosphate
AP	abasic apurinic/apyrimidinic sites
APE	AP endonuclease
APS	ammonium persulfate
ATP	adenosine triphosphate
BER	Base excision repair
BSA	bovine serum albumin
cDNA	complementary DNA
COFS	cerebro-oculo-facial-skeletal
Cp	crossing point
COFS	Cerebro-oculo-facial-skeletal
CPD	cyclobutane pyrimidine dimer
CRL	cullin-RING E3 ubiquitin ligase complex
CS	Cockayne syndrome
CSA	Cockayne syndrome protein A
CSB	Cockayne syndrome protein B
CSN	COP9 signalosome
Cul4A	Cullin 4A
DDB	DNA damage binding protein
DMSO	dimethylsulfoxide
DSB	double-strand break
dsDNA	double-stranded DNA
DTT	dithiothreitol
ECT	ectopic DNA sequence
EDTA	ethylenediaminetetraacetic acid
ER	estrogen receptor
ERCC	excision repair cross-complementing
FBS	fetal bovine serum
GCV	ganciclovir
GG-NER	Global genome repair
GR	glucocorticoid receptor
HD	helicase domain
ICL	interstrand crosslink
IGF	insulin growth factor

IHC	immunohistochemistry
IR	ionizing radiation
kDa	kilo Dalton
LB	Luria-Bertani broth
MB	magic buffer
mRNA	messenger RNA
mt	mitochondrial
NEIL1	endonuclease VIII-like protein 1
NER	Nucleotide excision repair
NLS	nuclear-localization signal
ORF	open reading frame
PAGE	polyacrylamide gel electrophoresis
PBS	phosphate buffered saline
PCNA	proliferating cell nuclear antigen
Pol	polymerase
PTB	phosphate transfer buffer
Puro	Puromycin
qRT-PCR	quantitative real time RT-PCR
RMCE	Recombinase Mediated Cassette Exchange
RNApol	RNA polymerase
ROC1	RING finger protein 1
ROS	reactive oxygen species
RPA	replication protein A
rpm	rotations per minute
rRNA	ribosomal RNA
RRS	recovery of RNA synthesis
RT	room temperature; reverse transcription
SDS	sodium dodecyl sulphate
SOC	super optimal broth with catabolite repression
SSB	single-strand break
ssDNA	single-stranded DNA
SWI/SNF	SWItch/Sucrose Non-Fermentable
TAP	tandem affinity purification
TBE	Tris-Borate-EDTA
TBS	Tris buffer saline
TC-NER	Transcription-coupled repair
TE	Tris-EDTA buffer
TEMED	N,N,N,N'-tetramethylenediamine
TFIIH	transcription factor IIH
TFIIS	transcription factor IIS
Tris	Tris(hydroxymethyl)aminomethane

TTD	trichothiodystrophy
TWB	TAP washing buffer
UBD	ubiquitin-binding domain
UDS	unscheduled DNA synthesis
UTR	untranslated region
UV	ultraviolet
$UV^{S}S$	UV sensitive syndrome
WB	western blot
wt	wild type
XP	xeroderma pigmentosum
6-4 PPs	pyrimidine(6-4)pyrimidone photoproducts
8-oxoG	8-dihydro-8-oxoguanine

1. Introduction

DNA is the repository of genetic information in each living cell, therefore its integrity and stability are essential to life. DNA, however, is not inert: rather, it is a chemical entity subject to constant threat of damage as a result of the exposure to both environmental and endogenous insults. The first hazard is intrinsic to the chemical nature of the DNA molecule itself that, although being the carrier of the genetic information, has limited chemical stability and can therefore undergo spontaneous reactions leading to the formation of abasic sites or base deamination. Second, the physiologic cellular metabolism generates *per se* DNA damaging catabolites that can induce single-strand breaks, such as reactive nitrogen and oxygen species, but also lipid peroxidation products, endogenous alkylating agents, estrogen and cholesterol metabolites, and reactive carbonyl species. Moreover, DNA lesions can be generated by a multitude of exogenous sources including ionizing radiations, the ultraviolet (UV) component of the sunlight and several chemical agents that can induce various types of DNA lesions, including single- and double-strand breaks, inter- and intra-strand crosslinks and distinct forms of base modifications. The outcome of DNA damage is varied and usually hostile, as errors can cause developmental abnormalities, tumorigenesis and aging. Therefore, DNA repair mechanisms must exist and are continually active under physiological conditions, having a remarkable influence on life from evolution through disease susceptibility. The Royal Swedish Academy of Sciences has celebrated the incredible value of DNA repair by awarding the 2015 Nobel Prize in Chemistry to three pioneers of basic research on DNA repair mechanisms, Tomas Lindahl, Aziz Sancar, and Paul Modrich.

To guide accurate repair, cells have evolved a highly specific response network to detect the damage sites with sensing molecules and then transmit the damage signals to transducers. Different checkpoints and repair systems, including cell cycle regulators, nucleases, helicases, polymerases, ligases, etc., are engaged in the execution of the repair of damage to preserve genomic integrity (reviewed in Par et al., 2016). The vital importance of DNA repair mechanisms is highlighted by their extreme conservation from unicellular bacteria and yeast to man. At present, five repair mechanisms are known to operate in mammals, namely base excision repair (BER), nucleotide excision repair (NER), recombinational repair which includes homologous recombination (HR) and non-homologous end-joining (NHEJ), and mismatch repair (MMR). BER mainly corrects single lesions or small alterations of bases, mostly but not solely of endogenous origin. NER is a complex process involving the removal of bulky DNA lesions that hinder DNA replication and transcription, thereby inactivating every gene on the transcribed strand. It has

therefore urged the development of a dedicated repair system called transcription-coupled repair, which assures great priority repair to the damage with the highest biological impact (reviewed in Hoeijmakers, 2009). NER includes a second sub-pathway, namely the global genome repair, devoted to the removal of DNA lesions occurring throughout the entire genome. Except for some oxidative damages, most NER lesions arise from exogenous sources, such as UV light and chemical agents. HR and NHEJ mainly work on double-strand break repair. NHEJ is an inaccurate but efficient system that operates throughout the cell cycle, whereas HR occurs specifically in late S and G2 phases and uses an undamaged homologous sequence as a repair template. MMR targets base substitution mismatches and insertion-deletion mismatches that arise because of replication errors that escaped the proofreading function of DNA polymerases, but is also involved in the processing of insertion/deletion loops that result from slippage during recombination events. Therefore, depending on the type of damage, cells have developed specific repair pathways, that can sometimes overlap. Cells also possess mechanisms specialized in direct reversal of base damage for the removal of certain type of photoproducts and alkylated bases. The genome protection network includes also the so-called DNA damage tolerance mechanisms. Tolerance pathways involve several distinct cellular responses that mitigate the potentially lethal effects of DNA replication arrest due to the presence of damaged bases. These processes, known as translesion synthesis (TLS), do not operate the removal of the initial lesion, but allow the cell to survive bypassing the arrest of the replication machinery. The tolerance mechanisms strongly contribute to the burden of spontaneous mutations that all replicating cells have to face.

Both prokaryotic and eukaryotic cells have evolved mechanism that greatly facilitate the efficiency of repair and damage tolerance. Various types of DNA damage and/or arrested replication can trigger specific cell cycle checkpoints that arrest the cell cycle progression, thus providing more time for repair or damage tolerance to occur and preventing genome duplication or cell division in the presence of damaged DNA. When the DNA damage is too severe to be adequately repaired, the outcome is cell death. On the other hand, when the damage is turned into a mutation by means of replication errors or faulty repair, the changes become permanent and exert their effect on the long-term even in descendant cells, in the form of point mutations affecting single genes and chromosome aberration that may involve multiple genes. Genome instability is the hallmark of all forms of cancer, but accumulation of lesions in the DNA may also result in the decline of physiological functions, thus leading to precocious aging. The type of occurring damage strongly influences the nature of the outcome. Some lesions are mainly mutagenic and strongly promote cancer, others are cytotoxic or cytostatic and trigger cell death or senescence. Finally, when mutations arise in the genome of reproductive cells, the offspring may be affected by a genetically inherited disorder (Figure 1).

The importance of DNA repair pathways in man is demonstrated by the existence of at least 27 human genetic disorders associated with a defective DNA damage response. In most but not all cases, there is an elevated cancer incidence, and many of them are characterized by multi-system defects such as developmental abnormalities, alteration of neurological functions and precocious aging.

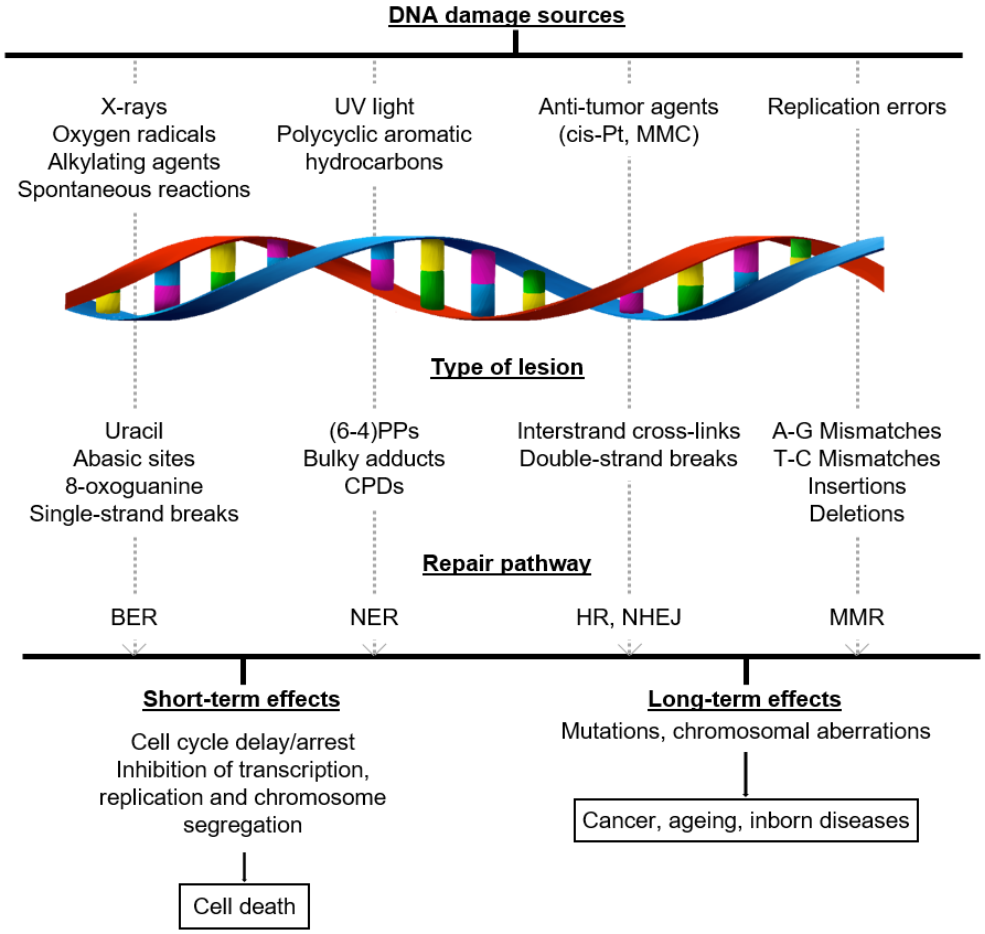

Figure 1. DNA damage, repair mechanisms and consequences. DNA lesions induced by common genotoxic agents (top), DNA repair mechanisms responsible for their removal (middle), and their biological effects (bottom). *Cis*-Pt, cisplatin; MMC, mitomycin; (6–4)PP, 6–4 photoproduct; CPD, cyclobutane pyrimidine dimer; HR, homologous recombination; NHEJ, non-end joining (adapted from Hoeijmakers, 2009).

2. Review of the literature

2.1 Cockayne syndrome

Cockayne syndrome (CS) is rare autosomal recessive multisystem disorder, first described by Edward Alfred Cockayne in 1936. The minimal incidence of CS has been evaluated in Western Europe at 2.7 cases per million birth (Kleijer et al., 2008). In recent years, higher incidence in countries where diagnostic tests are routinely available suggests that CS is still likely to be underdiagnosed. The progressive and devastating CS clinical symptoms are related to NER defects, a dysfunction shared by other hereditary disorder, specifically xeroderma pigmentosum (XP), trichothiodystrophy (TTD), cerebro-oculo-facio-skeletal syndrome (COFS) and UV-sensitive syndrome ($UV^{S}S$). The diagnostic criteria for CS include poor growth, neurodevelopmental and later neurological dysfunction with evidence of predominant white-matter involvement, at least three of the following clinical features: cutaneous photosensitivity, sensorineural hearing loss, dental caries, progressive pigmentary retinopathy and/or cataract, optic disk atrophy, miotic pupils or decreased lacrimation and a characteristic stance in the ambulatory patients (Nance and Berry, 1992) (Figure 2). Three major inter-related pathological processes underlie the CS symptoms, namely the severely compromised global growth and development, the premature and accelerated aging and neuropathological degeneration. Originally, CS patients were assigned to three clinical subtypes based on the observation that most symptoms are present in all CS cases, but the time of onset and the rate of progression can vary (Nance and Berry, 1992). Patients falling into the “classical” or “moderate” clinical subtype I (CSI) usually experience the first signs of the disease at the end of the first year of life (delayed developmental milestones or failure to thrive). Patients belonging to this group often learn to sit, stand, walk a few steps, and speak a few words or simple sentences, show severe growth failure and progressive sensory and neurological impairment. Average life expectancy is around 16 years and death mostly occurs from respiratory or renal failure. Patients belonging to the “severe” or clinical subtype II (CSII) typically manifest symptoms at birth. Clinical manifestations include congenital microcephaly, hypotonia or cataracts, severe nourishing difficulties, very limited neurological development, severe growth failure, severe contractures, and an average age of death around 5 or 6 years, mainly by respiratory failure or, less frequently, renal failure. Patients of the “late-onset” or “mild” subtype III (CSIII) may show the first clinical symptoms only after several years of life and present mild

developmental delay and limited growth failure. Progressive cerebellar symptoms, cognitive decline and hearing loss may be prominent symptoms in this subtype. Death occurs around 30 years, mostly because of respiratory failure (reviewed in Laugel, 2013).

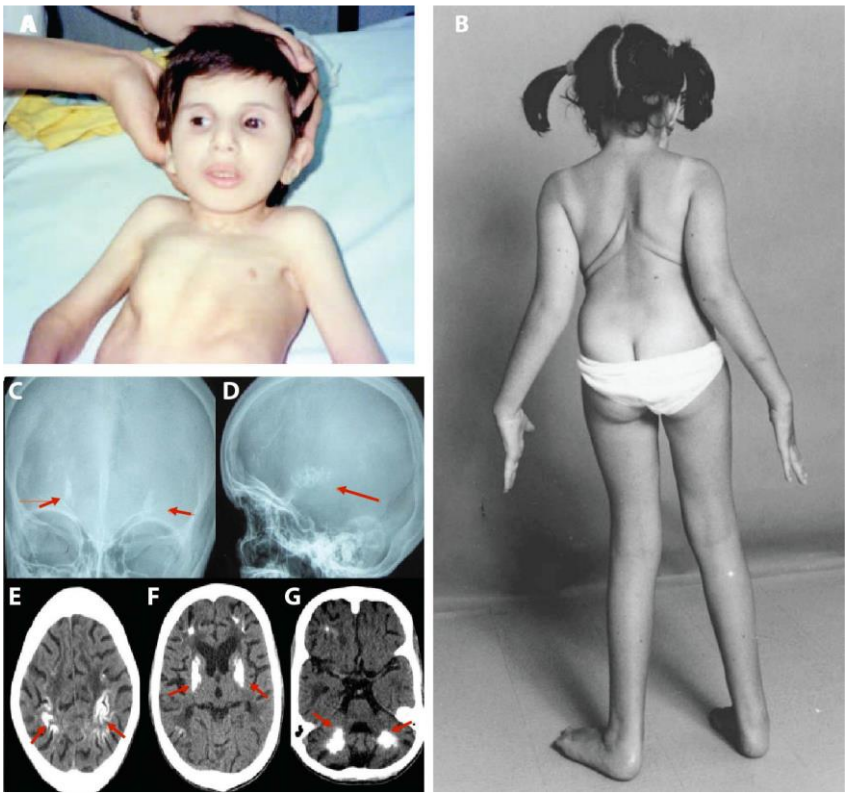

Figure 2. Phenotypic appearance and brain alterations in Cockayne syndrome (CS). (A) Typical facial appearance and **(B)** body disproportion with associated muscoloskeletal abnormalities. **(C,D)** Skull X-rays show basal ganglia calcification. (E) Brain CT shows calcification of subcortical regions, **(F)** basal ganglia and **(G)** dentate nuclei (modified from Stefanini and Ruggieri, 2008; Amalnath et al., 2015).

More recently, the clinical classification of several hundreds of CS patients has highlighted that CS phenotypes manifest throughout a continuous spectrum and that a clear threshold between the overlapping subtypes cannot be determined (Figure 3). In the 1970s and early 1980s, COFS and UV^{S}S were described as independent from CS, but ultimately proved to share the same cellular defect as the canonical CS patients. Therefore, the limits of this constantly expanding clinical spectrum have

been pushed even further with the inclusion of very severely affected patients as well as very mildly affected ones, who had been first considered as belonging to distinct entities but then found to be mutated in *CSA* or *CSB* genes (Graham et al., 2001).
COFS syndrome was first described within the Manitoba aboriginal population as an autosomal recessive disorder characterized by arthrogryposis, microcephaly, cataracts and microphthalmia, with a very early onset of the disease in the fetus. COFS patients show mutations mainly in the CSB gene, but there are also patients mutated in *XPD*, *XPG* or *ERCC1*.

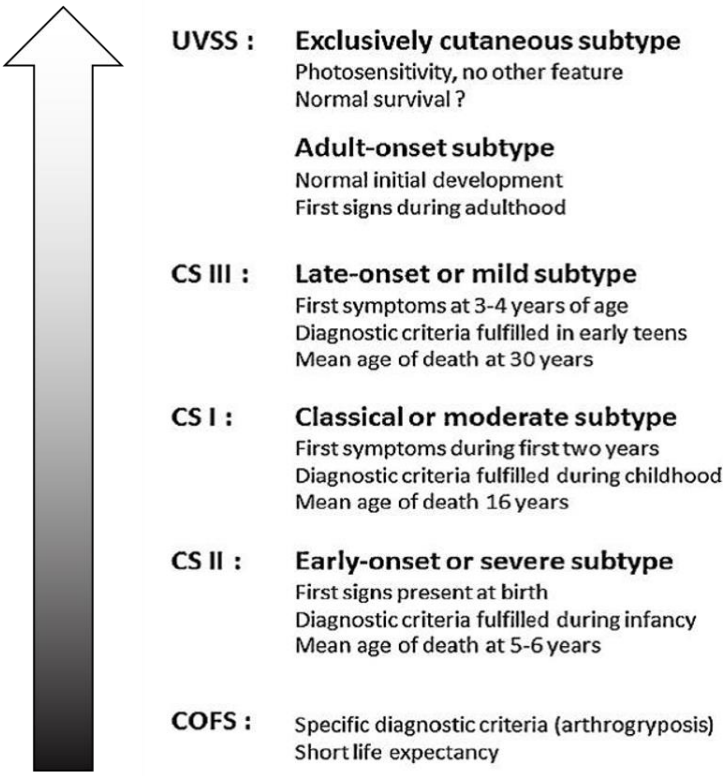

Figure 3. Continuous spectrum of severity in CS (modified from Laugel, 2013).

UV^{S}S is a very mild disorder only defined by cutaneous photosensitivity, without any other features typical of the CS picture and without cancer proneness.

Genes responsible for the UV^{S}S are *CSB*, *CSA* and *UVSSA*. Consequently, COFS and UV^{S}S are now considered as additional CS variants and constitute the opposite ends of the same continuous spectrum.

Particular cases are represented by rare patients showing combined features of CS and XP (XP/CS) caused by mutations in *XPB*, *XPD* or *XPG* genes. Most XP/CS patients manifest very severe symptoms, close to the type II CS with severe skin photosensitivity. Complex XP/CS-XP-B and XP/CS-XP-G genotypes are usually associated with inconstant development of multiple malignancies but survival into adulthood (reviewed in Laugel, 2013). Approximately 65% of CS patients characterized so far have mutations in the *CSB* gene. The clinical spectra of *CSA*- and *CSB*-linked phenotypes are largely overlapping and there are no specific symptoms or severity group linked to mutations in one gene in particular (Stefanini et al., 1996; Laugel, 2013). However, the phenotypic spectra are not rigorously identical and the most severe forms of the disease (COFS or CS type II) affect a significant number of CS-B patients, whereas *CSA* mutations seem to be preferentially associated with CS type I. Among the 101 CS patients whose clinical subtype could be determined from the literature or from personal unpublished data (28 CSA patients and 73 CSB patients), 56% of CSB patients met the CS type II criteria, whereas 75% of the CSA patients could be classified as type I (Figure 4) (Laugel, 2013). However, these results need to be verified on a larger scale to confirm this trend.

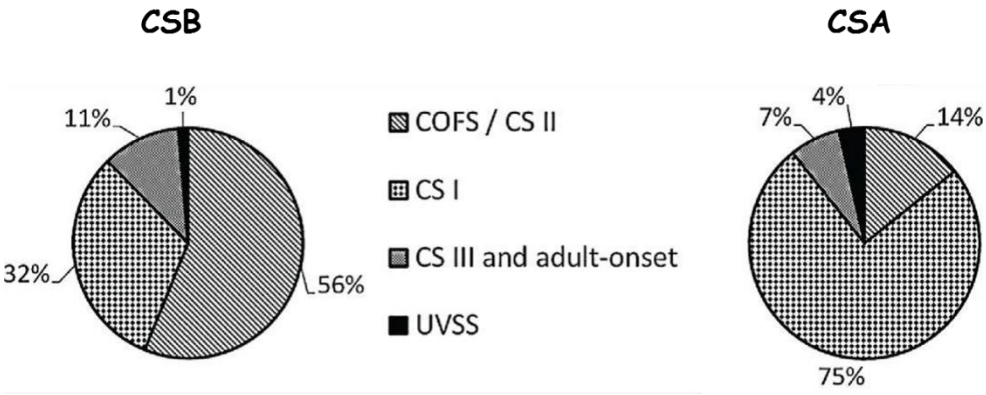

Figure 4. Distribution of the clinical subtypes of CS in *CSA* and *CSB* mutated patients (modified from Laugel 2013).

Neuroimaging analysis performed in the various clinical subtypes of CS patients from a cohort of biochemically and genetically verified cases revealed that calcifications, hypomyelination and brain atrophy were the main neuroradiologic features. Calcifications were typically found in the putamen and less often in the cortex and dentate nuclei. Progressive atrophy was seen in the supratentorial white matter, cerebellum, corpus callosum and brainstem. Patients with early-onset disease displayed more severe hypomyelination and prominent calcifications in the sulcal depth of the cerebral cortex, but atrophy was less severe in late-onset patients. Proton MR spectroscopy detected elevated level of lactate, whereas choline and N-acetylaspartate values were decreased. These combined neuroradiologic findings can help in the differential diagnosis of CS, distinguishing it from other leukoencephalopathies and/or cerebral calcifications in childhood (Koob et al., 2010).

2.2 CS proteins

Approximately 50% of the CS patients show altered cellular response to UV light, characterized by inability to recover normal RNA and DNA synthesis levels at late times after irradiation and hypersensitivity to the killing effects of UV exposure. Two distinct complementation groups have been defined by genetic analysis, namely CS-A and CS-B, corresponding to alterations in either the *CSA* or *CSB* genes, respectively. At the cellular level, CS cells of both groups are unable to repair UV-induced DNA damage occurring on the transcribed strand of transcriptionally active genes at the same rate of normal cells. Contrarily, they are able to repair the remaining parts of the genome at a normal rate. Therefore, the hypersensitivity to UV light observed in CS patients was attributed to functional alterations in TC-NER, the NER sub-pathway that specifically removes DNA damage blocking the progression of the transcription machinery in actively transcribed regions of DNA. Experimental evidence suggests that CS proteins exert additional roles in the repair of oxidative-induced lesions that might account for the neurological and ageing features typical of the disorder, which cannot be explained by the merely persistence of UV-induced lesions (reviewed in Karikkineth et al., 2016). Regarding the 50% of CS cases characterized by a normal response to UV light, at present no cellular markers have been identified and nothing is known about the genes responsible for the pathological phenotype.

2.2.1 CSA

CSA, the human homolog of the hamster *ERCC8* gene, maps on chromosome 5q12-q13. It is transcribed into a polyadenylated mRNA of 2044 bp and encodes a protein of 396 amino acids and 44 kDa. CSA belongs to the WD repeat (W, tryptophan; D, aspartic acid) family of proteins, indeed it contains seven putative WD40 repeats (Henning et al., 1995; Zhou and Wang, 2001; Lanzafame et al., 2013) (Figure 5).

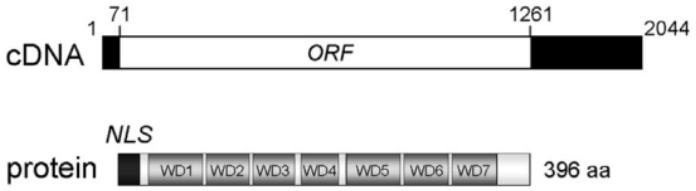

Figure 5. Schematic representation of the *CSA* cDNA and corresponding protein. In the cDNA structure, the white area corresponds to the open reading frame (ORF), whereas the black areas indicate the untranslated regions (GenBank NM_000082.3). Grey boxes represent the predicted WD functional domains, whereas the black box indicates the nuclear localization signal (NLS) (GenBank NP_000073.1)(modified from Lanzafame et al., 2013).

2.2.1.1 Structural and biochemical features

Based on its primary sequence, CSA was assigned to the WD40 repeat protein family. WD40 domains are approximately 40-60 amino acids long (Figure 6).

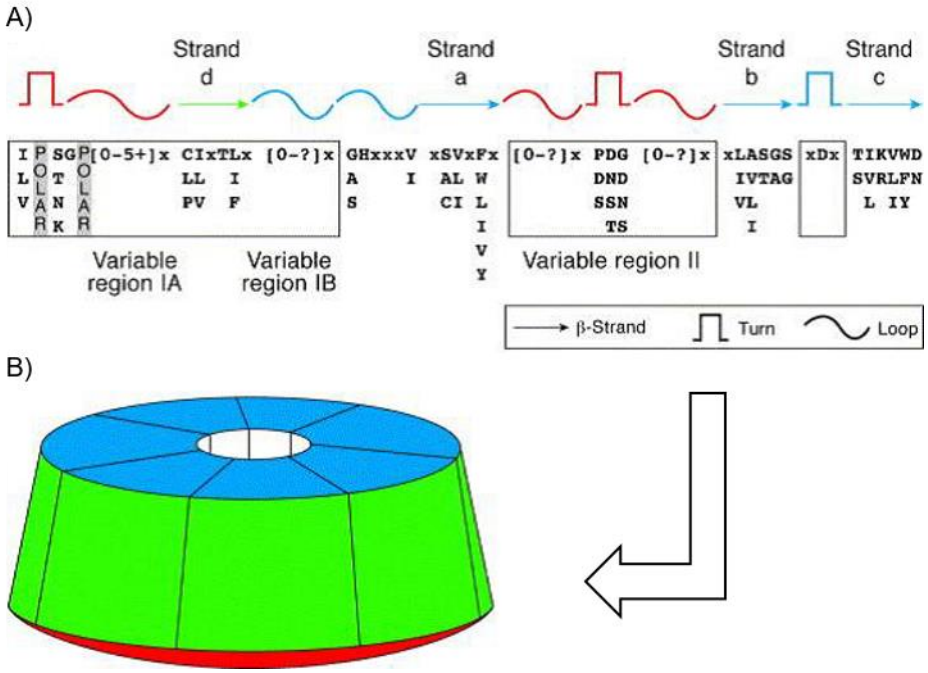

Figure 6. The WD repeat structure. (A) Schematic illustration of the structural elements within a single repeat. The alternative amino acids for each position are listed in approximate order of their frequency of occurrence. In the case of strand d, the listed alternative amino acids are only evident in about a third of the repeats. A surface-defining sequence pattern can be defined by replacing all the residues in strand a, strand b and strand c by 'x' (any residue). **(B)** Schematic representation of the positions of the elements shown in (A) in the three-dimensional structure of the fold. The predicted bottom of the flat surface regions is shown in red; the top flat surface is shown in lighter blue. The circumference, which is composed primarily of the β-strand residues, is shown in green (modified from Smith et al., 1999).

WD40 domains are initiated by a glycine-histidine (GH) dipeptide roughly 11 to 24 residues from the N-terminal, and end with a tryptophan-aspartic acid (WD) dipeptide at the C-terminal (reviewed in Li and Roberts, 2001; Smith, 2008). They exhibit a β-propeller architecture, typically containing seven blades, each composed of four anti-parallel β-sheets. It appears that these proteins share a common arrangement in which the WD repeat propeller structures create a stable platform that can coordinate sequential and/or simultaneous protein-protein interactions. Despite sharing a three-dimensional structure, the numerous proteins belonging to the WD repeat family exhibit a high degree of functional heterogeneity. Indeed, they can be involved in genome integrity maintenance, signal transduction, RNA

synthesis/processing, chromatin assembly, vesicular trafficking, cytoskeletal organization, DNA damage repair, cell cycle control and apoptosis (reviewed in Xu and Min, 2011). The seven WD-repeat structure of CSA (Figure 7) was predicted by sequence alignment with the crystal structure of the well-known WD40 family member subunit β of the transducin protein G (Zhou and Wang, 2001).

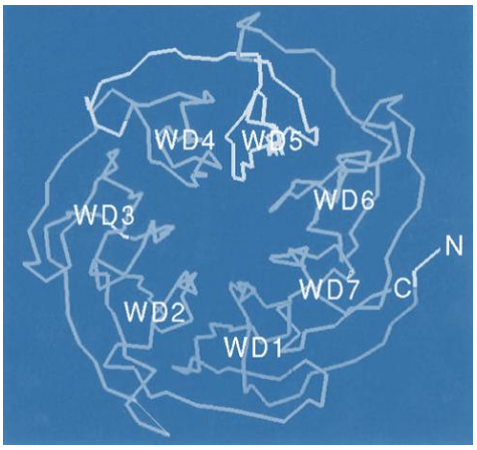

Figure 7. Structure model for the CSA protein. The seven WD repeats are labeled (modified from Zhou and Wang, 2001).

The β-propeller structure provides CSA with three potential interacting surfaces: the top, the bottom and the circumference (Figure 6B). The interior tunnel is probably too narrow to host protein-protein interactions, therefore it is not considered as a potential binding surface, although it might play important coordination roles. Molecular replacement experiments solved the structure of the CSA protein, which comprises seven WD repeats in the region including amino acids 30-365. The N-terminal region of CSA contains a helix-loop-helix motif directly involved in the binding with DDB1 (Fischer et al., 2011). The CSA protein localizes in nucleus and, likewise CSB, it has been detected in mitochondria in close association with the 8-oxoguanine glycosylase (OGG1) protein. Additionally, CSA increases its mitochondrial localization upon induction of oxidative stress (Kamenisch et al., 2010).

2.2.1.2 Mutational analysis

Most of the mutations identified in CS-A patients reported in literature result in severely truncated polypeptides as a consequence of either stop codons, frameshifts, splice abnormalities or genomic DNA deletions (Laugel, 2013)(Figure 8).

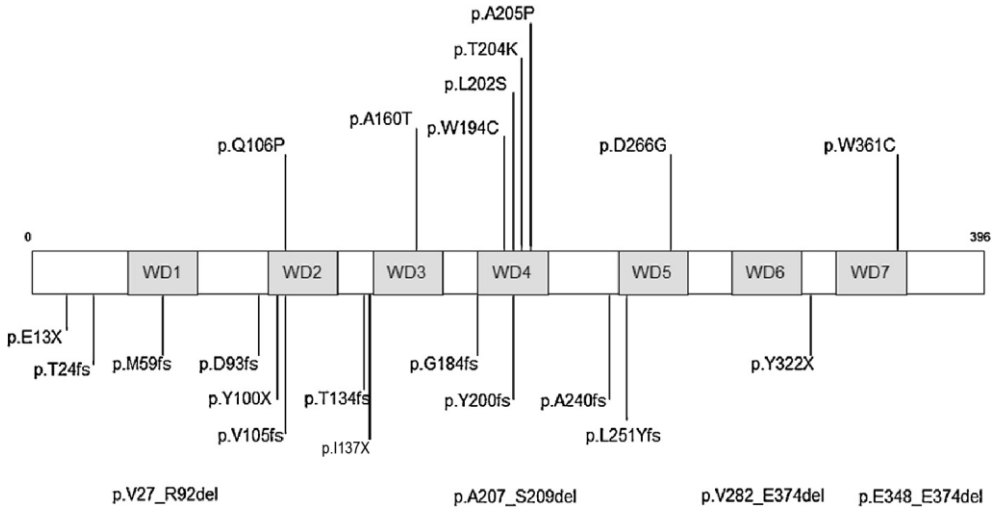

Figure 8. Updated linear map of the mutations in *CSA*. Missense mutations are indicated above the protein structure drawing; other point mutations and deletions are represented beneath the protein. WD repeats are shown in grey (modified from Laugel, 2013).

The nine missense mutations identified in *CSA* are located in the seven predicted WD40 repeats and in most cases modify evolutionarily conserved residues. Four missense mutations, namely p.Trp194Cys, p.Leu202Ser, p.Thr204Lys and p.Ala205Pro, are located within a conserved 14-residue stretch in the WD4 repeat that also harbors the short in-frame deletion p.Ala207_Ser209del. The p.Asp266Gly mutation, identified in two unrelated Dutch families (Laugel, 2013) and in a Brazilian family (Bertola et al., 2006) modifies WD5, one of the most conserved domains among all the WD motifs. The p.Gln106Pro mutation was identified in a Japanese patient and modifies a glutamine residue located in WD2. Even though this amino acid is poorly conserved, the substitution was described as conferring extreme cellular sensitivity to UV irradiation and to hinder the translocation of CSA to the nuclear matrix (Ren at al., 2003; Saijo et al., 2007). The p.Trp361Cys mutation occurs in the conserved tryptophan at the end of the WD7 repeat and is responsible for the unique UV^{S}S patient mutated in *CSA* (Nardo et al., 2009). Ten distinct splice

mutations have been identified in *CSA*. A founder effect has been suggested to explain the two splice mutations described in patients with the same ethnical background. The same genomic mutation c.618-1G>A has been reported in two Portuguese/Brazilian kindred (Laugel, 2013). This alteration of the intronic acceptor site activates another cryptic acceptor site located 9 bp downstream in exon 8 (CAG/TAGAG) and leads to an in-frame deletion of the first nine bases of exon 8. This is expected to result in the deletion of three amino acid residues from position 207 to 209 located within the WD4 motif. Five Somali patients presented a c.551-1G>A mutation in the intronic acceptor site, which resulted in the frameshifting insertion of the last 37 bases of intron 6 into the final mRNA sequence, through the activation of a cryptic acceptor site (TTTTTCAG/ATATCT) located 37 bp upstream of the normal intron-exon border (Laugel, 2013). An abnormal splicing pattern was also described in a patient with late-onset form of CS (Komatsu et al., 2004). The full-length *CSA* transcript was found in all families members except the proband, and multiple splicing variants were identified in all cases. No mutation could be found at the genomic level. An analogous situation was reported in a consanguineous French family of Turkish origin (Laugel et al., 2010). Unusual splicing variants but no full-length mRNA of *CSA* were found in the two affected brothers, without any detectable genomic alteration in the canonical donor and acceptor splice sites of each exon. This observation could be explained by the presence of unidentified mutations in the untranscribed regulatory or intronic sequences. Finally, a deletion of 277 kb affecting the whole *CSA* gene (exon 1-12) and two exons of the adjacent gene *NDUFAF2* was recently described in a Chinese patient (Ting at al., 2015). Besides indicating that *CSA* is not an essential gene, mutational analysis indicated that the molecular defect does not correlate with the severity of the clinical phenotype. This observation implies that the type and severity of the clinical features in CS-A patients must be influenced by factors in the intra-uterine environment and/or genetic background.

2.2.2 CSB

The *CSB* gene maps on the chromosome 10q11.23. It results in two transcripts of 5 and 7.5 kb. The longest mRNA encodes a protein of 1493 amino acids (168 kDa) (Troelstra et al., 1992) which belongs to the SWI2/SFN2 family of DNA-dependent ATPases (Figure 9).

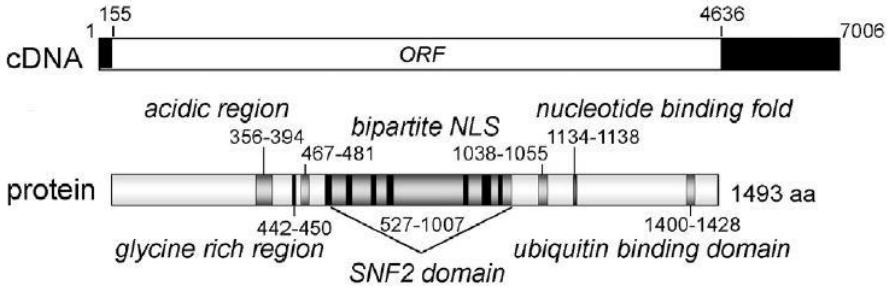

Figure 9. Schematic representation of the *CSB* cDNA and corresponding proteins. In the cDNA structure, the white area corresponds to the open reading frame (ORF), whereas the black areas indicate the untranslated regions (GenBank NM_000124.2). In the protein structure, boxes indicate the predicted functional domains (GenBank NP_000115.1). SNF2 domain contains the seven conserved ATPase motifs. NLS: nuclear localization signal (modified from Lanzafame et al., 2013).

2.2.2.1 Structural and biochemical features

Amino acid sequence similarity analysis assigned CSB to the SWI/SNF2 protein family of DNA-dependent APTases, a group of proteins involved in several cellular processes including chromatin remodeling, gene-specific transcriptional regulation, chromosome segregation and DNA repair. ATP-dependent chromatin remodelers use ATP as energy source to enable transitions between chromatin states. Their activity can lead to changes in nucleosome position, composition and conformation. The CSB protein contains seven conserved ATPases motifs distinctive of the SWI2/SNF2-like proteins, also present in DNA/RNA helicases (Figure 9). The seven ATPases motifs of CSB can be divided into two RecA-like domains (domain 1 and 2) wrapped around an interdomain cleft involved in DNA binding and ATP binding/hydrolysis. Conventional strand displacement assays have not yet clarified the enzymatic activity of CSB, likewise for other members of this protein family, whereas *in vitro* assays showed that CSB could alter the DNA conformation and induce chromatin structure changes by a direct interaction with core histones. *In vitro*, the activity of CSB depends on ATP binding but not hydrolysis (Citterio et al., 2000; Beerens et al., 2005). Furthermore, it has been demonstrated that ATP hydrolysis by CSB is essential for its stable interaction with chromatin following UV irradiation (Lake et al., 2010). Mutations in different CSB domains differentially affect the ATPase activity of the protein and, in this regard, the SNF2-like ATPase domain is critical. CSB catalyzes the annealing of complementary single-stranded DNA and performs strand exchange independent of ATP (Muftuoglu et al., 2006). Moreover, CSB contains an acidic region of unknown function, a glycine rich stretch

of seven residues at the N-terminus of the ATPase motif, a nucleotide-binding and a ubiquitin-binding domain (UBD) at the C-terminus (Anindya et al., 2010). The integrity of the UBD is essential for functional TC-NER, as demonstrated by the finding that cells expressing truncated forms of the protein lacking the UBD (UBD-less CSB) show features similar to cells lacking the whole CSB protein. UBD-less CSB is still able to assemble NER factors on the damage-stalled RNApol II, but fails to excise the lesion (Anindya et al., 2010). CSB also contains a bipartite nuclear localization signal (NLS), which explains its detection mainly in the nucleus, where it localizes in nucleoplasmic foci and nucleoli. CSB is also detected in the nuclear matrix together with the RNApol I and the XPB subunit of the transcription factor IIH (TFIIH) (Bradsher et al., 2002; Christiansen et al., 2003). The presence of CSB has been demonstrated in mitochondria and this localization increases following oxidative stress (Aamann et al., 2010; Kamenisch et al., 2010). CSB can undergo diverse post-translational modifications: *in vivo* and *in vitro* studies have demonstrated that CSB can be phosphorylated by the casein Kinase II (CKII or CK-2), an ubiquitous serine/threonine protein kinase that phosphorylates acidic proteins. CSB can be dephosphorylated by UV irradiation, indicating a phosphorylation-dependent regulation of its activity after DNA damage. Accordingly, it has been shown that the ATPase activity of CSB increases by 38% after CSB dephosphorylation by protein phosphatase 1 (Christiansen et al., 2003). CSB is also phosphorylated upon oxidative stress induction. Indeed, the SH3 domain of c-Abl, a tightly-regulated non-receptor tyrosine kinase activated in response to genotoxic or oxidative stress, interacts with CSB both *in vivo* and *in vitro* and phosphorylates CSB on the Tyr932 residue (Sun et al., 2000; Imam et al., 2007). CSB phosphorylation results in a re-distribution of the protein inside the nucleolus (Imam et al., 2007). Lastly, CSB can be ubiquitinated and this modification is required for the fully assembling of the NER complex and for DNA repair initiation (Anindya et al., 2010). CSA is responsible for the CSB ubiquitylation that licenses TC-NER, allowing the recovery of RNA synthesis (Groisman et al., 2006).

2.2.2.2 Mutational analysis

Mutational analysis has been accomplished in about fifty CS-B patients characterized by different severity degrees of pathological phenotype and coming from a wide range of ethnic backgrounds (reviewed in Stefanini and Ruggieri, 2008; Laugel, 2013). Seventy-seven *bona fide* inactivating mutations have been identified (Figure 10).

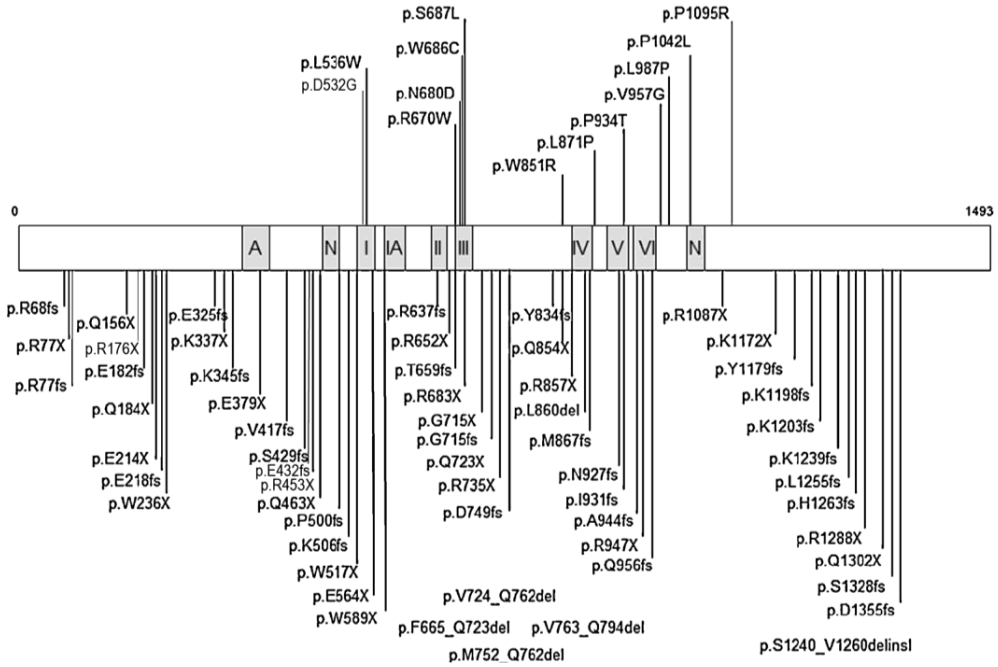

Figure 10. Updated linear map of the mutations in the CSB protein. Missense mutations are shown above the protein structure; other point mutations and deletions are represented beneath. Helicase motifs (I-IV), acidic domain (A) and nuclear localization signal (N) are indicated in grey (modified from Laugel, 2013).

It is worthwhile mentioning that at least ninety-nine polymorphisms have been documented in the CSB coding sequence alone, mostly located in the C-terminal region (Ensembl and NCBI SNP databases). The elevated mutation rate of CSB may hamper the immediate identification of the mutations responsible for the pathological phenotype and explain the lack of prenatal diagnosis procedures. Most of the inactivating mutations result in severely truncated polypeptides and in many cases both alleles are affected, likely resulting in non-functional proteins.
These findings suggest that CSB is not essential for cell viability and proliferation. Mutations in the *CSB* gene are distributed along the entire genomic sequence and almost all mutation types are represented.

Short genomic deletions or insertions account for nineteen out of seventy-seven inactivating mutations identified to date. Such mutations are located throughout the coding sequence and all but one result in frameshift changes. Most short insertions

are duplications of the wild-type sequence and most single-base deletions are located in runs of repetitive identical bases. Both types of genomic alterations probably result from error-prone replication slippage. Out of the twenty-four nonsense mutations, four (p.Arg453X, p.Arg735X and p.Arg1087X) have been found in more than one CS family. All the nonsense mutations involve the common transition due to a CpG hotspot effect from the CGA codon for arginine to the TGA stop codon. The majority of the twelve splice mutations affect the consensus AG sequence of the intronic acceptor site. The four in-frame deletions resulting from splice mutations are clustered between the helicase domains III and IV, in the linking segment between the two RecA-like domains of the protein. Out of the thirteen missense mutations, seven are located between position 851 and 1095, whereas four (p.Arg670Trp, p.Asn680Asp, p.Trp686Cys and p.Ser687Leu) map in a conserved amino acid stretch between position 670 and 687 in helicase domain III. It has been suggested that this domain could play a role in coupling the ATPase activity to DNA remodeling (Muftuoglu et al., 2002; Christiansen et al., 2003; Licht et al., 2003). Indeed, the helicase domain III is located in the DNA binding cleft, close both to the ATP binding site (motifs I and II) and RecA-like domain 2, suggesting that motif III is involved in the transduction of energy from the ATPase site on domain 1 to the second protein domain, thereby driving a conformational change required to perform the mechanical function of CSB (Laugel et al., 2010). *In vitro* studies have shown that point mutations in motif III are associated with a moderate increase in the cellular sensitivity to DNA-damaging agents, but mutational analysis shed new light on the potentially critical role of this particular motif (Christiansen et al., 2003; Licht et al., 2003).

No obvious genotype-phenotype correlation emerges from the data collected by mutation analysis in CS-B patients (reviewed in Laugel et al., 2010; Laugel, 2013). Severe truncations are present in patients with either classical or early-onset forms of the disease, as well as in three severe cases of CS without clinical photosensitivity. Conversely, both severe and moderate phenotypes are associated with truncating and missense mutations and even with the same set of mutated *CSB* alleles. The finding that the same inactivating mutation in the CSB gene was associated with distinct pathological phenotypes diagnostic, respectively, for CS and for a severe form of XP has further extended this notion.

The observation of a mild UV^{S}S patient lacking any detectable CSB product has suggested that the presence of truncated or abnormal CSB protein is more detrimental than the complete absence of CSB. Newman and collaborators (2008) have developed this hypothesis after the finding of a chimeric transcript, composed of the first 5 exons of *CSB* and of the open reading frame of the PGBD3 transposon nested in intron 5 of the *CSB* gene, translated into a fusion protein comprising the first 465 amino acids of CSB and the entire PGBD3 transposase. The authors

proposed that the fusion protein could play a deleterious role in absence of full-length CSB and therefore trigger the classical CS phenotype. According to this theory, mutations downstream of intron 6 would cause CS, whereas mutations upstream of intron 6 would only cause the mildest form of UV^{S}S. Similarly, a very late onset form of CS has been associated with an early truncating mutation and has raised the possibility that the same paradigm could also be applied to mild form of CS (Laugel et al., 2010).
Two out of the four mildly affected CS cases reported in literature presented with early truncating *CSB* mutations and seem to follow the same rule. However, the remaining two mild CS patients (Patient CS823VI and CS543VI) have mutations located downstream of intron 6, thus not supporting this hypothesis. The observation of two severely affected patients without any detectable CSB protein nor CSB-transposon fusion product do not support the proposed paradigm, either.
Five additional CS patients (Patients CS10LO, CS1PV, CS3PV, AEN74 and CS179VI) have mutations expected to prevent the translation of the fusion protein: the possibility of leaky stop codons and weak frameshifts has been put forward to account for these exceptions, but experimental evidence is still lacking (Newman et al., 2008). A systematic study at the protein level is needed to further investigate the potential link between the presence of the CSB-transposon fusion protein and the degree of clinical severity. Alternatively, the CS phenotype may be dependent on other genetic or environmental factors, such as modifier genes coding for proteins involved in the repair and transcription pathways that could modulate the effect of *CSA* or *CSB* mutations.
Endogenous or exogenous factors modifying the level of oxidative stress in the cell and the production of DNA lesions may also be of importance to determine the severity of the phenotype.

2.3 Functional roles of CS proteins

2.3.1 Nucleotide excision repair

A number of parallel developments have led to the discovery and subsequent elucidation of the Nucleotide excision repair (NER) system in humans (Figure 11). NER is organized in two sub-pathways: the GG-NER and the TC-NER. TC-NER rapidly removes DNA damages from the transcribed strands of transcriptionally active genes, thereby allowing recovery of RNA synthesis after UV irradiation. In contrast, GG-NER is a slow process that operates throughout the genome. Therefore, TC-NER mainly promotes survival, whereas GG-NER prevents mutations (Hoeijmakers, 2009). NER is a multistep process that requires coordinated and sequential action of more than 30 gene products and consists of several sequential

steps: damage recognition, local opening of the DNA helix, dual incisions on both sides of the lesion, displacement of the lesion-containing oligonucleotide, gap-filling DNA synthesis and ligation. Although the DNA damage is recognized by distinct mechanisms in each sub-pathway, the two pathways converge onto the same core NER reactions. Initiation of TC-NER likely occurs by the physical blockage of RNA polymerase II (RNApol II) on lesions (reviewed in Vermeulen and Fousteri, 2013). Lesion-stalled RNApol II subsequently triggers the recruitment of the NER machinery. In contrast to TC-NER, damage recognition by the GG-NER occurs independent of transcription and requires the concerted action of the XPC-HR23B and UV-DDB complexes. The further processing of lesions in both TC-NER and GG-NER occurs via a common pathway, in which the transcription factor IIH (TFIIH) comes first after the damage is recognized. The intrinsic helicase activity of TFIIH together with the XPA protein is required to verify the lesion. A lesion-bound complex involving at least TFIIH, XPA and RPA proteins provide the structural basis to load and properly orient the structure-specific endonucleases ERCC1/XPF and XPG, which incise, respectively, the damaged strand 5' and 3' to the lesion. The consequent 25-30 nucleotide gap is filled in by the replication machinery and sealed by DNA ligases. NER is a multistep mechanism devoted to recognize and repair a large number of structurally diverse DNA lesions. This versatility depends on the ability to recognize and verify chemical modifications in the DNA and distortions in the structure of the double helix. NER is critically important for the repair of lesions arising from different sources. The most characterized NER substrates are represented by the main DNA lesions induced by UV irradiation, i.e. cyclobutane pyrimidine dimers (CPDs) and (6-4)pyrimidinepyrimidone photoproducts (6-4PPs) (Vermeulen and Fousteri, 2013). CPDs and 6-4PPs differ in the number and position of the covalent bonds between two adjacent pyrimidines on the same DNA strand, which are generated into DNA upon exposure to short-wavelength UV light (UVB 290-320 nm and UVC < 290 nm).

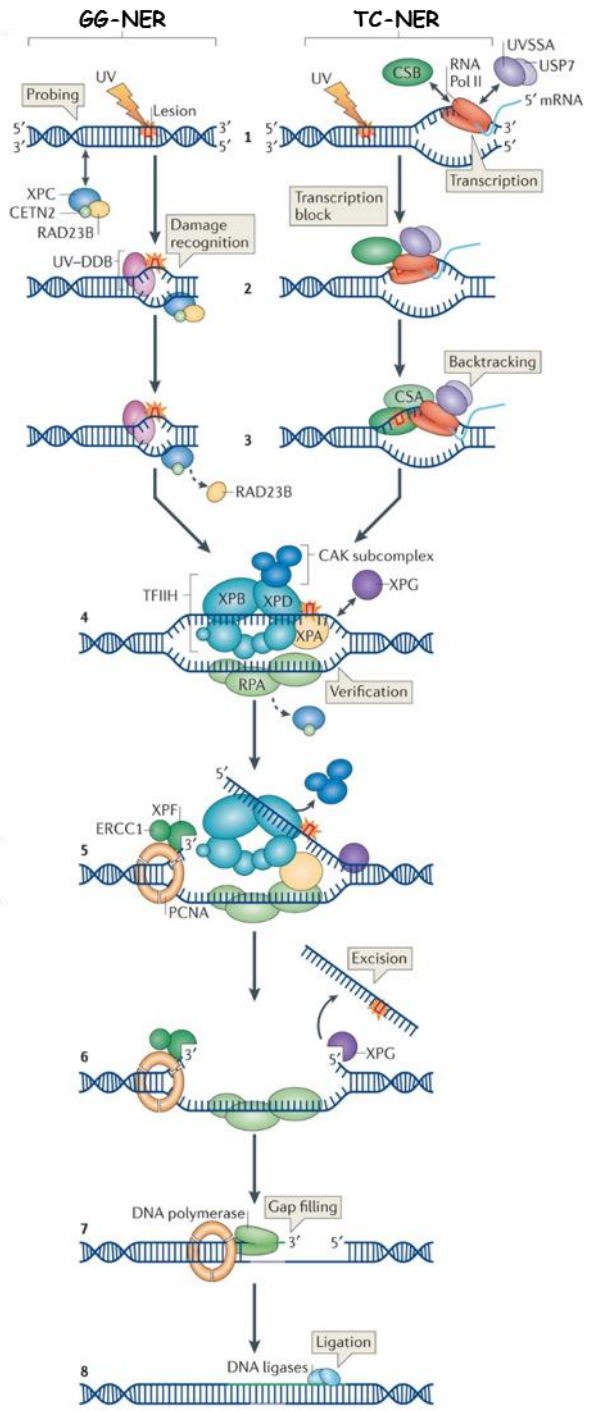
GG-NER
TC-NER
UV
Probing
Lesion
5′
3′
3′
5′
1
XPC
CETN2
RAD23B
Damage recognition
UV-DDB
2
UV
CSB
RNA Pol II
UVSSA
USP7
5′ mRNA
3′
5′
Transcription
Transcription block
Backtracking
CSA
3
RAD23B
CAK subcomplex
XPG
TFIIH
XPB
XPD
XPA
4
RPA
Verification
5′
XPF
ERCC1
3′
5
PCNA
Excision
6
3′
5′
XPG
DNA polymerase
Gap filling
7
3′
5′
Ligation
DNA ligases
8

Figure 11. Molecular mechanism of nucleotide excision repair in human cells.
Modalities of global genome repair (GG-NER) and transcription coupled repair (TC-NER) are illustrated (modified from Marteijn et al., 2014).

Additional NER substrates are the lesions caused by chemical agents that covalently bind DNA bases and form DNA bulky adducts. Examples of these chemicals include benzo[a]pyrene diol-epoxide, aromatic amines, aflatoxin, nitrosamines and 4-nitroquinoline oxide. In addition, endogenous cellular metabolic processes can yield some highly reactive products, such as lipid peroxidation that leads to the formation of malondialdehyde, an endogenous carcinogen that can also form DNA adducts. Other NER substrates are cyclopurins, which are bulky adducts characterized by the presence of a second bond between the purine and the deoxyribose in the DNA backbone (Brooks, 2007). Cyclopurins are caused either by reactive oxygen species generated by endogenous cellular processes or exposure to X-rays.
NER also deals with the lesions induced by crosslinking agents able to form covalent bonds with DNA, either on the same strand (intrastrand crosslinks) or across strands (interstrand crosslinks, ICLs). As far as the NER mechanism is concerned, intrastrand crosslinks are no different from bulky adducts, as long as they can be removed as part of a short oligonucleotide. Contrarily, ICLs pose a real challenge to NER, since both strands are damaged. NER requires an intact strand to serve as a template to repair the other, therefore ICLs repair necessitates a combination of NER factors with proteins implicated in translesion synthesis, homologous recombination, mismatch repair and the Fanconi anemia network (reviewed in Shen and Li, 2010; Wood, 2010). It was recently demonstrated that CSB coordinates the resolution of ICLs, possibly in a transcription-associated repair mechanism involving SNM1A, and that the defect in the process could contribute to post-mitotic degenerative pathologies associated with CS (Iyama et al., 2015).

2.3.2 CS proteins in TC-NER

In mammalian cells, TC-NER is strictly dependent on CSA and CSB (Figure 12). According to the most widely accepted model, the stalling of transcription at a DNA lesion site promotes a stronger interaction of RNApol II with CSB, which is also part of the normal transcription machinery. A recent study demonstrates that ATP hydrolysis by CSB is essential for stable CSB-chromatin association after UV irradiation and alterations in this process are likely involved in CS disorder. During normal cell growth, the association of CSB with chromatin is negatively regulated by the N-terminal region of the protein. In the absence of the negative regulatory

region, ATP hydrolysis becomes dispensable, indicating that CSB uses energy from ATP hydrolysis to overcome the inhibitory effect imposed by its N-terminal region. These results suggest that the recruitment of CSB to the lesion-stalled transcription is an ATP-dependent process that involves a gross conformational rearrangement in CSB (Lake et al., 2010). *In vitro* data indicate that the XPG protein facilitates the recognition of the stalled RNApol II by CSB. XPG interacts with RNApol II and enhances multiple CSB functions, including the stimulation of its ATPase activity (Sarker et al., 2005). However, in the context of chromatin XPG appears to act downstream of CSB (Fousteri et al., 2006). Once the distorted transcription bubble has been detected, the stalled RNApol II needs to be degraded or reverse translocated ("backtracked") from the lesion to allow the access of the repair machinery. Ubiquitination of the large subunit of RNApol II by Nedd4, an E3 ubiquitin ligase enzyme, has been reported to occur in human cells after UV irradiation. Nonetheless, ubiquitylation/degradation of RNApol II is not a damage response *per se*, but rather a consequence of the arrested RNApol II progression at the lesion site (Anindya et al., 2007). Regression and maintenance of the stalled RNApolII are obviously preferable for mammalian genes (Hanawalt and Spivak, 2008). At this purpose, the recently identified TC-NER factor UVSSA (UV-stimulated scaffold protein A), mutated in UVSS-A patients, forms a complex with the ubiquitin-specific protease 7 (USP7) and plays a protective role in the early steps of TC-NER. In this process, the UVSSA protein seems to provide substrate specificity to the pleiotropic deubiquitylating USP7 enzyme. The UVSSA-USP7 complex, which travels along with RNApol II and accumulates at damage-stalled transcription sites, stabilizes the RNApol II-CSB complex by counteracting polyubiquitylation of CSB and RNApol II (Vermeulen et al., 2013). Finally, the assembly of a functional TC-NER complex in eukaryotic cells does not require the dissociation of the stalled RNApol II from DNA (Jung and Lippard, 2006).

All the pre-incision NER core components are recruited to lesion-stalled RNApol II in a CSB-dependent manner: this suggests that CSB fulfils a transcription repair coupling function, while holding back the RNApol II to its template (Fousteri et al., 2006). Upon encountering a DNA lesion, RNApol II needs to backtrack to provide access for the NER factors to the damaged template. However, RNApol II backtracking can be obstructed by the process of nucleosome reassembling that naturally occurs behind the transcription machinery progression. This would render the 3' side of the damage, bound by RNApol II, inaccessible to the TC-NER factors. It has been proposed that a regulatory cascade of specific histone modifications, in concert with chromatin remodeling factors, is triggered by the CSB and CSA-dependent recruitment of p300 and HMGN1, presumably upstream of the RNApol II arrest site. These modifications and resulting remodeling events are required to create accessibility and/or affect RNApol II backtracking (Vermeulen et al., 2013).

Thus, removal of RNApol II by ubiquitylation and degradation might be a strategy when the arrest of RNApol II at the lesion site is prolonged because of DNA repair failure. CSA has no direct functions in coupling the pre-incision NER factors to stalled RNApol II and, therefore, it works differently from CSB. CSA is recruited to the stalled RNApol II as a part of an E3 ubiquitin ligase complex that includes DDB1, Cul4A and ROC1 (CRL4-CSA or CSA core complex). It has been shown that immediately after UV irradiation the CSN protein complex associates with the CSA core complex, thus inhibiting its E3 ubiquitin ligase activity (Groisman et al., 2003). By a mechanism dependent on CSB, the CSA core-CSN complex translocates to the nuclear matrix, where it co-localizes with the RNApol II (Kamiuchi et al., 2002). CSA is also required to recruit, in cooperation with CSB, the XPA binding protein 2 (XAB2) and the transcription factor TFIIS. XAB2 is an essential TPRs (tetratricopeptide)-containing protein involved in pre-mRNA splicing and transcription. Recently, XAB2 has been isolated in a multimeric protein complex made of hAquarius (IBP160), XAB2 (hSYF1), hPRP19, CCDC16, hISY1 and PPIE, which are known to be involved in pre-mRNA splicing (Kuraoka et al., 2008). Therefore, it has been suggested that this large complex is involved in transcription, pre-mRNA splicing and TC-NER. The transcription cleavage factor TFIIS is the last factor being recruited downstream of CSA and CSB and prior to the NER incision core complex. Following UV irradiation, the interaction between TFIIS and RNApol II increases significantly in normal cells, but not in CS-A and CS-B cells. Recent structure analysis of RNApol II associated with TFIIS revealed that TFIIS could enter into the RNApol II catalytic center, in close proximity to the nascent RNA molecule (Wang et al., 2009). Therefore, TFIIS can stimulate the cleavage activity of RNApol II, allowing the stalled RNApol II to restart elongation. Contradictory data on the possible role of TFIIS in TC-NER have been reported in two recent studies carried out in human cells by using an RNA interference strategy that showed a role for TFIIS in transcriptional recovery after UV irradiation.

CSB contains a UBD domain shown to be required for TC-NER *in vivo*. Cells expressing UBD-less CSB are still capable to assemble NER factors around the damage-stalled RNApol II, but the repair apparatus fails to excise the lesion (Anindya et al., 2010). Thus, the ability of CSB to bind ubiquitin is essential for measurable levels of damage incision to be triggered during TC-NER. At the late steps of the repair process, CSN dissociates from the CSA core complex restoring its ubiquitin ligase activity. CSB is then ubiquitinylated by the CSA core complex and degraded by the proteasome in a UV-dependent manner, a crucial step in the recovery of RNA synthesis after TC-NER (Groisman et al., 2006). Therefore, ubiquitylation acts as a quality control for the assembly of a fully functional TC-NER complex, but it is also required to license TC-NER.

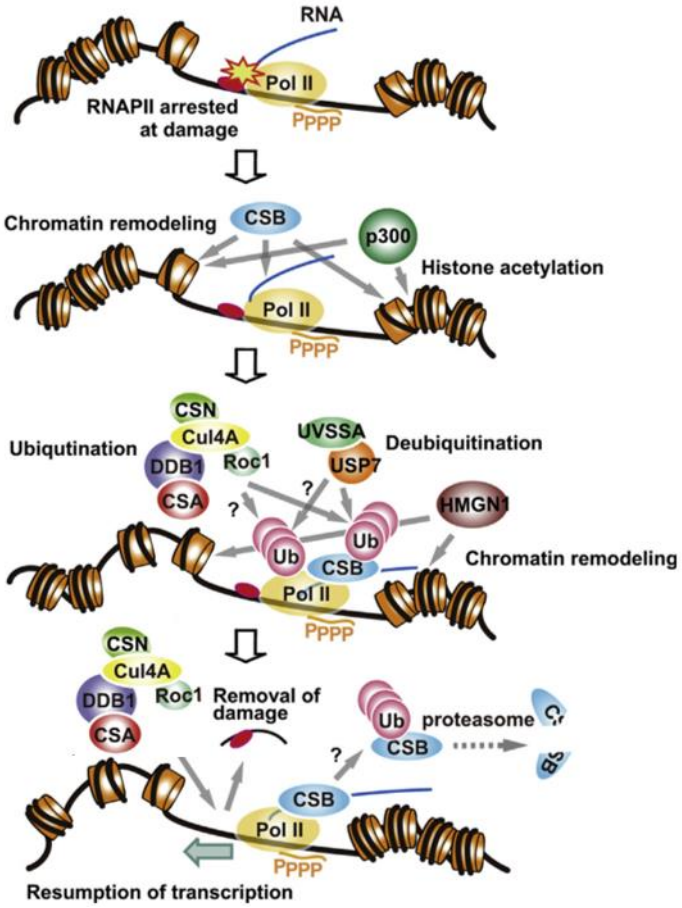

Figure 12. The roles of TC-NER factors around the stalled RNApol II site. A model for the roles of CSA, CSB and UVSSA proteins in TC-NER is shown. First, CSB is recruited to RNApol II stalled at a lesion. Then, the CSA and UVSSA complexes are recruited to the stalled RNApol II-CSB and function as ubiquitin ligase and deubiquitinase, respectively. CSB, p300 and HMGN1 function as chromatin remodeling factors around the stalled RNApol II site (modified from Saijo, 2013).

2.3.3 Roles of CSA and CSB in the oxidative stress response

A complex and unclear relationship exists between the clinical disease and the TC-NER molecular defects underlying the CS pathological phenotype. The elucidation of the biochemical functions of proteins mutated in hereditary diseases is often a

revelation to explain the characteristic symptoms of affected patients. In the case of CS, however, the causal relationship between the most prominent clinical symptoms and the established cellular roles of the CSA and CSB proteins has remained enigmatic (Khobta and Epe, 2013). The well-established and indispensable role of both proteins in TC-NER easily explains the diagnostically relevant UV sensitivity of CS patients. It is tempting to hypothesize that the degenerative symptoms of CS result from accumulation of unrepaired oxidative damage in either nuclear or mitochondrial DNA which, according to the free radical theory of aging, could give rise to elevated mutation frequency and, in consequence, early degeneration of tissues (Balaban et al., 2005; Fukui and Moraes, 2008).

Elevated levels of oxidatively generated mitochondrial DNA (mtDNA) damage, hypersensitivity to bioenergetic inhibitors as well as altered organization of mitochondrial respiratory complexes have been reported in CS-B cells (Osenbroch et al., 2009). The removal of oxidatively generated DNA modifications in all type of cells is predominantly carried out by specific and efficient mechanisms, in particular base excision repair (BER), which involves recognition throughout the genome by specialized proteins, namely repair glycosylases, that act independent of transcription (Svilar et al., 2011). However, some oxidatively generated DNA lesions are subject to NER, either because they cause a helix distortion recognizable by NER proteins such as XPC, or because they block transcription and therefore are able to trigger TC-NER.

CS symptoms, to some extent, resemble those observed in patients with inherited mitochondrial dysfunctions. Mitochondria are particularly exposed to reactive oxygen species (ROS) and, since they lack NER, a role of CSB and CSA in mtDNA damage repair has received special attention in the last years (Khobta and Epe, 2013). Some relevant indications for a direct involvement of CSB in the repair of oxidatively damaged DNA come from studies searching for physical interaction partners. Indeed, CSB has been shown to co-precipitate from cell extracts together with the repair glycosylase OGG1, which is known to recognize and excise 8-oxo-7,8-dihydroguanine (8-oxoG) from oxidatively damaged DNA in the initiation of BER (Klungland and Bjelland, 2007). The interaction between CSB and OGG1, however, appears to be indirect. OGG1 was detected in mitochondria of cultured human cells in a complex with CSA, CSB and mitochondrial DNA itself after treatment with H_2O_2 (Kamenisch et al., 2010). Relevant of note, CSA and CSB could not be detected in mitochondria in absence of oxidative stress, in agreement with the notion that neither TC-NER nor GG-NER are carried out in mitochondria (Cline, 2012). The re-localization of CSB to mitochondria was independently shown by others (Aamann et al., 2010), even though the precise role of CSB in the mitochondrion remains to be established. Moreover, CSB has been found to physically interact with several other proteins involved in BER, including NEIL1, a

repair glycosylase with associated β,δ-lyase activity, which excises lesions from single-stranded bubbles (Muftuoglu et al., 2009). Since NEIL1 is up-regulated during S-phase and interacts with PCNA and RPA, it might be involved in replication-associated BER (Banerjee et al., 2011). Another CSB interactor directly involved in BER is the apurinic/apyrimidinic (AP) endonuclease APE1 (Wong et al., 2007). APE1 initiates the repair of apparently all types of AP sites, including "free" sites of base loss generated by spontaneous depurination or reaction with ROS. The physical interaction with CSB takes place at the N-terminal domain of APE1, which is not required for the repair endonuclease activity, but essential for the interaction with the platform protein XRCC1 (Vidal et al., 2001) and for the additional role of APE1 as a redox-sensitive regulator of various transcription factors, such as AP-1, NF-kB and p53 (Kelley et al., 2012). The relevance of this interaction is underlined by the observation that CSB deficiency is associated with a three-fold hypersensitivity to methyl methanesulfonate (MMS), a chemical agent known to generate high levels of AP sites.
Another interaction demonstrated by co-immunoprecipitation is the DNA-independent binding of the N-terminal segment of CSB to poly(ADP-ribose) polymerase-1 (PARP1) (Thorslund et al., 2005). PARP1 immediately binds to free single-strand breaks (SSB) in DNA and might have an additional role in BER (Le Page at al., 2003). After binding to the SSB, PARP1 modifies various proteins by poly(ADP-ribosyl)ation, including itself, histones and probably CSB. Both nuclear and mitochondrial DNA repair are affected by mutations in *CSA* and *CSB* genes. CSA and CSB indeed can modulate the repair of oxidized DNA bases by acting both directly (by interaction with BER proteins) and indirectly (by modulating the expression of DNA repair genes). Whereas several lines of evidence highlight the role of CSB outside TC-NER, our knowledge on additional functional roles of CSA is much more limited (D'Errico et al., 2013). The phenotypic similarity between patients mutated in either *CSA* or *CSB* suggests that both proteins might be involved in similar cellular processes, or cooperate in the same pathways. Moreover, *CSA* and *CSB* are also mutated in a small number of photosensitive patients without neurological symptoms ($UV^{S}S$) (Horibata et al., 2004). Cells from these patients are not sensitive to ROS (Spivak and Hanawalt, 2006). This observation indicates that TC-NER proteins have additional functions that might account for the neurodegenerative phenotype of CS patients.

2.3.4 CS proteins in transcription

Several lines of evidence indicate that CS proteins might have a direct impact on the transcription process. CSB has been implicated in transcription driven by RNApol I, RNApol II and likely by RNApol III. In eukaryotic cells, RNApol I is the only

enzyme involved in ribosomal RNA (rRNA) synthesis, except for the 5S rRNA that is transcribed by RNApol III. CSB localizes at the site of ribosomal DNA (rDNA) transcription and is part of a protein complex that contains RNApol I, TFIIH and basal RNApol I transcription initiation factors (Bradsher et al., 2002). The rRNA transcription is largely regulated by chromatin remodeling and epigenetic changes, and some of these modifications are controlled by CSB. Indeed, CSB interacts with the histone methyl-transferase (HMT) G9a, which methylates lysine 9 of histone H3 (H3K9me). This post-translational modification and heterochromatin protein 1 gamma (HP1g) binding are required for rRNA synthesis initiation and elongation (Vélez-Cruz and Egly, 2013).
It has been demonstrated that CSB is also associated with NURD (nucleosome remodeling and deacetylation complex), another complex involved in transcriptional regulation of rRNA genes (Xie et al., 2012). In addition, CSB interacts with RNApol II stimulating its polymerase activity. Transcriptional defects have been reported in CS-B cells upon cellular response to stress, thus showing that CSB regulates processes such as transcriptional recovery after UV damage, p53 transcriptional response, response to hypoxia, response to insulin-like growth factor-1 (IGF-1), transactivation of nuclear receptors and transcription of housekeeping genes (Vélez-Cruz and Egly, 2013). The involvement of CSB in transcription was further investigated by transcriptome analysis in CS cells. Even in absence of DNA damage, CSB affects the expression of thousands of genes, both in primary fibroblasts as well as in neuronal cells. In addition, reprogramming of CS fibroblasts to neuron-like cells is defective, unless exogenous *CSB* gene is introduced. These findings could potentially explain the multiple neurodevelopmental defects observed in CS patients (Wang et al., 2014). Furthermore, recent studies indicate that CSB can potentially regulate the overall efficiency of the transcription machinery through its associated protein complexes. Indeed CSB is involved in the RNA polymerase elongation and splicing complexes (Nicolai et al., 2015). The involvement of CSB in transcription by RNApol III is less clear.

As far as CSA is concerned, it has been implicated only in transcription by RNApol I. It was recently demonstrated that CSA binds to the promoter and gene-internal regions of the active fraction of rDNA genes. CSA recruits the elongation factor CSB and TFIIH to the rDNA promoter and stimulates re-initiation of RNApol I transcription. Stable transfection of *CSA* in CS-A cells is followed by an increase in ribosome number, translation activity and cellular growth. Collectively, these data suggest a role for CSA in ribosomal biogenesis (Koch et al., 2014).

2.3.5 CS proteins in chromatin remodeling and maintenance

Changes in chromatin structure are known to be tightly associated to NER, and are required for efficient DNA repair in the context of condensed chromatin. During TC-NER, the CSA and CSB proteins are prerequisite factors for the assembly of chromatin remodelers such as HAT, p300 and HMGN1, since repair process requires efficient chromatin remodeling events to facilitate the rapid accessibility and assembly of repair factors at the DNA damage site. Moreover, it has been demonstrated that CSB itself, like many other members of the SWI2/SNF2 family, has nucleosome remodeling activity and binds to core histone proteins *in vitro* (Citterio et al., 2000). As previously discussed, the N-terminal region of CSB negatively regulates its association with chromatin. In the absence of this negative regulatory region, ATP hydrolysis becomes dispensable for chromatin association, indicating that CSB uses energy from ATP hydrolysis to overcome the inhibitory effect imposed by its N-terminal region (Lake et al., 2010). The role of CSB in chromatin maintenance is also supported by the observation that the transcription pattern of CS-B cells overlaps that of normal cells treated with the histone deacetylase inhibitor trichostatin A (Newman et al., 2006), thus indicating that CSB may decrease the amount of histone acetylation. The observation that acetylation of histone H4 in proximity of specific promoters is reduced in CS-B cells before and/or after UV irradiation suggests a CSB-dependent histone acetylase activity (Proietti-De-Santis at al., 2006). These studies indicate that the chromatin pattern is affected in CS-B cells, but it is not clear yet how CSB is involved in modifying histone acetylation. The recent identification of histone deacetylase 1 (HDAC1) as a CSB-interacting protein can raise interesting hypotheses (Nicolai et al., 2015). Recent studies showed that CSB interacts with four most prominent chromatin-remodeling factors (SMARCA1, SMARCA2, SMARCA4 and SMARCA5) belonging to the neural progenitors specific chromatin-remodeling complex (npBAF complex) and the neuron-specific chromatin-remodeling complex (nBAF complex). These data indicate that CSB may play a crucial role in preserving the functional integrity of different brain cell types (neural stem/progenitor cells, neurons and glial cells) through the coordination of transcription and chromatin remodeling activities (Nicolai et al., 2015).
A further role of CSB in telomere maintenance and stability has been recently demonstrated (Batenburg at al., 2012). CSB localizes at a small subset of human telomeres and it is required for preventing the formation of telomere dysfunction-induced foci in CS cells. In addition, CSB physically interacts with the telomeric repeat-binding factor 2 (TRF2), a duplex telomeric DNA binding protein essential for telomere protection. The finding that CSB-deficient cells accumulate telomere doublets (also known as fragile telomeres) and exhibit misregulation of TERRA, a large non-coding telomeric repeat-containing RNA, further strengthen the relevance

of CSB in telomere maintenance. Furthermore, overexpression of CS proteins promotes telomere-dependent telomere lengthening, a phenotype that is associated with a decrease in the amount of telomere-bound TRF1, a negative mediator of telomere length maintenance. Taken together, these findings suggest that CSB is important for telomere integrity and imply that CS patients may be defective in telomerase maintenance, event that may be associated with the premature aging phenotype of CS patients.

2.3.6 CS proteins in mitochondrial maintenance and metabolism

The neurodegenerative features of CS patients are strikingly similar to what is observed in many patients suffering from mitochondriopathies (reviewed in Scheibye-Knudsen, 2016). In recent years, a potential mitochondrial involvement has been proposed for this disease and, consistently, CSB has been reported to be present in the mitochondria (Aamann et al., 2010; Kamenisch et al., 2010). Electophoretic mobility shift assays and co-immunoprecipitation experiments revealed that mitochondrial DNA (mtDNA) associates to CS protein and, upon treatment with H_2O_2, CS proteins have been found to be recruited to mitochondria (Figure 13). Moreover, the finding that mtDNA mutations are highly increased in cells from CS patients and in the subcutaneous fat of aged $Csb^{-/-}$ and $Csa^{-/-}$ mutant mice suggests a role for CS proteins in counteracting mitochondrial mutagenesis and a new link between the neurodegerative and aging processes typical of CS (Kamenisch et al., 2010). Scheibye-Knudsen at al. in 2013 demonstrated that CSB-deficient cells showed increased membrane potential, increased free radicals production, increased oxygen consumption rate, increased carbonylcyanide-4-trifluoromethoxyphenlhydrazone (FCCP) uncoupled respiration (a sign indicating spare respiratory capacity) and increased mitochondrial content. In particular, this last feature might stem from a decreased mitochondrial degradation rate, due to defective mitophagy (the process by which mitochondria are selectively degraded). Based on the idea that CSA and CSB may be present in mitochondria it has been proposed that these enzymes may act within the mitochondrial matrix to sense mitochondrial DNA damage and induce mitophagy (reviewed in Scheibye-Knudsen, 2016). The above-mentioned features are unusual for a primary mitochondrial defect, where disruption of the electron transport chain would normally lead to decreased oxygen consumption and decreased membrane potential. The involvement of CSB in mitophagy was further investigated by treating CSB-deficient cells with the autophagy-stimulating drug rapamycin, which gave rise to a reversion of the phenotype. Furthermore, it has been demonstrated that primary fibroblasts from CS-A and CS-B patients present an altered redox balance with increased steady-state levels of ROS and decreased basal rate of oxidative phosphorylation (Pascucci et al.,

2012). Another possibility is that the mitochondrial alterations could be secondary to a nuclear DNA repair defect that leads to increased oxygen consumption, increased membrane potential and increased ROS production (Scheibye-Knudsen et al., 2013).

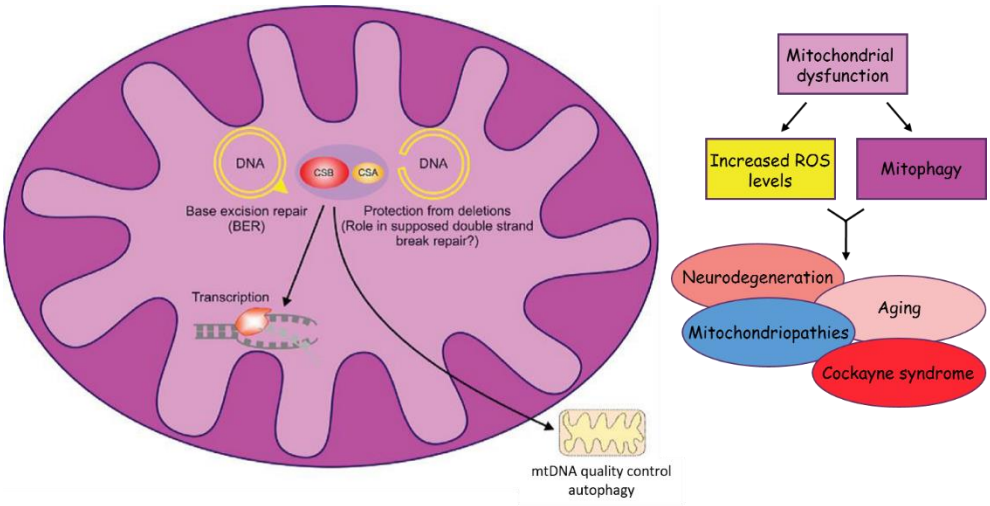

Figure 13. Schematic representation of CSA and CSB functions in the mitochondrion and contribution of mitochondrial dysfunction to a wide range of pathologies. Mitochondrial CSA and CSB proteins are involved in base excision repair, transcription, mitochondrial quality control and protection from mtDNA deletions (modified from Kamenisch et al., 2013).

CSB plays important roles in mitochondrial transcription through physical and/or functional interaction with the mtRNA polymerase, the mitochondrial transcription factor 2B and TFAM, the last one being a protein involved not only in nucleoid packaging, but also in DNA replication, transcription, and base excision repair (Kamenisch et al., 2013). Recent findings revealed a novel pathway that alters mitochondrial functions in CS cells. It was reported a CSA/CSB-dependent depletion of the mitochondrial DNA polymerase-γ catalytic subunit (POLG1), due to a dramatic increase in the levels of the high temperature requirement A (HTRA) 3 protease, which depends on altered nitroso-redox balance. HTRA3 accumulation was found in CS, but not in $UV^{S}S$ or control fibroblasts. Inhibition of serine proteases restored physiological POLG1 levels in either CS fibroblasts and in CSB-silenced cells. ROS scavengers and peroxynitrite normalized HTRA3 and POLG1 levels in

CS cells and increased mitochondrial oxidative phosphorylation, which is also altered in CS cells. Thus, by altering the expression of oxidases and antioxidants, CSB/CSA impairment promoted overproduction of serine proteases, which, in turn, depleted POLG1 and altered the mtDNA replication machinery. Altogether, these observations provide strong evidences for the importance of CSB in mitochondrial metabolism maintenance and support the idea that CS clinical features might result, at least in part, from mitochondrial dysfunction. Notably, much of the work investigating mitochondrial involvement in CS has been focused on the mutations in the CSB complementation group. Thus, much work is needed to investigate whether the same alteration are seen with CSA deficiencies.

3. Aims of the research

Cockayne syndrome (CS) is an autosomal recessive multisystem disorder, characterized by pre- or post-natal growth failure, skeletal abnormalities, progressive neurological dysfunction, cutaneous photosensitivity and signs of segmental premature aging. These alterations are caused by mutations in either *CSA* or *CSB* genes, which are both involved in transcription-coupled repair (TC-NER), the pathway that removes bulky adducts blocking the progression of the transcription machinery on the transcribed strand of active genes. The broad range in type and severity of CS phenotype and the lack of a clear genotype-phenotype relationship imply that CSA and CSB might have additional functions outside TC-NER. Whereas several lines of evidence highlight the involvement of CSB beyond TC-NER, our knowledge on additional functional roles of CSA is much more limited. CSA-defective (CS-A) cells are characterized by increased levels of intracellular reactive oxygen species (ROS) and mitochondrial anomalies, features that are known to play a part in aging and neurodegeneration. A recent study demonstrated that the CSA protein participates in the response to oxidative stress, in addition to its role in the removal of UV-induced lesions (reviewed in D'Errico et al., 2013). Furthermore it has been recently shown that the increased mitochondrial fragmentation in CS-A cells is rescued by overexpressing the Parkin protein (Pascucci et al., 2016). Taken together, these findings suggest that CSA is involved in other signaling pathways and likely carries out its other functions through the interaction with different protein/complexes. Notably, our laboratory has recently developed a cell system that allowed the purification of CSA-interacting proteins by Tandem Affinity Purification (TAP) and their subsequent identification through mass spectrometry by Prof. Luca Bini (University of Siena). From this analysis, forty-seven putative CSA-interacting proteins have been isolated, eleven of which represented by the well-known CSA binding partners operating in TC-NER, whereas the remaining thirty-six appeared as novel putative CSA interactors.

The main goal of this research study is to gain new insights into the still poorly understood role of the CSA protein outside TC-NER. Our strategy is to investigate the effect that specific *CSA* mutations have on the CSA protein interaction framework, both in basal condition and in response to different stressing agents. The selected CSA mutations were isolated from patient cells or conceived in the laboratory with the idea to target distinct WD domains. To overcome the limit imposed by the lack of a commercial antibody specific for CSA, which has so far hindered the investigation on CSA and its functional roles, we developed a panel of isogenic cell lines expressing the mutated forms of CSA tagged at the C-terminus

with the Flag and HA epitopes ($CSA^{Flag\text{-}HA}$). We then investigated the impact of CSA mutations on the transcript and protein stability as well as on the cellular response to stress inducing agents.
Among the recently identified CSA-interactors we identified two subunits (namely CCT3 and CCT8) of the TRiC/CCT chaperonin complex, which is involved in the folding of proteins characterized by complex topologies and regions of β-strand. Among the TRiC/CCT substrates, the WD repeat proteins are widely represented. We therefore investigated the impact of CSA mutations on the interaction with the CCT3 and CCT8 subunits of the TRiC/CCT complex and whether/how different cellular stressing agents affect these interactions or their cellular distribution. Then, we analyzed whether the knockdown of the TRiC/CCT complex could impair CSA functionality by assaying the cellular TC-NER activity upon UV-induced DNA damage, thus suggesting a role in the molecular pathways of CSA.

The second part of this research study is directed to the identification of new disease genes for Cockayne syndrome. We analyzed the case of an Italian patient with the clinical symptoms typical of the severe form of CS and cellular features characteristic of TC-NER alterations (reduced survival and decreased recovery of RNA synthesis but normal unscheduled DNA synthesis). Even though complementation assays were suggestive of genetic defects in the *CSB* gene, no inactivating mutations were found. Therefore, in the frame of a long lasting collaboration with our laboratory, Prof Tomoo Ogi (Research Institute of Environmental Medicine, Nagoya University, Japan) performed the whole exome sequencing (WES) analysis on primary cells from all the family members, identifying potentially pathogenic mutations in three distinct genes. In the attempt to validate which of these genes is causative of the CS phenotype in this unassigned case, we investigated whether the proteins encoded by the candidate genes interact with CSA. Next, we silenced the candidate genes in primary dermal fibroblasts from a healthy individual and subsequently tested CSA functionality by assaying the cellular TC-NER activity. This approach should allow us to define the conceivable involvement of the candidate gene in CS etiopathogenesis and, eventually, in CSA-dependent signaling pathways.

4. Materials and methods

4.1 Plasmids

4.1.1 Bacterial cultures

The bacterial strain TOP10 was used for plasmid cloning. TOP10 genotype is F- mcrA Δ(mrr-hsdRMS-mcrBC), φ80lac ZΔM15, ΔlacX74, recA1, deoR, araΔ139 Δ(ara-leu) 7697, galU, galK, rpsL (Strr), endA1, nupG. Bacterial cells were cultured in Luria Bertani (LB) medium (10 g/l bacto-tryptone, 5 g/l yeast extract and 5 g NaCl) or LB-agar (LB plus 15 g/l bacto-agar) supplemented with 100 μg/ml ampicillin (Pharmacia) or 50 μg/ml kanamycin (Sigma), depending on the plasmid.
50 μl of One Shot® TOP10 competent *E. coli* cells (Life Technologies) were transformed by heat shock using 5-50 ng of plasmid DNA or the ligation or Gateway reactions. According to the manufacture instructions, bacterial cells were gently mixed with the plasmid DNA, incubated for 30 min on ice, heat shocked for 30 sec at 42ºC and then maintained for 2 min on ice. 250 μl SOC medium (containing 2% bacto-tryptone, 0.5% yeast extract, 10 mM NaCl, 2.5 mM KCl, 10 mM $MgCl_2$, 10 mM $MgSO_4$, 20 mM glucose) were added to each sample that was then incubated for 1 hour at 37°C on shaker at a speed of 225 rpm, plated on a LB-agar plate and incubated overnight at 37°C.

4.1.2 Plasmid purification and screening

Small-scale (MiniPrep) and medium-scale (MidiPrep) DNA plasmid purifications were performed. For the MiniPrep, single bacterial colonies from the streaked LB-agar plates were isolated and inoculated in 5 ml LB medium supplemented with selective antibiotic and incubated overnight at 37°C with vigorous shaking. The cells were harvested at 6000 x g for 15 min at RT, resuspended in 250 μl buffer P1 (50 mM Tris·Cl, pH 8.0, 10 mM EDTA, 100 μg/ml RNase A), lysed in 250 μl buffer P2 (200 mM NaOH, 1% SDS), neutralized with 350 μl buffer P3 (3.0 M potassium acetate, pH 5.5) and centrifuged at 16000 x g for 10 min at RT. The supernatant was isolated and the plasmid precipitated by adding 1/10 volume of 3 M sodium acetate and 2.5 volumes ethanol 100%. After centrifugation at 16000 x g for 10 min, the pellet was washed in 70% ethanol and finally resuspended in 30 μl H_2O.

MidiPrep were performed using the HiSpeed® Plasmid Midi Kit (Qiagen). Briefly, 50 µl of the fresh miniprep culture were mixed with 50 ml LB medium supplemented with antibiotic, incubated overnight at 37°C with vigorous shaking and collected by centrifugation at 6000 x g for 15 min at 4°C. The pellet was resuspended in 6 ml Buffer P1, lysed in 6 ml Buffer P2 followed by 5 min incubation at RT, and neutralized with 6 ml chilled Buffer P3. The lysate was transferred to QIAfilter Cartridge, incubated 10 min at RT and transferred again to a HiSpeed Midi Tip previous equilibrated with Buffer QBT.
After gravitational flow, the HiSpeed Midi Tip was washed with 20 ml Buffer QC and the plasmid was eluted from the resin with 5 ml Buffer QF by gravity flow. The plasmid was precipitated by adding 3.5 ml isopropanol, incubated for 5 min at RT and transferred to a 20 ml syringe attached to the QIAprecipitator Midi Module. The solution was passed through the QIAprecipitator Midi Module, which was then washed with 2 ml 70% ethanol, and the DNA was eluted with 500 µl Elution Buffer from the kit.

4.1.3 Plasmid DNA digestion and ligation

Plasmid DNA was incubated for 1 hour at 37ºC with 1-2 U/ µg restriction enzyme in the appropriate digestion buffer. The digestion products were resolved by gel electrophoresis on a 1% TBE-agarose gel (0.5 g SeaKem® LE agarose, Cambrex, dissolved in 50 ml of an aqueous solution 89 mM Tris, 89 mM boric acid, 2 mM EDTA). DNA fragments were purified from the gel using the QIAquick Gel Purification Kit (Qiagen) whereas DNA fragments obtained from the polymerase chain reactions (PCR) were purified using the QIAquick PCR Purification Kit (Qiagen). Briefly, the DNA band excised from the gel was weighted and dissolved for 10 min at 50ºC in Buffer PIB (3 µl buffer per 1 mg of agarose gel), whereas DNA in solution was mixed with 5 volumes of Buffer PIB. The mixture was loaded into a QIAquick spin column and centrifuged at 16000 x g for 30 sec. The column was washed with 750 µl Buffer PE and centrifuged twice at 16000 x g for 1 min. DNA was eluted by adding 30 µl Buffer EB and centrifuged for 1 min.

DNA insert into the destination plasmid was performed through a DNA ligation reaction that was carried out in 10 µl final volume, containing 1x T4 DNA Ligase Buffer (Promega), ng of the insert, ng of plasmid (3:1 ratio), 1U T4 DNA Ligase (Promega). Samples were incubated for 3 hrs at 22ºC or overnight at 16ºC.
The amounts of plasmid and insert were calculated according to the formula:

$$\frac{\text{ng plasmid} \times \text{Kb insert}}{\text{Kb plasmid}} \times \text{molar ratio}\ \frac{(\text{insert})}{(\text{plasmid})} = \text{ng insert}$$

4.1.4 Generation of plasmids

To generate the CS3BE-E52V-CSA$^{Flag\text{-}HA}$, CS3BE-Q106P-CSA$^{Flag\text{-}HA}$ and CS3BE-K174A-CSA$^{Flag\text{-}HA}$ cell lines, the construction of *pRMCE-OriLB2-ECT-E52V-CSA$^{Flag\text{-}HA}$*, *pRMCE-OriLB2-ECT-Q106P-CSA$^{Flag\text{-}HA}$* and *pRMCE-OriLB2-ECT-K174A-CSA$^{Flag\text{-}HA}$* plasmids was required.
This is a multistep process that required first the cloning of intermediate entry plasmids (*pENTR11-E52V-CSA$^{Flag\text{-}HA}$*, *pENTR11-Q106P-CSA$^{Flag\text{-}HA}$* and *pENTR11-K174A-CSA$^{Flag\text{-}HA}$*, respectively).

4.1.4.1 Entry plasmids (*pENTR11-E52V-CSA$^{Flag\text{-}HA}$*, *pENTR11-Q106P-CSA$^{Flag\text{-}HA}$* and *pENTR11-K174A-CSA$^{Flag\text{-}HA}$*)

The DNA fragments containing the mutated sequence of *CSA* cDNA were obtained by PCR amplifications using as DNA template 5 ng of the *pENTR-CSA-K174A* plasmid (kindly given by J.C. Walte, Harvard Medical School, Boston, USA) or 50 ng of the cDNA that were reverse transcribed from the total RNA of CS3BE-CSA-E52V and CS3BE-CSA-Q106P cells (previously generated in our laboratory, unpublished observations) The primers used for the PCR reactions contained either the XhoI (forward) or the NotI (reverse) restriction enzyme sites to allow the generation of amplicons flanked by XhoI and NotI at the 5' and 3', respectively. The PCR reaction was performed in 50 µl containing 1X AccuPrime™ *Pfx* Reaction Mix (Life Technologies), 0.3 µM of the CSA primers (XhoI-CSA-Fw 5'-CATTCA**CTCGAG**CACCTATGCTGGGGTTTTTGTCCG-3' and NotI-CSA-Rev 5'-TTTCTA**GCGGCCGC**TCTAGATCCTTCTTCATCACTGCTGCT-3', where XhoI and NotI restriction sites for cloning *in frame* are in bold and the *CSA* sequence is underlined), and 1 U AccuPrime™ *Pfx* DNA polymerase (Life Technologies). Amplification was performed with one cycle of initial denaturation at 95°C for 3 min, four cycles at 95°C for 30 sec, 40°C for 1 minute and 68°C for 2 min, thirty cycles at 95°C for 30 sec, 55°C for 30 sec and 68°C for 2 min, and a final extension step at 68°C for 5 min.

PCR products were inserted into the destination plasmid *pENTR11$^{Flag\text{-}HA}$* (obtained from the *pENTR-wtCSA$^{Flag\text{-}HA}$*, previously generated in our laboratory and derived from the Gateway entry vector *pENTR11* (Life Technologies) by DNA ligation following restriction enzyme digestion. PCR products and destination plasmids were incubated at 37°C for 2 hrs with 1-2 U/µg of XhoI and NotI restriction enzymes (Promega) in the appropriate 1X Digestion Buffer (Promega). Next, the DNA fragments were separated by gel electrophoresis on a 1% Tris-Borate-EDTA (TBE)-agarose gel and the fragments of the predicted length were purified. Ligation reactions were performed in a final volume of 10 µl containing 1 µl of T4

DNA Ligase Buffer 10X (Promega), 1U of T4 DNA Ligase enzyme (Promega), 150 ng of the PCR amplified DNA fragment and 100 ng of the destination plasmid after XhoI/NotI restriction enzyme digestion. The ligase reaction was incubated for 3 hrs at 22°C or overnight at 16°C.
The ligation reaction was used to transform *E. coli* cells, which were subsequently selected in Kanamycin (Sigma)-containing media. The *pENTR11-E52V-CSA*$^{Flag\text{-}HA}$, *pENTR11-Q106P-CSA*$^{Flag\text{-}HA}$ and the *pENTR11-K174A-CSA*$^{Flag\text{-}HA}$ plasmids were purified (as described in section 4.1.2) and the correct insertion of the DNA fragment in the destination plasmid was verified by XhoI/NotI restriction enzyme digestion and gel electrophoresis on a 0.8% TBE-agarose gel.

4.1.4.2 *pRMCE-OriLB2-ECT-E52V-CSA*$^{Flag\text{-}HA}$, *pRMCE-OriLB2-ECT-Q106P-CSA*$^{Flag\text{-}HA}$ and *pRMCE-OriLB2-ECT-K174A-CSA*$^{Flag\text{-}HA}$ plasmids

To obtain the *pRMCE-OriLB2-ECT-E52V-CSA*$^{Flag\text{-}HA}$, *pRMCE-OriLB2-ECT-Q106P-CSA*$^{Flag\text{-}HA}$ and the *pRMCE-OriLB2-ECT-K174A-CSA*$^{Flag\text{-}HA}$ plasmids (also defined *cassette2*, in general terms), either the *E52V-CSA*$^{Flag\text{-}HA}$, *Q106P-CSA*$^{Flag\text{-}HA}$ or the *K174A-CSA*$^{Flag\text{-}HA}$ sequences were transferred from the respective entry clones (*pENTR11-E52V-CSA*$^{Flag\text{-}HA}$, *pENTR11-Q106P-CSA*$^{Flag\text{-}HA}$ and *pENTR11-K174A-CSA*$^{Flag\text{-}HA}$) to the destination vector *pRMCE-OriLB2-ECT-RfA* (kindly provided by Dr. FA Peverali, IGM-CNR, Pavia), taking advantage of the LR recombination reaction (Gateway® Technology, Life Technologies).
The Gateway recombination reaction was set up with 80 ng of each entry plasmids (*pENTR11*), 140 ng of *pRMCE-OriLB2-ECT-RfA* plasmid, 2 µl of 5x LR Clonase II enzyme mix and TE buffer (10 mM Tris(hydroxymethyl)aminomethane, Tris-HCl pH 7.5; 1 mM EDTA) to a final volume of 12 µl. Following overnight incubation at 25°C, 1 µl of Proteinase K (2 µg/µl) was added and incubated 10 min at 37°C to stop the reaction. The Gateway reaction mix was used to transform *E. coli* cells and, after antibiotic selection with Ampicillin (Pharmacia), each plasmid carrying the desired *CSA* mutation was purified. The correct integration of the insert was verified by XhoI/NotI restriction enzyme digestion, followed by gel electrophoresis on a 1% TBE-agarose gel.
Finally, the presence of the mutations of interest in the *CSA* sequence of the plasmids was verified by sequencing 0.5 µg of plasmid in the presence of 0.5 µl of the U497 primer (5'-CATCATATGTCTCCAGTCTCCAC-3') specific for *CSA*. The sequence was performed by the BMR Genomics Sequencing Service (University of Padova) through the 3730XL DNA Analyzer (Applied Biosystems).

4.2 Human cells

4.2.1 Primary cell strains and stable cell lines

The study was performed on primary (Table 1) and SV40-transformed (Tables 2 and 3) cultures of fibroblasts:

i) primary cells were established from skin biopsies of normal and CS donors (Table 1);
ii) SV40-transformed fibroblasts derived from a normal donor (MRC5) and a CS-A patient (CS3BE, c.400_481del, c.37G>T) (Table 2);
iii) CS3BE-derivative cell lines (isogenic cell lines) containing a single copy of either *cassette1* (pLNeoTkL2) or *cassette2*, the last one encoding the wtCSA or one of the mutated forms of CSA protein (E52V, Q106P or K174A) tagged with Flag-HA (Table 3).

Phenotype	Cell code	Sex	Age (years)[a]	Mutated gene	Altered protein	Notes
Normal	C3PV	M	-	-	-	
CS	CS7PV	F	0.5	*CSA*	p.Ala240GlyfsX8/ p.Ala240	u.o.
CS	CS15PV	M	5	*CSA*	p.Glu13X	u.o.

Table 1. Primary cell lines. Abbreviations: CS, Cockayne syndrome; u.o, unpublished observations. [a] age at diagnosis.

Cell line	Mutated gene	Altered protein	Notes
MRC5	None (normal donor)		A gift by Dr. A.R. Lehman
CS3BE (CS-A)	*CSA*	p.Glu13X/p.T134LeufsX13	Coriell C.R.

Table 2. SV-40 transformed cell lines.

Isogenic cell lines	Mutated gene	Exogenous allele
CS3BE-pLNeoTK1	*CSA*	Containing *cassette1*
CS3BE-wtCSA$^{Flag-HA}$	*CSA*	Expressing wtCSA$^{Flag-HA}$
CS3BE-E52V-CSA$^{Flag-HA}$	*CSA*	Expressing E52V-CSA$^{Flag-HA}$
CS3BE-Q106P-CSA$^{Flag-HA}$	*CSA*	Expressing Q106P-CSA$^{Flag-HA}$
CS3BE-K174A-CSA$^{Flag-HA}$	*CSA*	Expressing K174A-CSA$^{Flag-HA}$

Table 3. CS3BE-isogenic cell lines.

4.2.2 Culture conditions

Cells were routinely cultured at 37°C in humidified atmosphere conditioned with 5% CO_2. Primary fibroblasts and SV40-transformed cell lines were grown in Dulbecco's Modified Eagle Medium (DMEM, EuroClone) supplemented with 10% fetal bovine serum (FBS, Gibco by Life Technologies), 2 mM L-glutamine (EuroClone), 0.1 mg/ml Streptomycin (EuroClone) and 100 U/ml Penicillin (EuroClone). For culturing CS3BE-cassette1 cell line the medium was supplemented with 250 µg/ml Geneticin (G418, Gibco), whereas for the CS3BE-cassette2 cell lines the medium was supplemented with 0.15 µg/ml Puromycin (Life Technologies). Cells were routinely tested for a mycoplasma-free environment. Sub-culturing was performed by trypsinization and dilution. For cell preservation, aliquots were trypsinized, centrifuged at 1800 x g for 8 min, resuspended in 1 ml culture medium containing 10% dimethylsulfoxide (DMSO, Sigma), maintained for 24 hrs at -80°C in suitable box containing isopropanol (Cryostep, Nalgene) and then stored in liquid nitrogen at -196°C.

4.2.3 Recombinase Mediated Cassette Exchange (RMCE)

To generate CS3BE-derivative cell lines expressing the E52V-, Q106P-, K174A-CSA$^{Flag-HA}$ proteins, $2x10^6$ CS3BE-cassette1 cells were seeded in a 100 mm dishes in DMEM without selective antibiotics. After 24 hrs, 90-95% confluent cells were transfected with either the *pRMCE-OriLB2-ECT-E52V-CSA$^{Flag-HA}$*, *pRMCE-OriLB2-ECT-Q106P-CSA$^{Flag-HA}$* or *pRMCE-OriLB2-ECT-K174A-CSA$^{Flag-HA}$* plasmids (*cassette2*), along with the plasmid encoding the Cre enzyme (*pCre*) by using the Lipofectamine® LTX and Plus™ reagent (Life Technologies) according to manufacturer instructions. Briefly, 15 µg of each plasmid were diluted in 5 ml of OptiMEM I medium (Gibco) without serum, mixed with 30 µl Plus™ reagent and

15 µg of *pCre* plasmid (kindly provided by Dr. FA Peverali, IGM-CNR, Pavia). The solution was incubated at RT for 5 min, mixed with 50 µl Lipofectamine LTX reagent and incubated at RT for 30 min to allow the formation of the DNA-Lipofectamine complexes. Cells were first incubated for 5 min in OptiMEM I medium and subsequently supplemented with the DNA-Lipofectamine solution, mixed by gentle rocking and incubated at 37°C for 24 hrs. Afterwards, cells were trypsinised, diluted 1:10 in DMEM and seeded in 100 mm culture dishes. The following day the medium was replaced with fresh medium containing 0.3 µg/ml Puromycin for one week, and then transferred in medium supplemented with 0.3 µg/ml Puromycin and 2 µg/ml Ganciclovir (GCV) to positively select cells containing *cassette2* (Table 4). Clones were isolated and grown in DMEM supplemented with 0.15 µg/ml Puromycin. In parallel, cell aliquots were cultured in DMEM supplemented with 250 µg/ml G418 to test the loss of *cassette1* that provides the G418 resistance. Clones resistant to Puromycin and GCV but sensitive to G418 were further screened by PCR analysis (see below).

Antibiotic	Reference	Concentration	Plasmid
Geneticin (G418)	Gibco (10131)	250 µg/ml	*pL1NeoTK2*
Puromycin	Life Technologies	0.15 µg/ml or 0.3 µg/ml	*pRMCE-OriC-ECT*
Ganciclovir	InvivoGen (sud-gcv)	2 µg/ml	*pL1NeoTK2*

Table 4. Antibiotics used for clone selection.

4.2.4 Cell treatments

Cells were exposed to UV light using a Philips TUV 15W lamp (predominantly 254 nm, i.e. UVC). The UV intensity was measured before cell exposure with a calibrated radiometer (WXL Radiometer, Vilber Lourmat).

The treatment with $KBrO_3$ 20 mM (Sigma-Aldrich) and menadione 100 µM (Sigma-Aldrich) was performed in DMEM culture medium without serum, for 1 hour at 37°C.

4.2.5 RNA interference

Silencing of *CCT3*, *CCT8*, *CS11/9_A* and *CS11/9_B* expression was achieved applying pools of four distinct siRNA (Table 5) on primary fibroblasts from the normal donor C3PV. Cells were grown to about 70% confluence in 60 mm plates

in DMEM supplemented either with 10% or 2% FBS. The siRNA pools were diluted in DMEM medium without serum, mixed with 20 µl of HiPerFect Reagent (Qiagen) to reach a final volume of 100 µl. In parallel, a control reaction by using the AllStar negative control siRNA was carried out. The mix was then drop-wise distributed onto cells by diluting the siRNA solution on the cell culture media to reach a final concentration of either 50 or 100 nM. Plates were gently swirled to ensure uniform distribution of the transfection complexes and incubated at 37°C with 5% CO_2. After 48 hrs, the medium was replaced and fresh siRNA solutions added. Gene silencing was monitored 24, 48 and 96 hrs after transfection. For each time point, whole cell extracts were obtained for protein analysis.

Target mRNA	siRNA Code (Qiagen)	Target sequence
CCT3	Hs_CCT3_5	CAGACTGACATTGAGATTACA
	Hs_CCT3_9	AGCGGCCAAGTCCATGATCGA
	Hs_CCT3_8	ATCCACGTATGCGGCGCTATA
	Hs_CCT3_7	CTTGCGTGGAGTCATGATTAA
CCT8	Hs_CCT8_8	TCGTACCTCCATAATGAGTAA
	Hs_CCT8_7	TAGAGTGGATCAGATCATCAT
	Hs_CCT8_6	AAGGTGATGTAACATCTGTCA
	Hs_CCT8_5	AAACGTTGGATTAGATATTGA
CS11/9_A	Hs_ CS11/9_A_5	Not detailed
	Hs_ CS11/9_A_4	
	Hs_ CS11/9_A_2	
	Hs_ CS11/9_A_1	
CS11/9_B	Hs_ CS11/9_B_5	Not detailed
	Hs_ CS11/9_B_4	
	Hs_ CS11/9_B_3	
	Hs_ CS11/9_B_1	
None	AllStars Negative Control siRNA	Not detailed

Table 5. siRNAs used for RNA interference experiments.

4.2.6 Colony-forming ability assay

Cell survival after UV or menadione exposure was determined by standard clonogenic assays. Briefly, the isogenic cell lines expressing either *cassette1*, the wtCSA$^{Flag\text{-}HA}$ protein or any of the mutated forms of CSA$^{Flag\text{-}HA}$ were incubated overnight in standard medium supplemented with 10% FBS. Dishes in duplicate

were then exposed to increasing energy levels of UV light (5, 10 and 15 J/m^2) or increasing menadione concentrations (25, 50, 100 and 200 µM), which was maintained for 1 hour and then replaced with fresh standard medium supplemented with 10% FBS. Cells were cultured under standard conditions for 10-15 days and subsequently fixed. The number of clones was counted and compared with that of the normal cell line MRC5 processed in parallel. The number of colonies in treated cultures was expressed as a percentage of that in untreated cultures.

4.3 DNA and RNA analysis

4.3.1 Polymerase chain reaction

To identify clones that stably integrated a single-copy of *cassette1* or that successfully recombined *cassette1* with *cassette2* through the Cre-mediated RMCE methodology, were investigated by PCR reaction. Genomic DNA was obtained from single colonies growing in 12-well tissue culture plates. Briefly, cells were washed in phosphate buffered saline (PBS, Oxoid), trypsinised and centrifuged at 1800 x g for 8 min at RT. Cell pellet was resuspended in 1 ml PBS and fragmented by chilling for 5 min on dry ice and heating for 10 min at 94°C. 2 µl Proteinase K (10 mg/ml) were added to the samples and incubated at 50°C for 90 min. Following Proteinase K inactivation by heat shock for 8 min at 94°C, PCR reactions were carried out or samples were stored at -20°C.

Three different PCR assays were performed in a final volume of 20 µl. Details on primers and reactions are listed in Table 6 and 7.

Target sequence	Code	Primer Sequence (5' – 3')	Amplicon size (bp)
Recombined *loxP*	LoxP-Fw FPuro3-Fw	GCTGTACAAGAAGCTTATAACTTCG AGGCCCACCGACTCTAGAGG	350
Recombined *lox2272*	Lox2-Rev mCSA-Fw	CCATGGTGGCCTCGAGATAAC AATCGAATGAGGCTCTGGAA	957
ECT sequence	B48II_dx B48_sx	GACTGGAAACTTTTTTGTAC TAGCTACACTAGCCAGTGACCTTTTTCC	170/135

Table 6. Primers used for the PCR screening and corresponding product. Abbreviations: *ECT*, Ectopic DNA sequence; *LoxP*, *LoxP* site; *Lox2272*, *Lox2272* site.

Recombined *LoxP*					
Reaction mix			***Cycling protocol***		
Reagent	**Final conc.**	**Volume (µl)**	**°C**	**Time**	**Cycles**
H_2O	add to 20 µl	12.4	95	3’	1
Buffer 5X (Promega)	1X	4	95	20’’	40
dNTPs (10 mM)	200 µM	0.4	54	20’’	
LoxP-Fw (100 µM)	0.05 µM	0.2	72	20’’	
FPuro3-Fw (100 µM)	0.05 µM	0.2	72	7’	1
Template DNA		2			
DMSO 100%	3%	0.6			
GoTaq (5U/ul) (Promega)	0.02 U/µl	0.2			
Recombined *Lox2272*					
Reaction mix			***Cycling protocol***		
Reagent	**Final conc.**	**Volume (µl)**	**°C**	**Time**	**Cycles**
H_2O	add to 20 µl	12.4	95	3’	1
Buffer 5X (Promega)	1X	4	95	20’’	40
dNTPs (10 mM)	200 µM	0.4	54	20’’	
mCSA_Fw (100 µM)	0.05 µM	0.2	72	20’’	
Lox2_Rev (100 µM)	0.05 µM	0.2	72	7’	1
Template DNA		2			
DMSO 100%	3%	0.6			
GoTaq (5U/ul) (Promega)	0.02 U/µl	0.2			
***ECT* sequence**					
Reaction mix			***Cycling protocol***		
Reagent	**Final conc.**	**Volume (µl)**	**°C**	**Time**	**Cycles**
H_2O	add to 20 µl	13.8	95	3’	1
Buffer 5X (Promega)	1X	2	95	30’’	40
$MgCl_2$ 25 mM (Promega)	1 mM	0.8	56	10	
dNTPs (10 mM)	200 µM	0.4	72	20’’	
B48II_dx (100 µM)	0.1 µM	0.4	72	2’’	
B48_sx (100 µM)	0.1 µM	0.4			
Template DNA		2			
GoTaq (5U/ul) (Promega)	0.02 U/µl	0.2			

Table 7. PCR reaction protocols adopted for clone screening.

PCR products were resolved by gel electrophoresis on a 1.5% TBE-agarose (SeaKem Le Agarose, Lonza) gels and stained with ethidium bromide.

4.3.2 Analysis of transcript levels

Total RNA was isolated using the RNeasy Mini Kit (Qiagen) according to manufacturer instructions. Briefly, $3x10^5$ cells cultured at confluence in 6 cm dishes were collected, rinsed with PBS and centrifuged at 2000 x g for 8 min. Pellet was resuspended in 300 µl RLT Buffer supplemented with 3 µl β-mercaptoethanol. The lysate was homogenized by passing at least 5 times through a blunt 20-gauge needle (0.9 mm diameter), mixed with 300 µl 70% ethanol, transferred into a RNeasy spin column and centrifuged at 10000 x g for 15 sec. The spin column was then washed with 700 µl RW1 Buffer and with 500 µl RPE Buffer. RNA concentration was determined by using the NanoPhotometer™ P330 (Implen). RNA was reverse-transcribed into first-strand cDNA using the iScript cDNA synthesis kit (BioRad) according to manufacture instructions. Briefly, 1 µg of total RNA was incubated with 4 µl 5X iScript reaction mix and 1 µl iScript reverse transcriptase at 25°C for 5 min. Reverse transcription reactions were carried out at 42°C for 30 min. Samples were then maintained at 48°C for 15 min and at 85°C for 5 min for the enzyme inactivation.
Quantitative real time RT-PCR (qRT-PCR) was performed using the LightCycler 480 Real-Time PCR system (Roche Diagnostics) in 96 well plates. Detection of PCR products was achieved through SYBR Green I fluorescent dye (Biorad). Each reaction was performed in 20 µl final volume containing 10 µl 2x PCR buffer iQ SYBR Green Supermix (Biorad), 5 µM forward and reverse primers (Table 8) and 2 µl template DNA.

Gene	Primer code[a]	sequence (5'-3')	Product[b]	Amplicon size (bp)
CSA	F-CSA R-HA	TGGGTTCCATCCTTATATGA GTAGTCGGGCACGTCGTAGG	*Recombinant CSA*	192
CSA	CSA-F1 CSA-R1	GACTATATCTTGGCAACAG GTGACTTTTTCCCATTATGT	*Total CSA*	109
RPL13A	RPL-F1 RPL-R1	CTCAAGGTCGTGCGTCTGAA TGGCTGTCACTGCCTGGTACT	*RPL*	94

Table 8. Primers pairs used for qRT-PCR reactions. [a]F, forward primer; R, reverse primer. [b]*Recombinant CSA* primers map in the 3' portion of *CSA* exon 11 and in the HA coding sequence, respectively; *Total CSA* primers map in exons 7 and 8 of *CSA*, respectively, and amplify both the endogenous and the ectopic *CSA* mRNA.

The reaction was initiated by activation of Taq Polymerase at 95°C for 5 min, followed by 40 three-step amplification cycles consisting of denaturation at 95°C for 25 sec, annealing at 60°C for 25 sec and extension at 72°C for 25 sec. A final

dissociation stage was run to generate a melting curve that revealed the amplification product specificity. qRT-PCR was monitored and analysed by the LightCycler 480 Software (Roche Diagnostics). Quantification was achieved using the crossing point (C_P) measured with the second derivative maximum method. Standard curves were obtained for each primer set with serial dilutions of cDNA. Amplification of the housekeeping gene *RLP13A* was used as reference gene to normalize the cDNA amounts.

4.4 Protein analysis

4.4.1 Whole cell extracts

10^6 cells were washed with ice-cold PBS and scraped off in 50 µl 3X Laemmli buffer solution (254 mM Tris-HCl pH 6.8, 8% SDS, 0.02% bromophenol blue, 40% glycerol, 3% β-mercaptoethanol). Afterwards, cell suspension was exposed to 3 cycles of sonication by using the Branson Sonifier 250 instrument (power setting 1). Each cycle consisted of 10 sec pulse and 10 sec rest on ice. Following sonication, samples were stored at -80°C or -20°C for long- or short-time storage, respectively.
For studies of protein-protein interactions by Tandem Affinity Purification (TAP), cells were lysed and processed according to the Nuclear Complex Co-IP kit (Active Motif). Briefly, cells cultured in 100 mm Petri dish were washed with ice-cold PBS and gently scraped off in 1 ml PBS supplemented with Phosphatase Inhibitors. Cell suspension was centrifuged at 4°C for 5 min at 2000 x g. The supernatant was discarded while the pellet was resuspended in 350 µl 1X Hypotonic buffer, followed by incubation on ice for 15 min. Then, 20 µl Detergent were added and the suspension centrifuged at 14000 x g for 30 sec at 4°C. The supernatant fraction was collected.
For co-immunoprecipitation (co-IP) analysis, cells cultured in 100 mm Petri dish were washed with ice-cold PBS and gently scraped off in 1 ml PBS supplemented with Phosphatase Inhibitors. Cell suspension was centrifuged at 4°C for 5 min at 2000 x g, the supernatant was discarded and the pellet resuspended in 350 µl Cell Lytic M buffer (Sigma-Aldrich), incubated 15 min on ice, centrifuged at 16000 x g and the supernatant fraction was collected.

4.4.2 Immunoblotting

Proteins were separated on Mini-PROTEAN® TGX™ Precast 4-20% gradient gels (Biorad) assembled in the Mini PROTEAN® III Cell system (Biorad). The chambers were filled with 1X Protein Running buffer prepared from a 10X stock

solution (3% Tris pH 7.5, 1% SDS, 14.4% glycine). Precision Plus Protein™ All Blue (Biorad) was used as a molecular weight marker. The electrophoresis was performed at a constant voltage of 200 V for about 40 min. Alternatively, proteins were loaded on SDS-polyacrilamide gels composed of a 5% stacking gel and a 12% running gel, and separated for 1 hour at 100 V. Protein transfer was achieved through the Trans-Blot® Turbo® Transfer System Midi Transfer Pack (Biorad), applying the Biorad pre-programmed protocols for mixed molecular weights (7 min at 2.5 A constant, up to 25 V). Alternatively, proteins were transferred onto a 0.2 μm nitrocellulose membrane (Whitman) in phosphate transfer buffer (12.2 mM $Na_2HPO_4.2H_2O$, 7.8 mM $NaH_2PO_4.H_2O$) by applying an electrical current of 1.16 A at 4°C for 1 hour. Following the transfer, the nitrocellulose membrane was incubated at RT for 1 hour in blocking solution made of 1X Magic buffer (MB; 500 mM Tris-HCl pH 7.5, 500 mM NaCl, 1.5% Tween 20) supplemented with 5% skim milk (Difco). Then, the membrane was incubated overnight at 4°C in blocking solution containing the primary antibody. The dilution of each antibody is indicated in Table 9.

Antibody	Dilution	Origin	Reference
Anti-CCT3	1:1000	Rabbit	Bethyl, A303-458A
Anti-CCT8	1:1000	Rabbit	Bethyl, A303-446A
Anti-CS11/9_A	1:1000	Rabbit	Not detailed
Anti-CS11/9_B	1:2000	Rabbit	Not detailed
Anti-CS11/9_C	1:1000	Rabbit	Not detailed
Anti-HA	1:1000	Rat	Roche, 11 867 423 001
Anti-DDB1	1:1000	Rabbit	A gift from Dr. R. Groissman
Anti-GAPDH	1:1000	Mouse	Santa Cruz, sc-32233
Anti-Mouse-HRP (H+L)	1:10000	Donkey monoclonal	Jackson Immunoresearch, 715-005-150
Anti-Mouse-HRP (L)	1:10000	Goat monoclonal	Jackson Immunoresearch, 115-055-174
Anti-Rabbit-HRP (H+L)	1:10000	Donkey monoclonal	Jackson Immunoresearch, 711-055-152
Anti-Rabbit-HRP (L)	1:10000	Goat	Jackson Immunoresearch, 211-032-171
Anti-Rat-HRP (L)	1:10000	Goat	Jackson Immunoresearch, 112-035-175

Table 9. Antibodies used for immunoblot analysis.

At the end of the incubation, the membrane was washed three times for 7 min each in 1X MB and incubated at RT for 1 hour with horseradish-peroxidase-(HRP)-conjugated secondary antibodies (see Table 9) diluted in blocking solution.
Following this second hybridization, the membrane was washed three times for 7 min each in 1X MB and developed using the LiteAblot® EXTEND Long Lasting Chemiluminescent Substrate (EuroClone) or the Western Lightning® Ultra Extreme Sensitive Chemiluminescent Substrate (PerkinElmer), according to the manufacturer instructions. The chemiluminescent signals were then detected using the ChemiDoc XRS system (BioRad) and quantified using the software ImageJ (Abramoff et al., 2004).

4.4.3 Immunofluorescence

Cells grown on glass coverslips were washed in PBS, fixed in 3.7% paraformaldehyde for 12 min at RT and washed three times in PBS. Permeabilization occurred in PBS containing 0.1% Triton X-100 for 5 min at RT for primary fibroblasts, whereas in PBS containing 0.1% Triton X-100 for 2 min at RT in case of transformed cells. Samples were then washed twice in PBS for 5 min, and once in PBS containing 0.05% Tween 20 (PBS-T) for 5 min. Samples were blocked with blocking solution (PBS-T containing 5% BSA) at RT for 1 hour, followed by 1 hour incubation at RT in blocking solution containing the primary antibody at the dilution detailed in Table 10. Cells were washed three times in PBS for 5 min each, incubated for 1 hour at RT in PBS-T containing the secondary antibody conjugated with a fluorophore (see Table 10) and washed three times with PBS-T for 5 min. For double labelling, the two-antibody staining was performed sequentially. DNA staining was carried out by incubating the coverslips in a DAPI solution (1:1000 in PBS) for 10 min at RT, followed by three washing steps in PBS. Slides were mounted in Mowiol® 4-88 mounting medium (Sigma-Aldrich).

Antibody	Dilution	Origin	Reference
Anti-CCT3	1:200	Rabbit	Bethyl, A303-458A
Anti-CCT8	1:200	Rabbit	Bethyl, A303-446A
Anti-HA	1:300	Rat	Roche, 11 867 431 001
AlexFluor 488-conjugated anti-rabbit IgG	1:400	Goat	Jackson Immunoresearch, 111-545-045
Cy3-conjugated anti-rabbit IgG	1:400	Goat	Jackson Immunoresearch, 111-165-045

Table 10. Antibodies used for indirect immunofluorescence analysis.

Fluorescent images were obtained using an Olympus IX71 inverted microscope equipped with a CCD camera (Robert Scientific Phomometric) and analysed using the ImageJ software.

4.4.4 Co-immunoprecipitation

All the procedures described in this section were carried out at 4°C and all the buffers were supplemented with Protease Inhibitor Cocktail (Active Motif). For each immunoprecipitation and pre-clearing step, 30 µl of 50% slurry containing Dynabeads® Protein G (Novex by Life Technologies) were used. Beads were washed once in PBS containing 0.02% Tween 20, twice in washing buffer (WB, IP low buffer 1X supplemented with PIC, Active Motif) and then saturated in WB containing 0.1 mg/ml BSA overnight in constant rotation. Whole cell extracts were pre-cleared by incubation with saturated beads for 1 hour in constant rotation. The suspension was then placed in a magnetic rack, the beads were pulled apart and the supernatant was separated, mixed with the primary antibodies and incubated overnight in constant rotation. The following day, saturated beads were added to the sample containing the antibody and incubated 1 hour and 30 min in constant rotation. At the end of the incubation step, the beads were pulled apart and the supernatant stored as flow-through. The recovered beads were washed three times for 5 min in WB containing 1 mg/ml BSA and three times in WB alone in constant rotation. The elution step was performed in 40 µl 2X NuPage®-LDS Sample buffer (Life Technologies) supplemented with 50 mM DTT and stored at -80°C or analysed by immunoblotting.

4.4.5 Tandem Affinity Purification

Whole cell extracts from $5x10^7$ cells were incubated overnight at 4°C on a rotating wheel with 120 µl of beads conjugated with anti-Flag antibodies (Anti-Flag® M2 Affinity Gel, Sigma) previously washed in WB. Samples were centrifuged at 3000 x g for 2 min and the beads transferred into a SigmaPrep Spin column (Sigma) where they were washed 5 times in WB. Complexes were eluted with two subsequent incubations for 1 hour at 4 °C with 500 µl of Flag peptide (Sigma, 0.2 µg/ml) in TBS buffer (10 mM Tris pH 7.4, 150 mM NaCl). Eluates were further purified by immunoprecipitation with 100 µl of anti-HA agarose affinity resin (Sigma) previously washed in WB buffer. Samples were incubated overnight at 4°C on a rotating wheel and subsequently centrifuged at 3000 x g for 2 min. Beads were transferred into a SigmaPrep Spin column (Sigma) and washed 5 times in WB. Finally, complexes were eluted by 10 min incubation at RT with 60 µl of 2X

NuPAGE® LDS Sample Buffer (Life Technologies) and centrifugation at 3000 x g for 1 min. Samples were supplemented with 50 mM dithiothreitol (DTT), incubated at 70°C for 10 min and stored at -80°C.

4.5 Recovery of RNA Synthesis assay

UV-induced DNA repair synthesis in siRNA-treated cells was analysed by autoradiography as described in Stefanini et al. 1986 and 1996. Briefly, cultures were prepared by seeding fibroblasts in 3 cm dishes (10^5 cells/dish), each containing a round glass coverslip, in DMEM medium supplemented with 10% FBS and cultured under standard conditions. Cells were then exposed to a UV dose of 20 J/m^2 and incubated again with DMEM containing siRNA solutions. After 96 and 120 hrs, cells were incubated in medium containing 10 μCi/ml ^{3}H-uridine (NER Radiochemicals, specific activity 26.4 Ci/mmol) for 1 hour, washed in PBS and fixed in Bouin's solution. Autoradiographic preparations were performed using a photographic emulsion (Ilford K2). After 3 days at 4°C, the slides were developed and stained with May-Grunwald (BDH Prolabo) and Giemsa (BDH Prolabo) solutions. RRS was evaluated by counting the number of autoradiographic grains on at least 50 nuclei of G1/G2 phase cells.

4.6 Whole Exome Sequencing

Whole exome sequencing analysis was performed by Prof. Tomoo Ogi (Research Institute of Environmental Medicine, Nagoya University, Japan). The analysis was carried out in primary dermal fibroblasts and/or lymphoblastoid cells from all the CS11/9_PV family members. Briefly, whole exome sequencing was made by using the SureSelect human whole exome target enrichment system v5 (Agilent), followed by paired-end sequencing on the Illumina Hiseq2500 sequencer (Nakazawa et al., 2012). 10 Gbps reads per sample were obtained. Bioinformatic analyses for the exome data were also carried out by Prof. Tomoo Ogi taking advantage of a standard exome analysis pipeline. Quality filtered sequence reads were aligned to the human reference genome (hg19) with the Burrows-Wheeler Aligner software. GATK haplotype caller was used to determine genetic variants. All variants were annotated with ANNOVAR. To identify potentially pathogenic mutations, Prof. Tomoo Ogi focused the analysis on rare functionally significant variants. Using a recessive model of inheritance, potentially pathogenic mutations were identified in three genes for the CS phenotype in the CS11/9_PV family, to which we refer at as *CS11/9_A*, *CS11/9_B* and *CS11/9_C*.

4.7 Statistical analysis

All the experiments were repeated at least two-three times. P-values were obtained by the unpaired two-tailed student t-test. Fisher F-ratio at a probability level (p-value) of 0.05 was used to compare variances among the analysed groups. Data are reported as mean ± standard error (SE). P-values <0.05 were considered significantly different.

5. Results

The following research study has been focused on these specific objectives: *i)* generation and characterization of a cell system aimed to investigate the consequences of CSA mutations on the cellular response to different stressing agents *(section 5.1), ii)* characterization of CSA interaction with the TRiC/CCT chaperonin complex *(section 5.2), iii)* identification of novel disease genes for an unassigned CS case *(section 5.3).*

5.1 Generation and characterization of a panel of isogenic cell lines expressing distinct mutated forms of CSA$^{Flag\text{-}HA}$

In a previous study performed in our laboratory, we generated a cell line expressing at physiological levels the wild type CSA protein (wtCSA) fused *in frame* at its C-terminus with the Flag and HA epitope tags (CSA$^{Flag\text{-}HA}$) with the purpose to purify CSA, its interacting proteins and concomitantly overcome the absence of commercially available antibodies specifically directed against CSA. To generate a panel of cell lines expressing different versions of the CSA protein within the same cellular background (isogenic cell lines), we took advantage of the Recombinase Mediated Cassette Exchange (RMCE) approach to insert, within the same genomic *locus*, a single copy of the cDNA encoding distinct mutated forms of CSA$^{Flag\text{-}HA}$. The selected mutations affect different WD domains: the E52V amino acidic change resides in the first WD repeat (WD1), the Q106P substitution modifies WD2, whereas the K174A change affects WD3 (Figure 14). We analyzed the consequences of such mutations on the stability of *CSA* transcript, of CSA protein and its subcellular localization. Moreover, we determined whether/how the selected CSA mutations impact on the survival of the isogenic cell lines to different stressing agents.

5.1.2 Generation of isogenic cell lines expressing mutated forms of the CSA protein

Three vectors expressing the *CSA* cDNA containing mutations either found in CS patients (Q106P) or conceived in the laboratory (E52V and K174A) were generated and used to produce derivatives of the CS3BE cell line expressing different versions of the CSA protein (Figure 14). The amplified cDNA fragments were first cloned into the *pENTR11*$^{Flag\text{-}HA}$ expression vector and subsequently the

entry plasmids were used to generate by Gateway cloning (Life Technologies) the destination plasmids pRMCE-CSA$^{Flag\text{-}HA}$ needed for the Recombinase Mediated Cassette Exchange (RMCE).

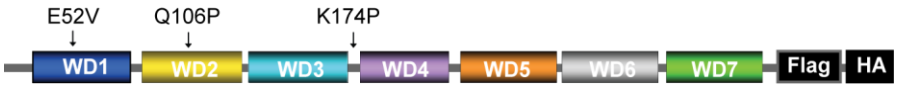

Figure 14. Schematic representation of the CSA$^{Flag\text{-}HA}$ protein and position of the amino acid changes investigated in this study. WD repeat domains are indicated by alternating colors. W, tryptophan; D, aspartic acid. The CSA protein is tagged at its C-terminal with Flag-HA.

5.1.2.1 Recombinase Mediated Cassette Exchange (RMCE)

The RMCE is a powerful molecular genetic tool based on the Cre-mediated site-specific recombination that allows the swapping of a DNA fragment integrated into a pre-determined genomic locus with a second DNA fragment. Both fragments are flanked by heterotypic *LoxP* sites (García-Otín and Guillou, 2006).
In the strategy that we have applied, a recipient DNA cassette (*cassette1*) was previously integrated in single copy in the genome of the CSA-defective (CS-A) cell line CS3BE (CS3BE-cassette1). *Cassette1* carries the neomycin and Herpes Simplex Virus 1 thimidine kinase (HSV-TK) transcription units flanked by the heterotypic *LoxP* and *Lox2272* sites. The *Lox2272* site is a mutated form of *LoxP* that impairs the Cre-mediated intra-molecular recombination events usually occurring between two identical *LoxP* sites, thus avoiding the excision of the integrated cassette.
CS3BE-cassette1 cells were subjected to the RMCE assay, which allowed the integration of *cassette2* DNA fragment (Figure 15).

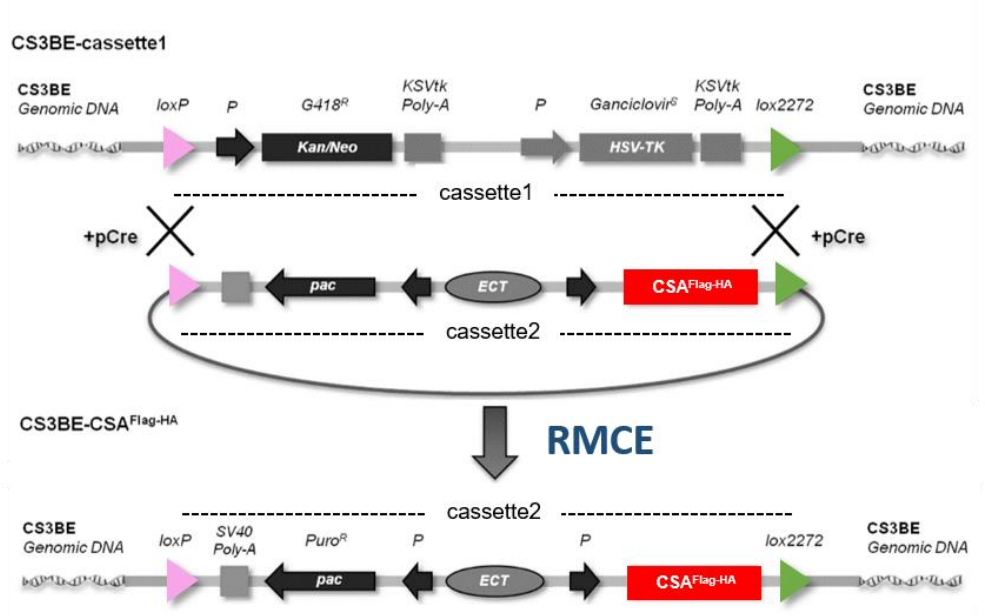

Figure 15. Cre-mediated Recombinase-Mediated Cassette Exchange (RMCE). RMCE allows the exchange of *cassette1* with *cassette2*. *ECT*, ectopic sequence; $G418^R$, geneticin resistance; *HSV-TK*, Herpes Simplex Virus 1 thymidine kinase; Kan, kanamycin; Neo, neomycin; *P*, promoter; pCRE, plasmid containing CRE recombinase; Poly-A, polyadenylation; $Puro^R$, puromycin resistance.

Cassette2 is also flanked by *LoxP* and *Lox2272* sites and, besides the *pac* gene that confers resistance to puromycin, it contains the cDNA encoding one of the mutated forms of $CSA^{Flag\text{-}HA}$ (E52V-$CSA^{Flag\text{-}HA}$, Q106P-$CSA^{Flag\text{-}HA}$ or K174A-$CSA^{Flag\text{-}HA}$). The CS3BE-cassette1 cells were co-transfected with the plasmid containing *cassette2* and the Cre-expression vector. The expression of Cre recombinase allowed the exchange of the integrated *cassette1* with *cassette2* by specifically recombining the identical *Lox* sites provided in *trans* (site-specific recombination). Positive clones were selected in medium containing puromycin. Gancyclovir (GCV) was also used to counterselect the *TK* gene present in *cassette1*. Clones sensitive to G418 ($G418^S$) and resistant to GCV (GCV^R) were investigated for the recombination process using specific set of primers (Figure 16). In each PCR reaction, one primer maps within the *cassette2* sequence, whereas the second one is specific for the still inserted sequence of *cassette1*, located either upstream of the *LoxP* site or downstream of *Lox2272*. Using these primer pairs, amplification can only occur in the clones that successfully recombined. To identify single integration events of *cassette2*, the ectopic DNA region (*ECT*) that corresponds to

a deleted form of an endogenous DNA sequence (*enECT*) was also analyzed by PCR.

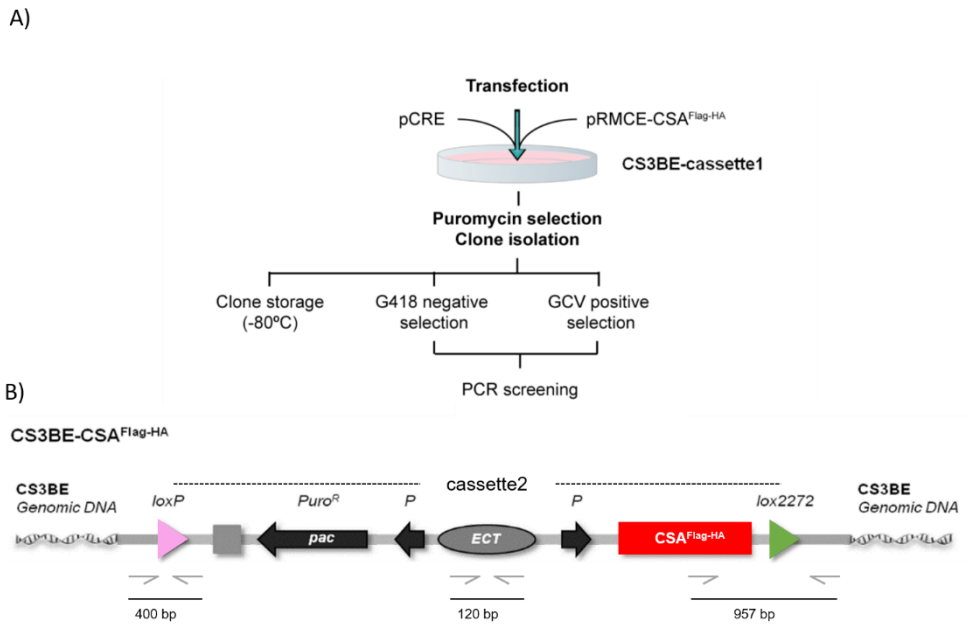

Figure 16. Selection of RMCE positive clones. (A) Following transfection and selection in puromycin, RMCE clones were negatively selected in geneticin (G418) and positively selected in ganciclovir (GCV). Clones were further analyzed by PCR. **(B)** Schematic representation of a successfully integrated *cassette2* into the genome of CS3BE cells. The DNA sequences left behind from *cassette1* are located either upstream of *LoxP* or downstream of *Lox2272*. The position of the primers used for amplification and the size of the corresponding products are indicated. *ECT*, ectopic sequence; Puro^{R}, puromycin resistance; *P*, promoter.

5.1.3 Impact of *CSA* mutations on the recombinant *CSA$^{Flag\text{-}HA}$* mRNAs

The expression levels of the recombinant *CSA$^{Flag\text{-}HA}$* mRNA was tested by quantitative real time RT-PCR (qRT-PCR) in all the isogenic cell lines, in the parental cell lines CS3BE and CS3BE-cassette1, as well as in the normal cell line MRC5. At first, we used primers pairs mapping in exon 7 and exon 8 of the *CSA* coding sequence. As a consequence, the PCR amplified both the endogenous and the recombinant *CSA* transcripts (Figure 17). The *CSA* expression level observed in the CS3BE-wtCSA$^{Flag\text{-}HA}$ is about 2-folds the level obtained in the normal MRC5 cells, in CS3BE and CS3BE-cassette1 cells that do not express the recombinant

CSA transcript. These findings indicate that the transcription of *wtCSA*$^{Flag\text{-}HA}$ driven by the SV40 promoter results in mRNA levels that are similar to the mRNA levels from the endogenous CSA promoter and, therefore, may exclude excessive over-expression of the recombinant gene. The observation that CS3BE and CS3BE-cassette1 cells present equal amount of *CSA* transcript indicates that the integration of *cassette1* in the genome of CS3BE cells did not influence the expression of the endogenous CSA gene. In addition, all the isogenic cell lines expressed higher amounts of total *CSA* transcripts (Figure 17), with the CS3BE-Q106P-CSA$^{Flag\text{-}HA}$ cell line showing the highest *CSA* expression levels.

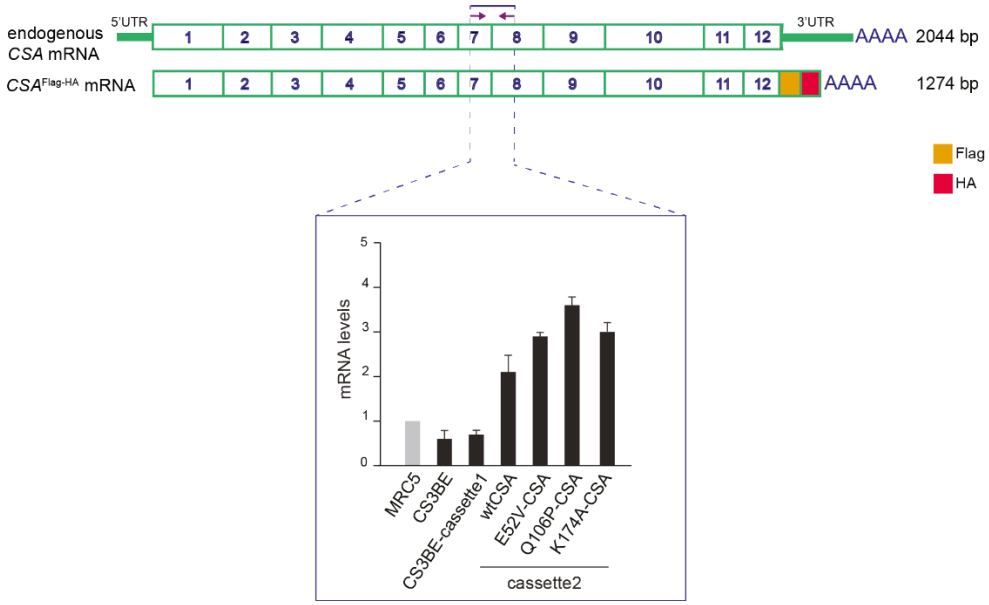

Figure 17. Total (endogenous and recombinant) *CSA* expression levels in CS3BE and CS3BE-derivative cell lines. The *CSA* expression level was normalized to the expression level of the *GAPDH* housekeeping gene and then to the expression level in control MRC5 cells. Reported values represent the mean of three independent experiments. The cartoon represents the *CSA* mRNAs and the position of the PCR primers (arrows). Empty boxes indicate the coding sequences. Numbers indicate exons. Bars indicate SE.

Next, we used primers mapping in the 3' portion of CSA exon 11 and in the HA coding sequence, respectively, thus generating a PCR amplification product specific for the *cassette2*-containing cells (Figure 18). Among the isogenic cell lines, those expressing the recombinant Q106P-CSA$^{Flag\text{-}HA}$ protein revealed the highest transcript levels, almost equivalent to 2.5-folds the *wtCSA*$^{Flag\text{-}HA}$ mRNAs.

Similarly, K174A-CSA$^{Flag-HA}$ expressing cells transcribed higher amounts of recombinant *CSA* than CS3BE-wtCSA$^{Flag-HA}$ cells, whereas a normal expression level was observed in E52V-CSA$^{Flag-HA}$ expressing cells.
Overall, these findings indicate that the E52V, Q106P and K174A mutations do not impair the stability of *CSA* mRNA.

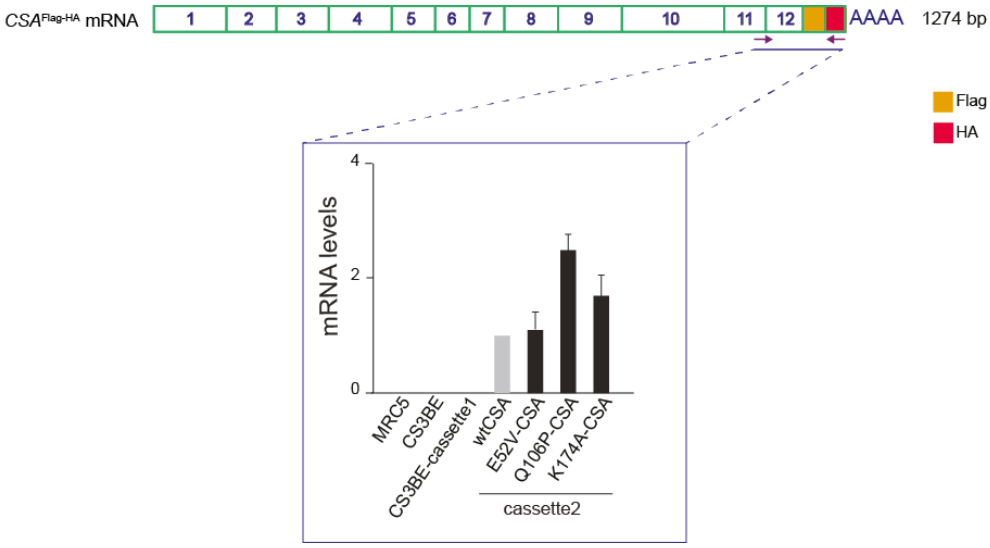

Figure 18. Recombinant *CSA*$^{Flag-HA}$ expression levels in CS3BE and CS3BE-derivative cell lines. *CSA*$^{Flag-HA}$ expression level was normalized to the expression level of the housekeeping gene *RPL13A* and then to the expression level in CS3BE-wtCSA$^{Flag-HA}$ cells. Reported values represent the mean of three independent experiments. The cartoon represents the *CSA* mRNAs and the position of the PCR primers (arrows). Empty boxes indicate the coding sequences. Numbers indicate exons. Bars indicate SE.

5.1.4 Impact of *CSA* mutations on the stability of the recombinant CSA$^{Flag-HA}$ proteins

Whole cell extracts from CS3BE-wtCSA$^{Flag-HA}$, CS3BE-E52V-CSA$^{Flag-HA}$, CS3BE-Q106P-CSA$^{Flag-HA}$, CS3BE-K174A-CSA$^{Flag-HA}$ and CS3BE-cassette1 cell lines were analysed by immunoblotting with antibodies directed against the HA epitope tag. As shown in Figure 19, the HA antibody recognized in all the isogenic cell lines expressing the recombinant CSA$^{Flag-HA}$ proteins a single band of approximately 48 kDa corresponding to the predicted molecular weight of the CSA$^{Flag-HA}$ protein. As expected, no protein band was observed in the parental cell

line CS3BE-cassette1. We found that the recombinant CSA protein was detected at very high levels in the CS3BE-wtCSA$^{Flag\text{-}HA}$ cells. Because of a lack of antibodies that specifically recognize CSA proteins and no other WD-repeat proteins with similar molecular weight, we cannot compare the intracellular amounts of wtCSA$^{Flag\text{-}HA}$ with that of the endogenous protein. In addition, despite a high transcription level of *Q106P-CSA*$^{Flag\text{-}HA}$ and *K174A-CSA*$^{Flag\text{-}HA}$, the amount of all mutated forms of CSA$^{Flag\text{-}HA}$ was markedly reduced.

These studies clearly revealed that the selected *CSA* missense mutations do not impair the stability of *CSA* transcripts but rather interfere with the stability of the corresponding proteins.

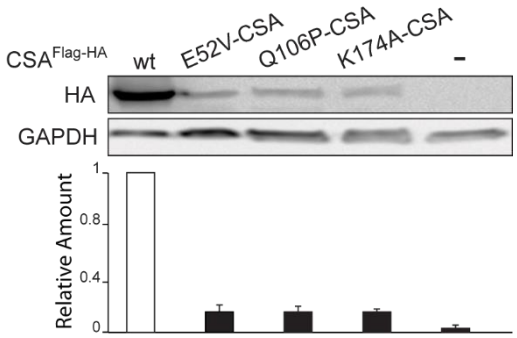

Figure 19. HA immunoblot analysis in total cell lysates from CS3BE-derivatives cell lines. The immunoblot signal of HA protein was normalized to the amount of GAPDH and the values reported in the diagram below. Bars indicate SE.

5.1.5 Subcellular localization of the recombinant CSA$^{Flag\text{-}HA}$ proteins

To investigate the subcellular localization of the isogenic cell lines expressing either the wt or any of the mutated forms (E52V, Q106P or K174A) of the CSA$^{Flag\text{-}HA}$ protein, we performed indirect immunofluorescence analysis in the isogenic cell lines with antibodies directed against the HA epitope tag. We observed that the wtCSA$^{Flag\text{-}HA}$ protein localized in the nucleus and was excluded from the nucleoli. This finding is in agreement with previous observations on the subcellular localization of the endogenous CSA protein (Bradsher et al., 2002), thus indicating that the recombinant protein is distributed in the same cellular compartment of the endogenous one.
In contrast, CSA$^{Flag\text{-}HA}$ proteins with the single amino acid changes E52V and Q106P resided mainly in the cytoplasmic and perinuclear region, whereas those

with the K174A substitution showed a signal distributed both in the cytoplasm and in the nuclear compartment (Figure 20). These results highlighted that single amino acid changes can interfere with the subcellular localization of the recombinant protein. The observation that the wtCSA$^{Flag\text{-}HA}$ protein localizes in the same subcellular region of the endogenous one prompted us to conclude that the altered distribution of the mutated forms of CSA$^{Flag\text{-}HA}$ is the direct consequence of CSA mutations.

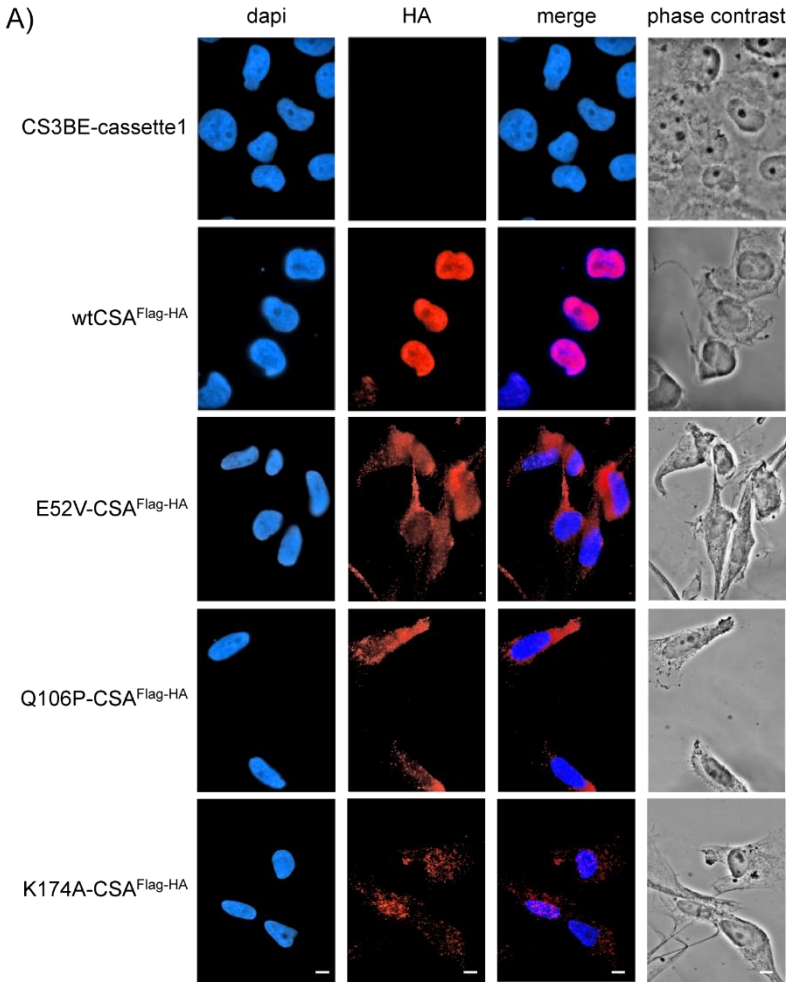

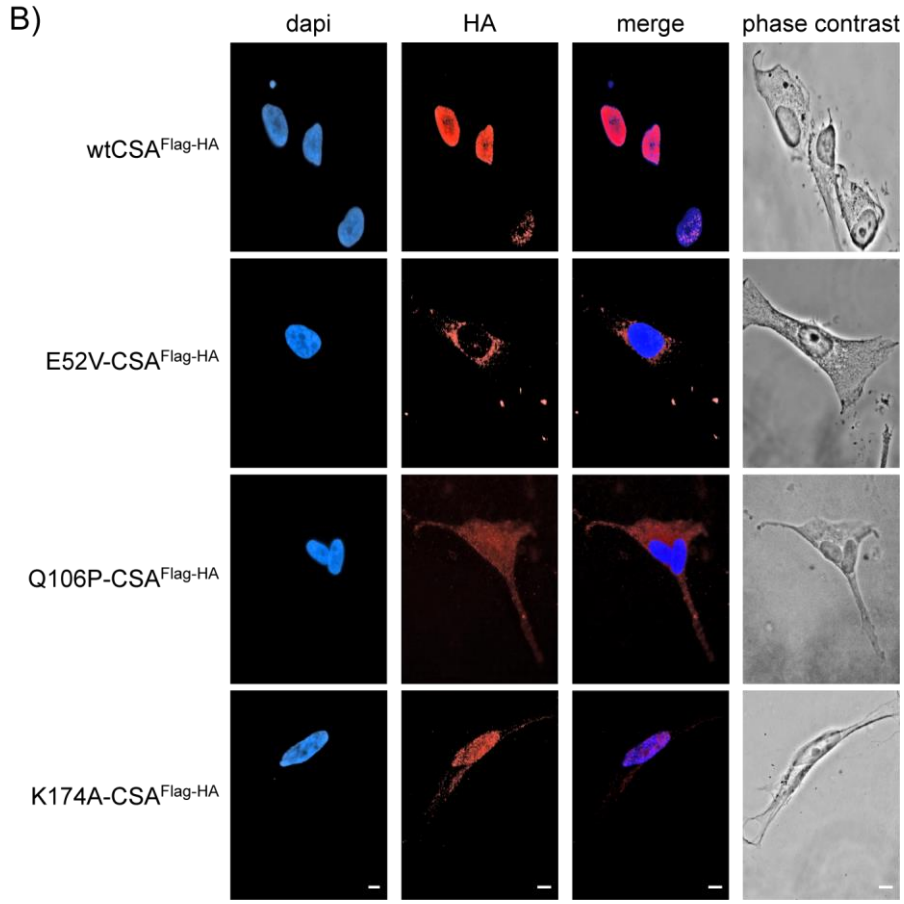

Figure 20. Subcellular localization of the recombinant CSA$^{Flag-HA}$ proteins in the isogenic cell lines. (A) Indirect fluorescence staining with antibodies directed against the HA epitope tag (*red*). Nuclei are visualized by DAPI staining (*blue*); **(B)** Higher magnification of cells treated as in (A). Bars, 2 μm.

5.1.6 Impact of CSA$^{Flag-HA}$ mutations on the cellular response to stress-inducing agents

Next, we evaluated the cellular response of all the isogenic cell lines to different stress-inducing agents, namely UV irradiation or menadione (MD) treatment. MD causes oxidative stress by generating and accumulating cellular reactive oxygen

species (ROS), such as superoxide radicals, singlet oxygen and hydrogen peroxide. The cell survival was investigated by colony-forming assay (Figure 21). After irradiation with increasing energy levels of UV light (5, 10 and 15 J/m^2) or increasing MD concentrations (25, 50, 100 and 200 µM), we found that the expression of wtCSA$^{Flag\text{-}HA}$ resulted in resistance to both treatments, with survival levels approaching those of the normal MRC5 cells. In contrast, the CSA-defective cells CS3BE-cassette1 showed reduced levels of survival. Therefore, the expression of wtCSA$^{Flag\text{-}HA}$ *per se* is sufficient to fully recover the sensitivity of the parental CS3BE-cassette1 cells to UV and MD, confirming that the ectopically expressed CSA protein is fully functional. In contrast, all the mutants showed a strong UV and MD sensitivity, as the parental cell line. Upon UV irradiation, we observed a higher variability in the residual level of survival among the isogenic cell lines expressing mutated CSA$^{Flag\text{-}HA}$ forms. In particular, the K174A mutation appeared to be the most deleterious, whereas the effect of the E52V mutation is comparable to the absence of CSA of the parental cell line CS3BE-cassette1. Therefore, all the analyzed *CSA* mutations are unable to complement the UV-sensitive phenotype of CS3BE cells, whereas one of them (K174A) confers extreme sensitivity to the killing effects of UV light.

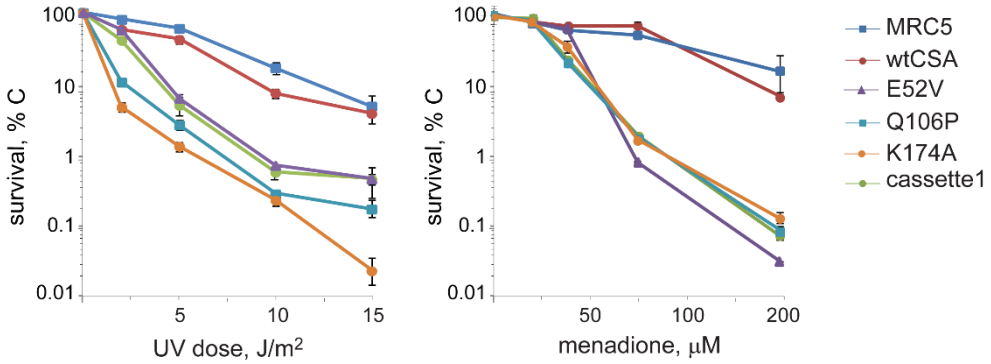

Figure 21. Sensitivity to UV irradiation and menadione (MD) treatment of the isogenic cell line CS3BE-E52V-CSA$^{Flag\text{-}HA}$, CS3BE-Q106P-CSA$^{Flag\text{-}HA}$, CS3BE-K174A-CSA$^{Flag\text{-}HA}$, CS3BE-wtCSA$^{Flag\text{-}HA}$ and CS3BE-cassette1 as well as the normal cell line MRC5. Survival values in irradiated samples are expressed as percentages of those in the corresponding non-irradiated samples. Bars indicate SE.

Overall, the results of this study indicate that mutations in different sites of CSA impair the stability of the protein, may affect its subcellular localization and severely affect the cellular ability to survive after UV or MD treatment.

5.2 Characterization of the CSA interaction with the TRiC/CCT chaperonin complex

The presence of the Flag and HA epitope tags at the C-terminus of the wtCSA$^{Flag-HA}$ protein has recently allowed our laboratory to purify and identify novel CSA-interacting complexes by tandem affinity purification (TAP) followed by mass spectrometry (the latter analysis was performed by Prof. Luca Bini, University of Siena). Relevant of note, among the newly identified CSA interactors we found CCT3 and CCT8, two of the subunits of the multimeric chaperonine complex TRiC/CCT involved in the folding of proteins characterized by complex topologies. Among the proteins that commonly use TRiC/CCT complex to achieve their native conformations, those containing WD repeats are widely represented, including Cdc20 and Cdh1 (Camasses et al, 2003). Indeed, the propeller-shaped β-sheet structures of WD repeat proteins seem to fit within the dimensions of the TRiC/CCT cavity (Craig, 2003).
Because of our previous finding demonstrating that *CSA* mutations impair the stability of the protein (session 5.1.4), we decided to investigate the functional meaning of CSA interaction with CCT3 and CCT8 and whether CSA may represent a new folding substrate for the TRiC/CCT complex.

5.2.1 Characterization of CSA$^{Flag-HA}$ interaction with CCT3 and CCT8

As a first step, we investigated the interaction of CSA with CCT3 and CCT8 proteins by using the TAP technique, which is based on two sequential immunoprecipitation experiments performed with the anti-Flag and anti-HA antibodies, followed by immunoblotting analysis.

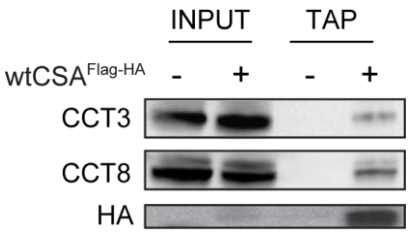

Figure 22. The CCT3 and CCT8 proteins co-immunoprecipitate with the recombinant wtCSA$^{Flag-HA}$ protein. Immunoblot analysis of total cell lysate (INPUT) and the co-immunoprecipitated proteins following Tandem Affinity Purification (TAP) in CS3BE-wtCSA$^{Flag-HA}$ cells (+) and in the parental cell line CS3BE-cassette1 (-).

As shown in Figure 22, we found that in total cell lysates of CS3BE-wtCSA$^{Flag-HA}$ cells the CCT3 and CCT8 proteins co-immunoprecipitated with wtCSA$^{Flag-HA}$. No immunoprecipitation of the TRiC/CCT subunits was observed in the parental cell line (CS3BE-cassette1) that lacks wtCSA$^{Flag-HA}$ expression.
Next, we performed co-immunoprecipitation (co-IP) experiment using anti-CCT3 or anti-CCT8 antibodies in CS3BE-cassette2 cells expressing the recombinant wtCSA$^{Flag-HA}$ protein. As shown in Figure 23, we observed that wtCSA$^{Flag-HA}$ co-immunoprecipitated with CCT3 and CCT8. As expected, the CCT8 subunit co-immunoprecipitated also with the CCT3 subunit, whereas no clear signal of CCT3 was observed in CCT8 immunoprecipitation. This suggests that the anti-CCT8 antibody is less efficient in immunoprecipitating the TRiC/CCT complex.

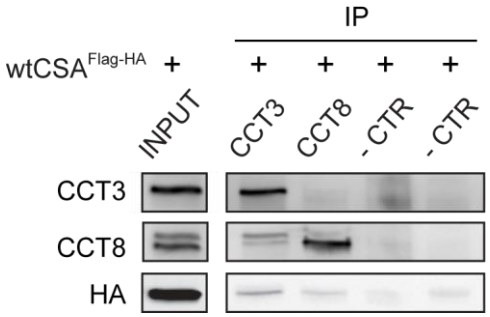

Figure 23: The recombinant wtCSA$^{Flag-HA}$ co-immunoprecipitates with the CCT3 and CCT8 subunits of the TRiC/CCT complex. Immunoblot analysis of total cell lysate (INPUT) and proteins co-immunoprecipitated with antibodies directed against the CCT3 and CCT8 subunits in CS3BE-wtCSA$^{Flag-HA}$.

5.2.2 Impact of CSA$^{Flag-HA}$ mutations on the interaction with CCT3 and CCT8

As we previously demonstrated, the E52V, Q106P and K174A mutations alter the cellular localization and protein stability of CSA. Therefore, we investigated the effects of CSA mutations on the interaction with the TRiC/CCT complex by TAP followed by immunoblotting. We observed that, despite the low cellular level of E52V-CSA$^{Flag-HA}$, Q106P-CSA$^{Flag-HA}$ and K174A-CSA$^{Flag-HA}$ mutated proteins, their interaction with CCT3 and CCT8 was very high (Figure 24). We are tempted to speculate that the increment of co-immunoprecipitated proteins observed after TAP analysis reflects a more stable interaction of the analyzed proteins with the mutated forms of CSA. Notably, CCT3 and CCT8 showed similar patterns of interactions toward the mutated forms of CSA$^{Flag-HA}$ (Figure 24), in agreement with the observation that these two proteins are part of a unique chaperonin complex, whose

function is to protect multidomain proteins characterized by intricate structures and regions of β-strand, predicted to be slow-folding and/or aggregation-prone.

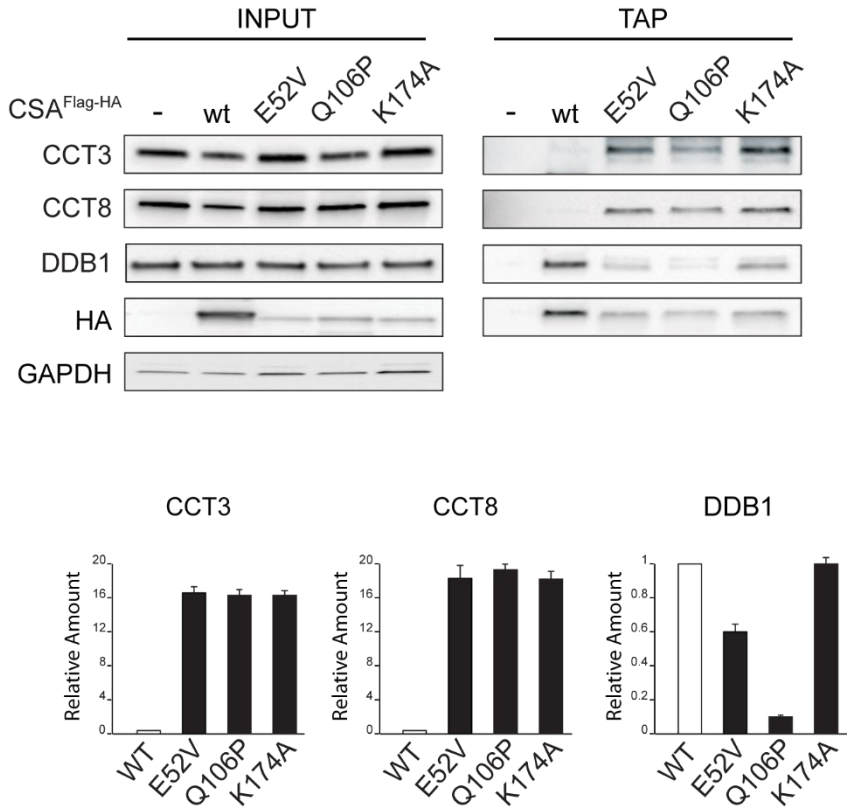

Figure 24. Interaction of CCT3, CCT8 and DDB1 with the mutated CSA$^{Flag-HA}$ proteins. Immunoblot analysis of total cell lysates (INPUT) and the proteins co-immunoprecipitated by Tandem Affinity Purification (TAP) in CS3BE-wtCSA$^{Flag-HA}$, CS3BE-E52V-CSA$^{Flag-HA}$, CS3BE-Q106P-CSA$^{Flag-HA}$ and CS3BE-K174A-CSA$^{Flag-HA}$ cells and in their parental cell line CS3BE-cassette1 (-). The levels of the co-immunoprecipitated proteins showed in the upper panel were normalized and quantified to the amount of HA protein bands. GAPDH was used as loading control. Bars indicate SE.

Moreover, we examined the co-immunoprecipitation of DDB1, a well-known interactor of CSA and member of the CSA core complex. As expected, DDB1 co-immunoprecipitated with the wtCSA$^{Flag-HA}$ as well as the E52V and K174A

mutated forms of $CSA^{Flag\text{-}HA}$, whereas it failed to co-immunoprecipitate with the Q106P-$CSA^{Flag\text{-}HA}$ recombinant protein. This finding indicates that the Q106P mutation hampers the interaction of CSA with DDB1, in agreement with the notion that this amino acid change alters the propeller structure of CSA, relevant for protein-protein interactions (Zhou and Wang 2001).

5.2.3 Effect of $CSA^{Flag\text{-}HA}$ mutations on CCT3 and CCT8 subcellular localization

Since all the analyzed mutations impact on the CSA protein stability, alter its subcellular localization and increase its interaction with the TRiC/CCT complex, we investigated whether the expression of the mutated form of CSA may alter the cellular distribution of the chaperonine complex. Therefore, we performed indirect immunofluorescence analysis in the parental cell line CS3BE-cassette1 as well as in all the isogenic cell lines expressing either the wild type or mutated forms of $CSA^{Flag\text{-}HA}$. As shown in Figure 25 and 26, we observed a comparable cytoplasmic signal in all the CS3BE-derivative cell lines for both the subunits of the TRiC/CCT complex.

Therefore, mutations in CSA do not impact on the subcellular localization of the CCT3 and CCT8 proteins.

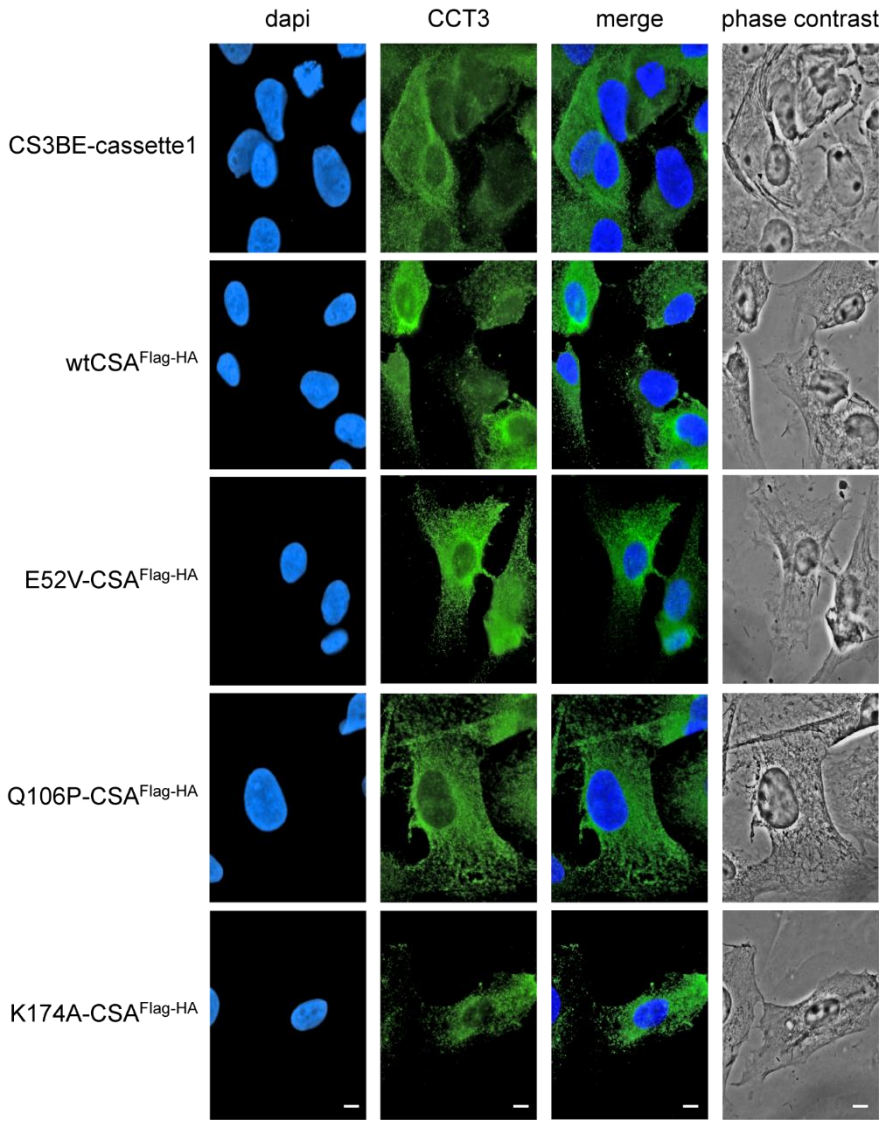

Figure 25. Subcellular localization of the CCT3 protein in the isogenic cell lines. Indirect fluorescence staining with antibodies directed against the CCT3 protein (*green*). Bars, 2 μm.

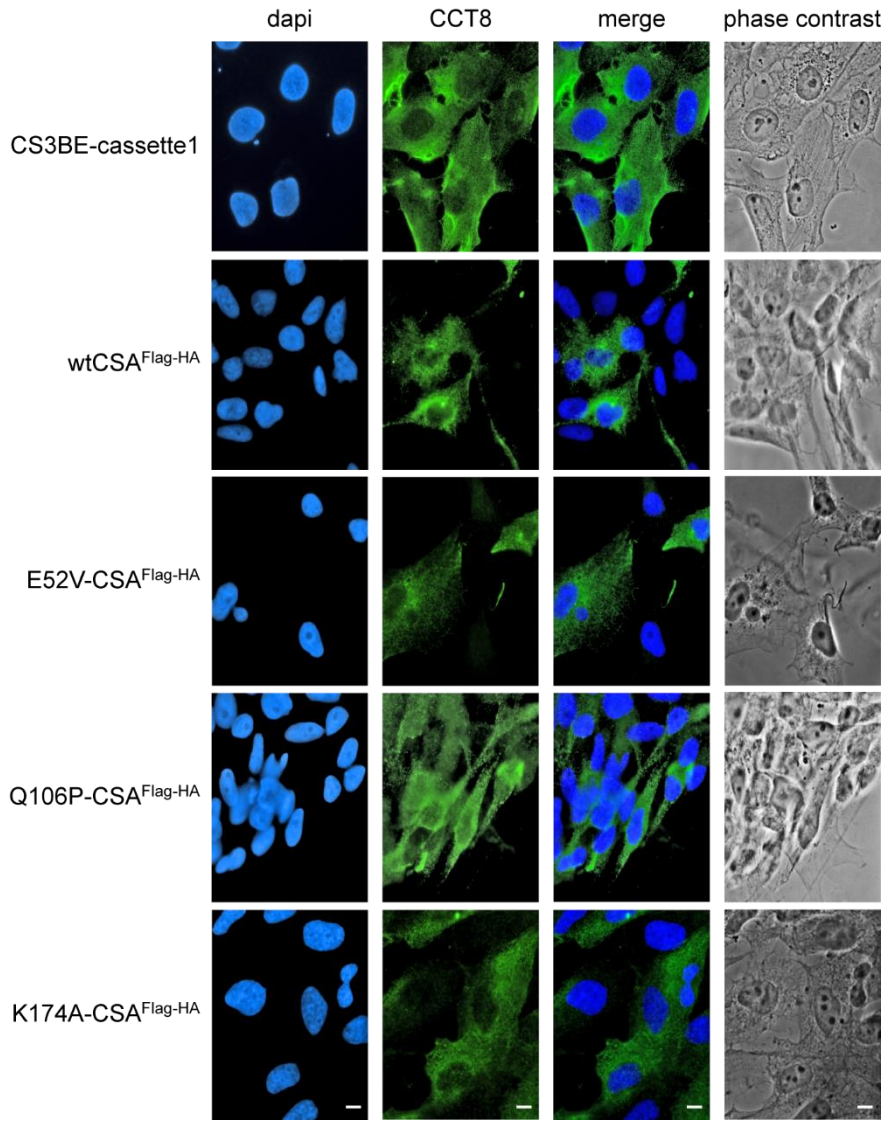

Figure 26. Subcellular localization of the CCT8 protein in the isogenic cell lines. Indirect fluorescence staining with antibodies directed against the CCT8 protein (*green*). Bars, 2 μm.

5.2.4 Dynamic of CSA$^{Flag-HA}$ interaction with CCT3 and CCT8 in response to specific cellular stresses

Since we are tempted to believe that the TRiC/CCT chaperonine complex is required for the proper folding of CSA, and given the pivotal role of CSA in UV and oxidative DNA damage response, we decided to investigate whether different stressing agents can alter the interaction of CSA with CCT3 and CCT8 (Figure 27).

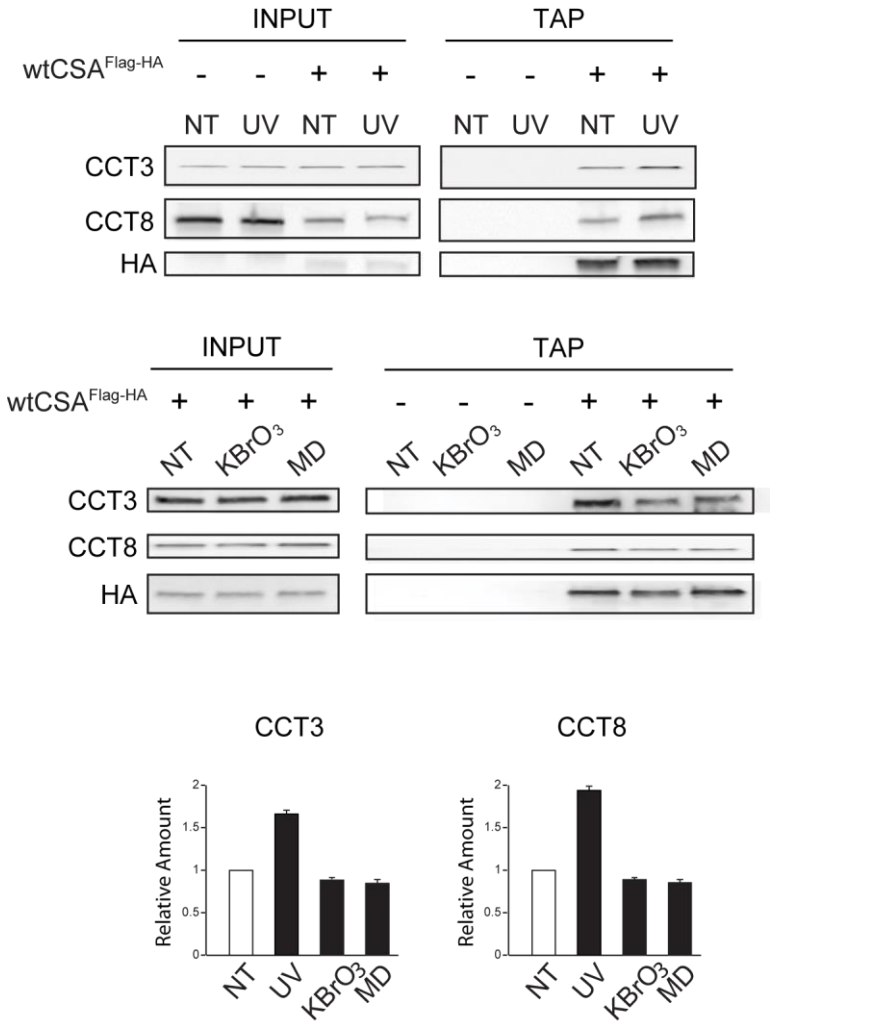

Figure 27. Interaction of the CCT3 and CCT8 proteins with the recombinant wtCSA$^{Flag-HA}$ protein upon treatment with cellular stressing agents. Immunoblot analysis of total cell lysates (INPUT) and the proteins co-immunoprecipitated with Flag and

HA antibodies by Tandem Affinity Purification (TAP) in CS3BE-wtCSA$^{Flag-HA}$ cells (+) and in the parental cell line CS3BE-cassette1 (-). Cells were irradiated with UV light (10 J/m^2) or treated with menadione (MD, 100 μM) or potassium bromate ($KBrO_3$, 20mM). The levels of CCT3 and CCT8 showed in the upper panel were normalized and quantified to HA levels and expressed as fold increase of the corresponding not treated (NT) cells. Bars indicate SE.

The susceptibility of CSA interaction with CCT3 and CCT8 proteins to UV or oxidative stress was investigated following irradiation of CS3BE-wtCSA$^{Flag-HA}$ cells with UV light (10 J/m^2) or treatment with the oxidative stress-inducing agents $KBrO_3$, (200 mM) or MD (100 μM). After treatment, we isolated by TAP the wtCSA$^{Flag-HA}$-interacting proteins and evaluated by immunoblotting the presence of CCT3 and CCT8 among the co-immunoprecipitated proteins.

Untreated and CS3BE-cassette1 cells were processed in parallel. In agreement with the observation that these two proteins belong to the same complex, we detected a similar pattern of interaction of CCT3 and CCT8 with wtCSA$^{Flag-HA}$, which slightly increased upon treatment with UV light. On the contrary, cell exposure to oxidative stress did not alter the interaction of CSA$^{Flag-HA}$ with the two TRiC/CCT subunits.

5.2.5 Subcellular localization of CCT3 and CCT8 in response to stressing agents in CSA-defective fibroblasts

Since we observed a higher interaction of CSA with the TRiC/CCT complex following UV irradiation, we decided to investigate whether distinct cellular stressing agents or CSA mutations present in CS patients can affect the cellular distribution of CCT3 and CCT8. To this purpose, we analyzed the cytoplasmic localization of CCT3 and CCT8 in primary fibroblasts from the healthy donor C3PV (Figure 28) or the CS patients CS7PV (Figure 29) and CS15PV (Figure 30), both mutated in the *CSA* gene and carrying in homozygous conditions the r.719_843del (exon 9) and the r.37g>u mutations, respectively. The subcellular distribution of the TRiC/CCT subunits was analyzed either in basal conditions, in response to UV irradiation (10 J/m^2) or following potassium bromate (200 mM) or menadione (100 μM) treatment.
CCT3 and CCT8 staining gave superimposable results in all the analyses, therefore we decided to show only the images obtained with the antibodies directed against CCT8, which has a sharp signal and low levels of background. In the fibroblasts from the healthy donor (C3PV) we found no major differences in the cytoplasmic localization of CCT3 and CCT8 even though after MD or UV treatment we observed the appearance of a mild nuclear staining. Similar results were obtained from the CS-A patient fibroblasts, indicating that pathological alterations in the

CSA protein do not affect the subcellular localization of the two CCT proteins. This data are in agreement with our previous observations from the isogenic cell lines (5.2.3).

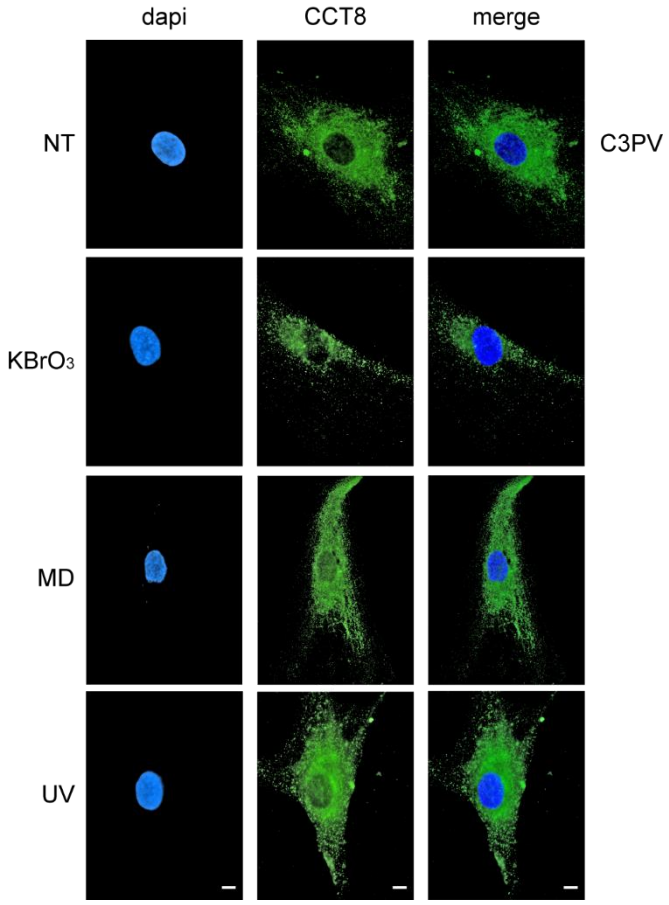

Figure 28. Subcellular localization of the CCT8 protein in fibroblasts from the healthy donor C3PV. Cells were treated with potassium bromate ($KBrO_3$, 20mM) or menadione (MD, 100 µM) or irradiated with UV light (10 J/m^2). Indirect fluorescence staining with antibodies directed against the CCT8 protein (*green*). Bars, 2 µm.

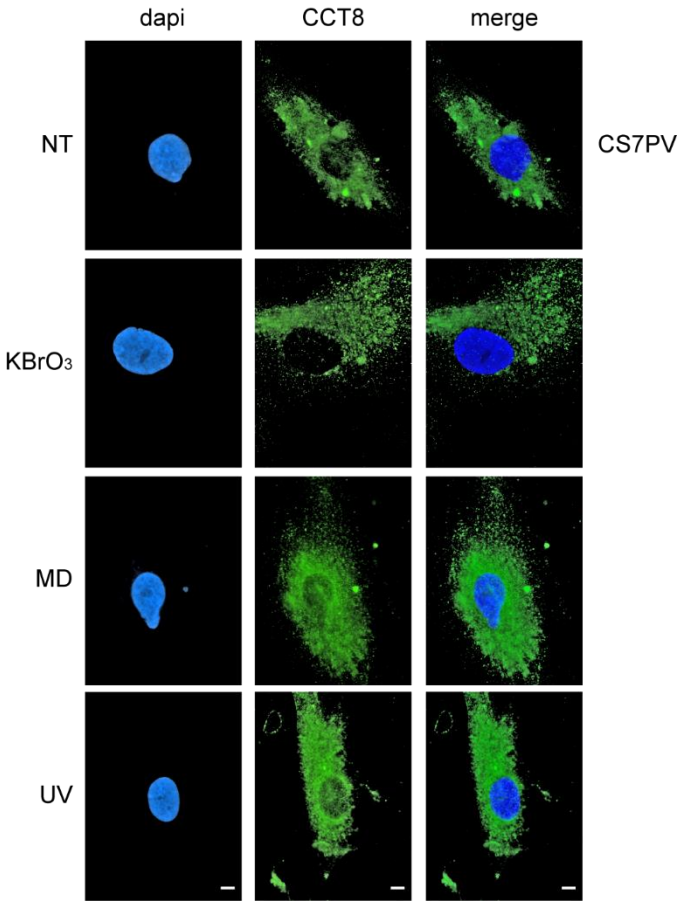

Figure 29. Subcellular localization of the CCT8 protein in fibroblasts from the CS7PV patient. Cells were treated with potassium bromate ($KBrO_3$, 20mM) or menadione (MD, 100 µM) or irradiated with UV light (10 J/m^2). Indirect fluorescence staining with antibodies directed against the CCT8 protein (*green*). Bars, 2 µm.

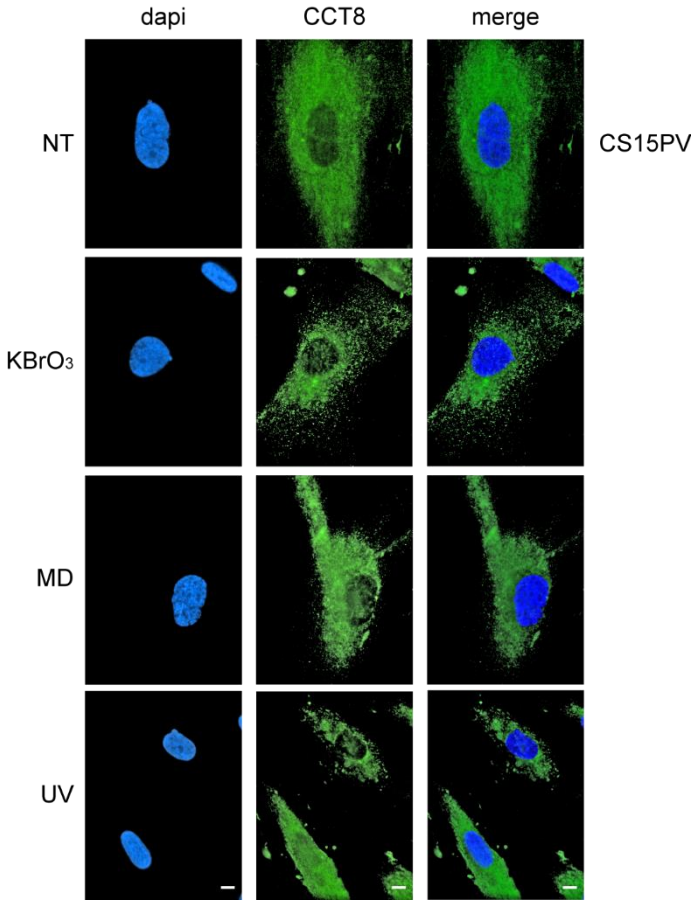

Figure 30. Subcellular localization of the CCT8 protein in fibroblasts from the CS15PV patient. Cells were treated with potassium bromate ($KBrO_3$, 20mM) or menadione (MD, 100 µM) or irradiated with UV light (10 J/m^2). Indirect fluorescence staining with antibodies directed against the CCT8 protein (*green*). Bars, 2 µm.

5.2.6 Silencing of the *CCT3* and *CCT8* genes

Next, we searched for the biological relevance of the TRiC/CCT complex interaction with the CSA$^{Flag\text{-}HA}$ protein. By silencing experiments, we reduced the intracellular levels of the chaperonine complex and afterwards we assayed the functionality of CSA in TC-NER. Therefore, at first, we set up the experimental conditions for TRiC/CCT silencing. Normal primary dermal fibroblasts from a healthy donor (C3PV) were transfected with siRNA molecules for 48 or 96 hrs and the levels of CCT3 and CCT8 investigated by immunoblot analysis. Upon 96 hours of siRNA treatment, we appreciated a considerable reduction of CCT3 and CCT8 protein amount (Figure 31). Notably, we observed that the reduction of the targeted TRiC/CCT subunit was paralleled by decreased levels of the other analyzed subunit, thus indicating that silencing one subunit may affect the entire chaperonine complex.

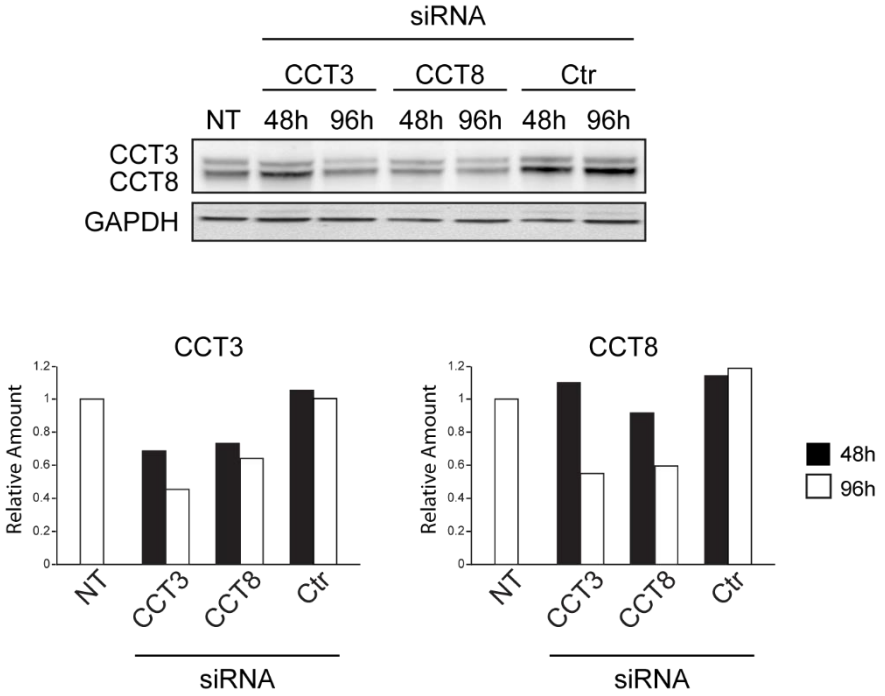

Figure 31. *CCT3* and *CCT8* silencing in C3PV cells. Immunoblot analysis of total cell lysates from C3PV cells transfected with *CCT3* or *CCT8* siRNA molecules. The protein levels of CCT3 and CCT8 shown in the upper panel were normalized to GAPDH levels and their quantification reported in the lower panel. Bars indicate SE. CTR, control siRNA; NT, not treated.

From this analysis, we set our experimental conditions for TRiC/CCT knockdown on 96 hrs of siRNA transfection.

5.2.6.1 RRS analysis after *CCT3* and *CCT8* silencing

To investigate CSA functionality in TC-NER, we evaluated the Recovery of RNA Synthesis (RRS) after UV irradiation in primary dermal fibroblasts from the C3PV healthy donor, in which we knocked down either *CCT3* or *CCT8* by RNA interference. The *CCT3* or *CCT8* genes were silenced for 96 hrs and 24 hrs before RRS analysis, cells were irradiated with UV light (20 J/m^2). In parallel, CS-A primary cells (AS440) were used as control.
As shown in Figure 32B, C3PV fibroblasts silenced for *CCT8* exhibited level of RRS after UV-induced DNA damage comparable to the level of the corresponding unirradiated (NT) sample and to the cells transfected with control siRNA (Ctr). On the other hand, the results from RRS investigations in C3PV cells silenced for *CCT3* pointed toward a defective capacity to repair UV-induced damage, as indicated by the lower level of RRS in irradiated cells (Figure 32B). Although the RRS reduction observed upon *CCT3* knockdown is not conspicuous, it is nevertheless consistent with RRS level sometimes observed in CSA-defective fibroblasts from CS patients.

In summary, we demonstrated that the wild type CSA protein interacts with the TRiC/CCT complex and this event is relevant for CSA functionality in TC-NER. Mutations impairing CSA stability result in increased interaction with the chaperonin complex. Overall, these findings open the possibility of a TRiC/CCT involvement in CS pathogenesis.

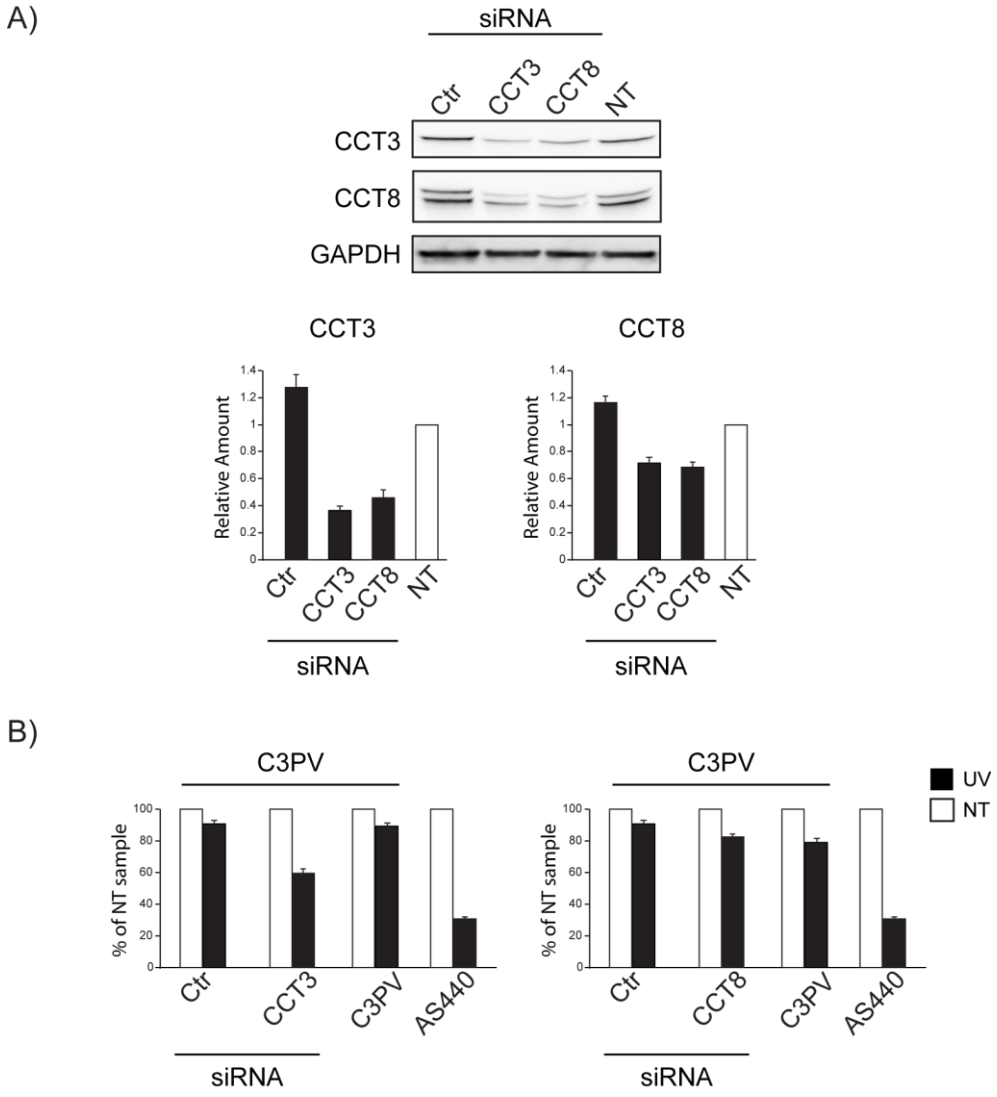

Figure 32. *CCT3* knockdown in normal C3PV cells impairs RRS 24 hrs after UV irradiation. (A) Immunoblot analysis of total cell lysates from C3PV cells transfected with *CCT3* or *CCT8* siRNA molecules for 96 hrs. The levels of the CCT3 and CCT8 proteins were normalized to GAPDH levels and their quantification reported in the lower panel; **(B)** RRS levels 24 hrs after UV (20 J/m^2) irradiation in normal C3PV cells either transfected with *CCT3/CCT8* siRNA or not transfected, and in primary CS-A (AS440) fibroblasts. The mean number of autoradiographic grains per nucleus in irradiated samples is expressed as percentages of those in the corresponding unirradiated cells. Ctr, control siRNA; NT, not treated. Bars indicate SE.

5.3 Identification of putative causative genes in an unassigned CS case

Up to now, research studies directed to the identification of novel disease genes and mutations causative for CS have been fundamental to disclose the molecular mechanisms underlying TC-NER pathway and to understand the functional basis of CS proteins.
Therefore, as part of this PhD study, we also focused on the identification of causative gene for CS phenotype in an unassigned case reported to our laboratory and represented by the CS11/9_PV patient.

5.3.1 The CS11/9_PV patient

Case report:
The CS11/9_PV patient was the firstborn of two healthy unrelated parents who also gave birth to a healthy girl. The boy was born by Caesarean section at forty weeks and three days of gestation, with a birth weight of 3380 g (25° percentile), a birth length of 50 cm (40° percentile) and a head circumference of 35 cm (50° percentile). Apgar scores were 6 at one minute and 9 at five minutes. At birth, a number of dysmorphic features were noted: the patient presented with microcephaly, micrognathia, camptodactyly, hypotony, tremors and polypnea for which he required oxygen supplementation. Routine laboratory tests were normal. In the post-natal period the patient showed contractures, retinal degeneration, nystagmus and physical and psychomotor delay. Magnetic resonance imaging (MRI) analysis revealed thinned corpus callosum and basal ganglia calcifications. Percutaneous endoscopic gastrostomy (PEG) was required to overcome feeding and swallowing difficulties. The patient died at age three because of a general worsening of the physical conditions.

Primary dermal fibroblasts from all the family members were collected to investigate for a suspected diagnosis of COFS. Primary dermal fibroblasts from the patient showed cellular features typical of TC-NER alterations, such as reduced survival and decreased RRS levels (Figure 33), but normal unscheduled DNA synthesis (UDS) after 20 J/m^2 UV irradiation (Figure 34).

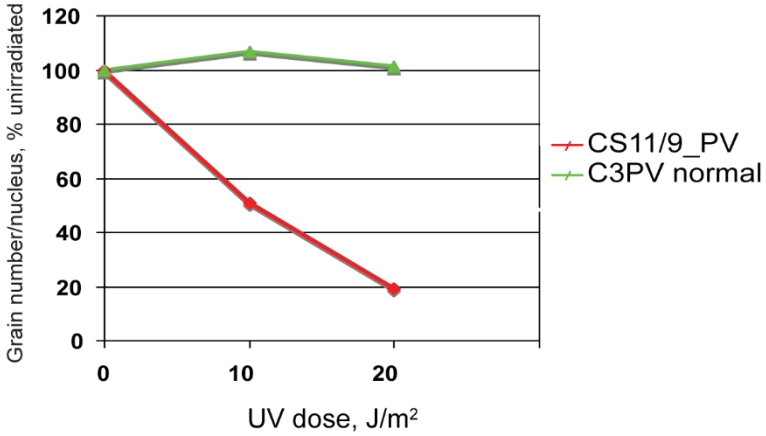

Figure 33. RRS analysis 24 hrs after UV irradiation in normal fibroblasts from a healthy donor (C3PV) and CS11/9_PV patient. The mean number of autoradiographic grains per nucleus in irradiated samples is expressed as percentages of those in unirradiated cells.

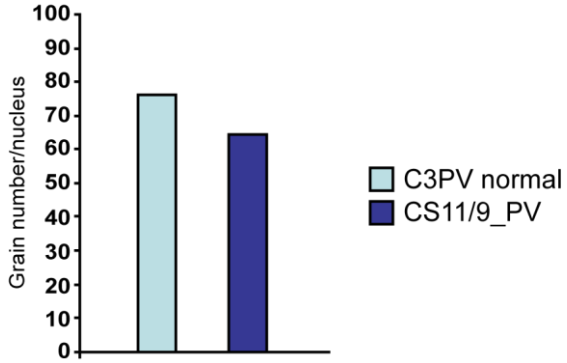

Figure 34. UV-induced DNA repair synthesis (UDS) after UV irradiation (20 J/m^2) in normal fibroblasts from a healthy donor (C3PV) and CS11/9_PV patient. UDS is expressed as mean number of autoradiographic grains/nucleus.

Complementation assay revealed a recovery of TC-NER alterations after fusion of CS11/9_PV fibroblasts with CS-A but not CS-B fibroblasts, thus indicating that mutations in the *CSB* gene could be responsible for the CS phenotype of the CS11/9_PV patient (Figure 35).

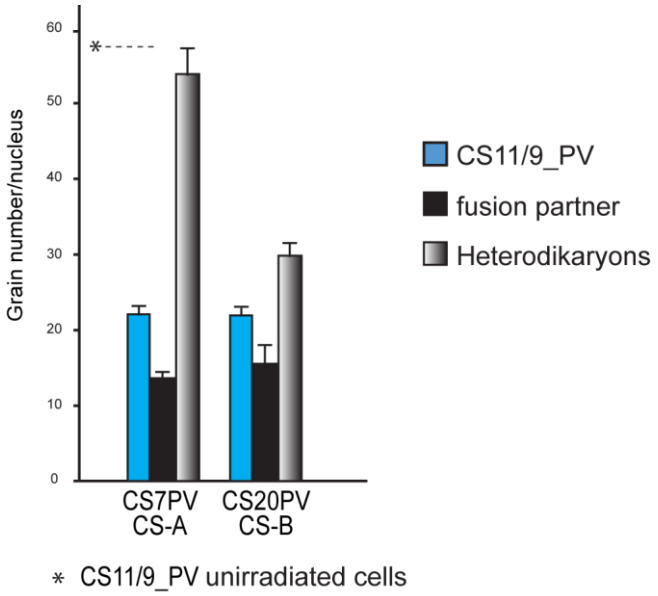

Figure 35. Complementation analysis in heterodikaryons obtained by fusion of CS11/9_PV fibroblasts with cells representative of different excision repair-deficient groups (CS-A, CS7PV; CS-B, CS20PV). The RRS analysis performed 24 hrs after UV irradiation was analyzed 73 hrs after cell fusion. Column heights indicate the mean number of autoradiographic grains per nucleus in homodikaryons and heterodikaryons. Bars indicate SE.

Even though the results of the complementation assay are suggestive of a genetic defect in the *CSB* gene, sequencing analysis did not reveal inactivating mutations in the cDNAs of *CSB*, *CSA*, *UVSSA* or *UPS7* genes (data not shown). Nevertheless, immunoblotting analysis on primary dermal fibroblasts from the CS11/9_PV patient showed nearly absent levels of CSB or of the CSB-transposon fusion protein CSB-PGBD3 (Figure 36), despite a normal level of *CSB* transcript (Figure 37). Notably, the reduced CSB protein amount is not ascribable to a transcriptional defect, since CS11/9_PV fibroblasts present normal *CSB* transcript levels (Figure 37). Therefore, we are prompted to exclude that the mutation affecting *CSB* and causing such a reduced protein amount resides in the promoter or other regulatory regions.

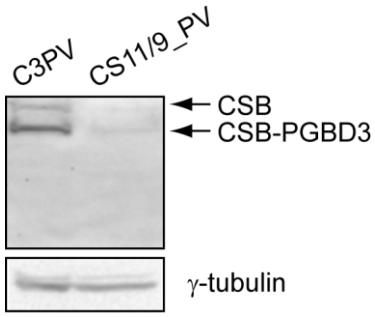

Figure 36. CSB protein levels. Immunoblot analysis with antibodies directed against CSB protein in total cell lysates of fibroblasts from a healthy donor (C3PV) and the CS11/9_PV patient.

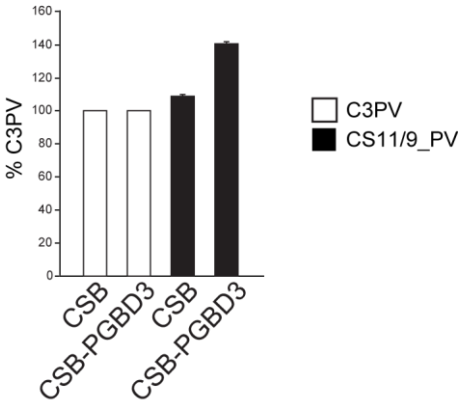

Figure 37. *CSB* and *CSB-PGBD3* transcript levels. Real-time PCR analysis in fibroblasts from a healthy donor (C3PV) and the CS11/9_PV patient. Transcript levels are expressed as percentages of the amount detected in the corresponding normal cells analyzed in parallel. Bars indicate SE.

To identify putative causative genes for this unassigned CS case, we sent CS11/9_PV cells to the laboratory of Prof. Tomoo Ogi (Research Institute of Environmental Medicine, Nagoya University, Japan), who performed the whole exome sequencing (WES) analysis in fibroblasts and/or lymphoblastoid cells from all the CS11/9_PV family members. From the bioinformatic analysis of the exome data, Prof. Ogi identified potentially pathogenic mutations in three genes. This work is part of a long lasting collaboration with the group headed by Prof. Ogi, and partners are required to not reveal the identity of the candidate genes until

completion of the research. Therefore, we will refer to the candidate genes as follows: *CS11/9_A*, *CS11/9_B* and *CS11/9_C*.
CS11/9_A encodes for a co-activator of hormone receptor and acts as co-regulator for several nuclear receptors. It can associate with chromatin, interact with histone-modifying complexes and promote cell proliferation.
The CS11/9_B protein is widely recognized as a key regulator of inflammation and immunity, whereas CS11/9_C protein belongs to a protein family of RNA helicases that plays different roles in RNA processing and metabolism, including transcription, alternative splicing and degradation.

5.3.2 Co-immunoprecipitation analysis of CSA with CS11/9_A, CS11/9_B and CS11/9_C

Taking advantage of the cell system developed in our laboratory, we decided to investigate whether the putative causative genes identified by WES analysis represented novel CSA interactors. To this purpose, we performed TAP analysis in the CS3BE-wtCSA$^{Flag\text{-}HA}$ cell line. The parental cell line CS3BE-cassette1 was processed in parallel as a negative control. As shown in Figure 38, we observed that CS11/9_A and CS11/9_C co-immunoprecipitated with CSA$^{Flag\text{-}HA}$, whereas no interaction was detected for CS11/9_B.

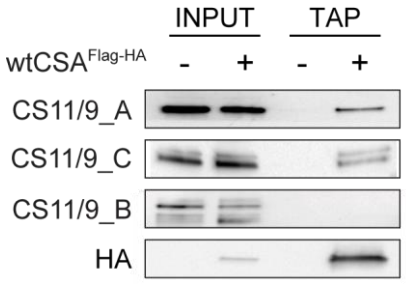

Figure 38. The CS11/9_A and CS11/9_C proteins co-immunoprecipitate with the recombinant wtCSA$^{Flag\text{-}HA}$ protein. Immunoblot analysis of total cell lysate (INPUT) and the proteins co-immunoprecipitated following Tandem Affinity Purification (TAP) in CS3BE-wtCSA$^{Flag\text{-}HA}$ (+) cells and in the parental cell line CS3BE-cassette1 (-).

Next, we performed co-IP analysis in whole cell lysates of CS3BE-wtCSA$^{Flag\text{-}HA}$ fibroblasts with antibodies directed against CS11/9_A or CS11/9_C proteins (Figure 39). We found that wtCSA$^{Flag\text{-}HA}$ co-immnoprecipitated with CS11/9_A, confirming the TAP result, whereas a very faint signal of wtCSA$^{Flag\text{-}HA}$ was found in the CS11/9_C immunoprecipitation.

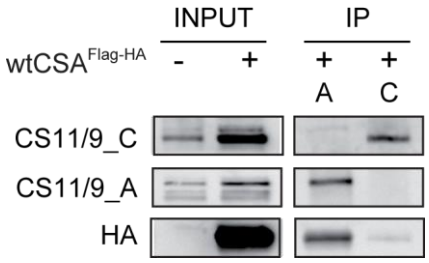

Figure 39: The recombinant wtCSA$^{Flag-HA}$ protein co-immunoprecipitates with the CS11/9_A protein. Immunoblot analysis of total cell lysate (INPUT) and the proteins co-immunoprecipitated with antibodies directed against CS11/9_A (A) and CS11/9_C (C) in CS3BE-wtCSA$^{Flag-HA}$ cells (+) or in the parental CS3BE-cassette1 (-) cell line.

Overall, these results strongly suggest that potential CS-causative genes encode proteins physically interacting with CSA (namely, CS11/9_A and CS11/9_C).

5.3.3 Silencing of the candidate genes

To gain further insights into the functional meaning of CSA interaction with CS9/11_A, we knocked down by RNA interference *CS11/9_A* gene in primary dermal fibroblasts from the C3PV healthy donor and subsequently performed recovery of RNA synthesis (RRS) analysis after UV-induced DNA damage.
As a control, we decided to knockdown also *CS11/9_B* gene. Firstly, we investigated the CS9/11_A and CS9/11_B protein levels 48 and 96 hrs after siRNA transfection (Figure 40).

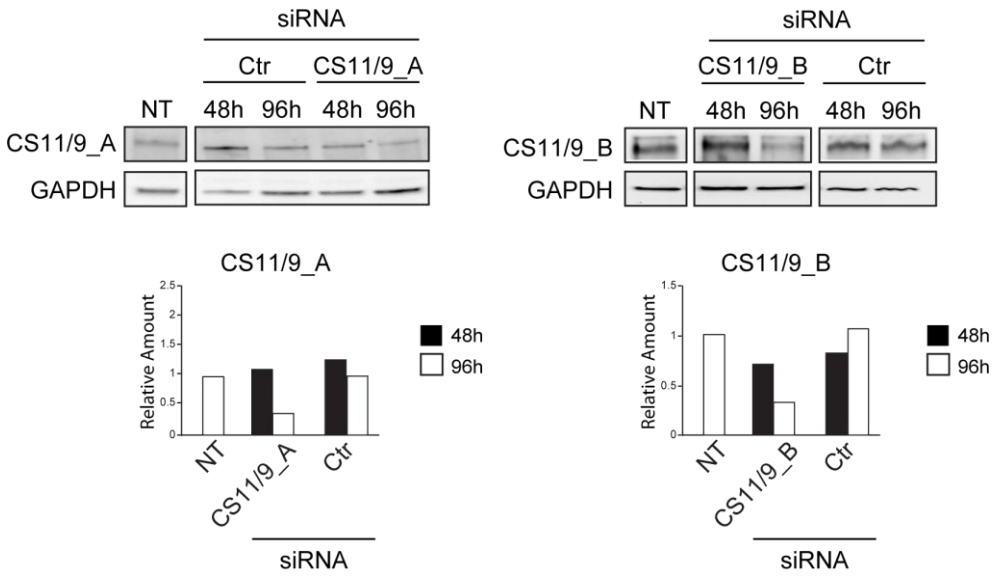

Figure 40. Knockdown of *CS11/9_A* and *CS11/9*_B in C3PV cells by RNA interference. Immunoblot analysis of total cell lysates from C3PV cells transfected with siRNAs against *CS11/9_A* and *CS11/9_B* for 48 or 96 hrs. The levels of CS11/9_A and CS11/9_B proteins reported in the upper panel were normalized to GAPDH levels. Bars indicate SE.

We therefore established that siRNA treatment led to optimal *CS11/9_A* and *CS11/9_B* silencing at 96 hrs after transfection.

5.3.4 RRS analysis after *CS11/9_A* and *CS11/9_B* silencing

Finally, 24 hrs after UV irradiation we performed RRS analysis in cells from the healthy donor C3PV silenced for 96 hrs with either *CS11/9_A* or *CS11/9_B*. C3PV fibroblasts silenced for *CS11/9_B* exhibited normal levels of RRS after UV-induced damage, comparable to the level in the corresponding unirradiated (NT) sample and to the sample transfected with control siRNA (Ctr). As expected, the CSA-defective cells AS440 revealed a quite strong reduction of RRS levels, indicative of TC-NER defects (Figure 41).

Relevant of note, a mild but reproducible reduction of RRS was observed following UV irradiation DNA in CS3BE cells silenced for *CS11/9_A*, thus indicating a defective capacity to repair UV-induced DNA damage (Figure 41).

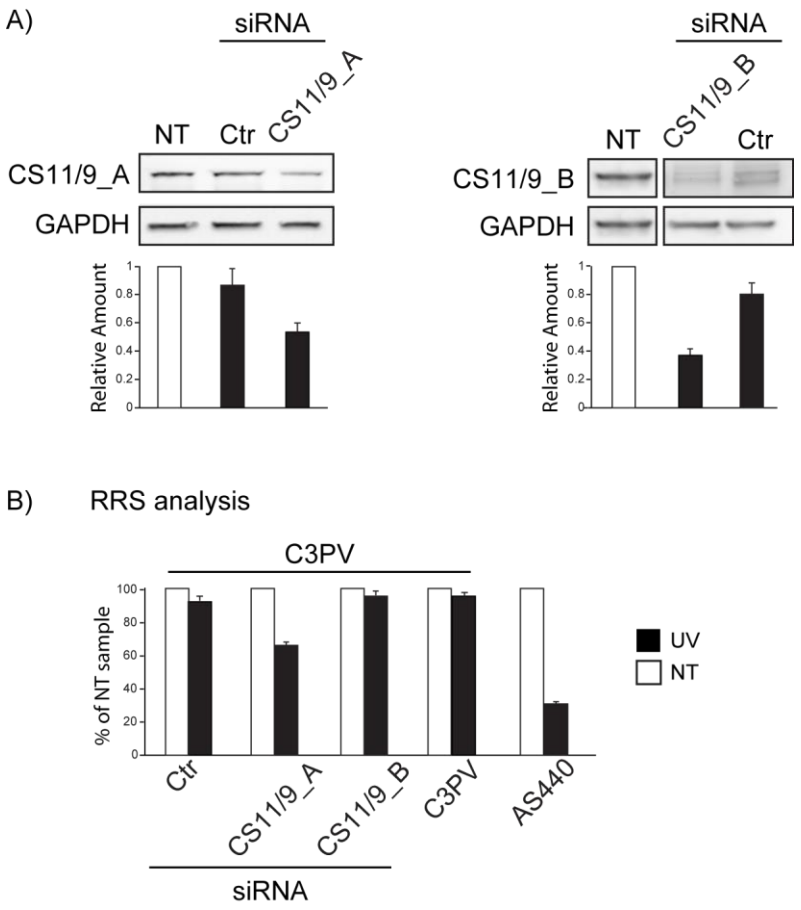

Figure 41. *CS11/9_A* knockdown affects RRS levels in C3PV cells. (A) Immunoblot analysis of total cell lysates from C3PV cells transfected with *CS11/9_A* or *CS11/9_B* siRNAs for 96 hrs. The levels of the CS11/9_A and CS11/9_B proteins shown in the upper panel were normalized to GAPDH levels; **(B)** RRS levels 24 hrs after UV irradiation (20 J/m^2) in primary fibroblasts from CS-A (AS440) patient or the healthy donor C3PV. C3PV cells were silenced either for *CS11/9_A* or *CS11/9_B* gene or transfected with control siRNA (Ctr), or not treated (C3PV). The mean number of autoradiographic grains per nucleus in irradiated samples is expressed as percentages of those in the corresponding unirradiated cells. NT, not treated. Bars indicate SE.

This observation is indicative of an involvement of the CS11/9_A protein in the CSA-dependent signaling pathways. Even though further experiments are required,

this finding opens the possibility that CS11/9_A may be the causative gene for the CS phenotype in this unassigned case.

6. Discussion and conclusions

Cockayne syndrome (CS) is an autosomal recessive multi-system disorder characterized by pre- or post-natal growth failure, premature aging and progressive neurological dysfunction associated to other clinical features including gait defects, cataracts, skeletal abnormalities, impaired sexual development, sensorineural hearing loss, dental caries, and cutaneous photosensitivity (Laugel, 2013). The neuropathological changes include neuronal and myelin loss with deposits of calcium and iron in the vessels of the cerebellum, basal ganglia and cerebrum. The most common neurological manifestation is mental retardation, and the other classical features include retinitis pigmentosa and photosensitive retinitis (Mundaganur, 2012). About half of patients clinically diagnosed as CS reveal skin photosensitivity which is associated with an altered cellular response to UV light caused by a defect in nucleotide excision repair (NER), the DNA repair pathway that removes a wide spectrum of DNA lesions, including UV-induced damage. (Stefanini and Ruggieri, 2008). CS is caused by defects in one of two genes, designated *CSA* and *CSB*, which are both involved in the sub-pathway of NER called transcription-coupled nucleotide excision repair (TC-NER) that removes DNA lesions blocking the progression of the transcription machinery in the transcribed regions of DNA (reviewed in Lanzafame et al., 2013). Conversely, the NER sub-pathway called global genome repair (GGR), which removes the two major UV-induced photoproducts and other bulky DNA adducts from the silent regions of the genome, is unaffected in CS. The function of CSA and CSB in TC-NER is quite well characterized.

The wide range of phenotypic manifestations as well as the lack of clear genotype-phenotype relationship obtained from mutational analysis in CS patients support the notion that CS proteins might have additional functions outside TC-NER. In particular, the lack of skin cancer despite the persistency of DNA damage as well as the premature aging coupled with neurological deterioration are suggestive of transcriptional impairment and/or accumulation of oxidative damage, rather than accumulation of UV-induced DNA lesions. According to these observations, it has been suggested that *CSA* and *CSB* might have additional roles outside TC-NER.

In this study, we have generated a panel of isogenic cell lines with the purpose to investigate the effect of specific mutations on CSA functionality, their impact on the cellular response to specific stress factors and on the CSA protein interaction framework. The use of the Cre-mediated Recombinase Cassette Exchange (RMCE) technique allowed to integrated in the same genomic *locus* of a recipient CSA-defective cell line (CS3BE-cassette1) a single copy of cDNA encoding mutated forms of CSA (E52V-CSA$^{Flag\text{-}HA}$, Q106P-CSA$^{Flag\text{-}HA}$ or K174A-CSA$^{Flag\text{-}HA}$). The

finding that CS3BE-cassette1 contains the same levels of *CSA* transcripts as the parental cell line CS3BE demonstrated that the genomic insertion of *cassette1* did not affect the endogenous *CSA* transcription. Similarly, the replacement of *cassette1* with *cassette2* by RMCE did not impair *CSA* expression, as demonstrated by the observation that *CSA* mRNA level in CS3BE-wtCSA$^{Flag\text{-}HA}$ cells is about 2-folds the level obtained in the normal MRC5 cells and in the parental cell lines CS3BE and CS3BE-cassette1. Therefore, we can reasonably exclude excessive over-expression of the recombinant gene in our cell system. Notably, the Q106P-CSA$^{Flag\text{-}HA}$, E52V-CSA$^{Flag\text{-}HA}$ and K174A-CSA$^{Flag\text{-}HA}$-expressing cell lines showed transcript levels comparable or even higher than those observed in the wtCSA$^{Flag\text{-}HA}$ cells, indicating that the selected point mutations did not reduce the stability of *CSA* mRNA (Figure 17 and 18). In contrast, the levels of the mutated CSA$^{Flag\text{-}HA}$ proteins were markedly reduced compared to the levels of wtCSA$^{Flag\text{-}HA}$ (Figure 19). Thus, we believe that all the analyzed mutations impair the stability of the recombinant CSA protein, without altering the stability of the transcript.

CSA is a 396 amino acid protein belonging to the large WD-repeat family. WD repeats are minimally conserved domains of about 40 to 60 amino acids that end with a tryptophan-aspartic acid (WD) dipeptide at the C-terminal (reviewed in Smith 2008). CSA contains seven WD repeats organized into a circular propeller-like structure with seven blades, each made up of four β-strands. This structure creates a stable platform with three potential interacting surfaces likely committed to the interaction with other proteins, thus coordinating sequential and/or simultaneous binding to various partners.
The E52V, Q106P and K174A mutations we have generated are aimed to disrupt the interaction of CSA with specific partners and therefore to affect specific signaling pathways that rely on CSA functionality. Nevertheless, all the isogenic cell lines we generated showed similar cellular sensitivity to UV irradiation as well as to oxidative-stressing agents whether they express any of the mutated forms of CSA or lack the expression of wild type CSA (CS3BE-cassette1) (Figure 21). This indicates that the mutants cannot recover, even partially, CSA functionality. A possible explanation to justify this issue is that the effect of CSA mutations is devastating for the protein structure and therefore it fully hampers CSA functioning. The reduced cellular levels of all the mutated CSA recombinant proteins support this hypothesis (Figure 19).
Notably, we found that E52V and K174A mutants can efficiently co-immunoprecipitate the DDB1 protein partner of the CSA core complex (Figure 24), indicating that part of the mutated proteins can indeed bind to CSA interactors. It is likely that a portion of the mutated forms of CSA can be folded into a circular propeller-like structure, but the presence of the amino acid change impairs CSA activity or, even if the mutated CSA proteins can partially perform their task, the

cellular protein amounts are too low to partially recover CSA activity in TC-NER or in the removal of oxidative damage. Indeed, we found that most of the E52V and Q106P mutants are trapped in the cytoplasm (Figure 20), thus precluding their access to the genomic DNA.
We cannot exclude that the presence of the Flag-HA epitope tags at the C-terminus of the CSA recombinant proteins affects the protein cellular localizations or even impact on their protein stability. However, the finding that the wtCSA$^{Flag\text{-}HA}$ is mainly localized in the nucleus rules out this possibility (Figure 20). We conclude that the occurrence of single amino acid changes impacts on the subcellular distribution of the recombinant proteins and likely on their nuclear import. Nothing is known about the mechanisms of CSA nuclear translocation. Catera and Pedrini (personal communication) found that the transport of CSA into the nucleus is time-dependent and that the first 21 residues, containing a putative nuclear location signal (NLS), are necessary for the proper localization of the protein even though they are not sufficient to promote nuclear translocation. We found that the E52V and Q106P alterations drastically interfere with the nuclear localization of the CSA protein, whereas the K174A amino acid change is the one that interferes less.

The identification of proteins and protein complexes interacting with CSA is a promising strategy to unravel the still unidentified functions of CSA, which may be relevant for the definition of phenotype-genotype correlations in CS patients. The presence of the Flag and HA epitopes at the C-terminus of the recombinant CSA protein allowed the purification of CSA-binding partners by Tandem Affinity Purification (TAP) and their subsequent identification through mass spectrometry. By this analysis, we isolated not only eleven well-known CSA interactors participating in TC-NER, including DDB1, cullin 4A (Cul4A), all the subunits of the COP9 signalosome (CSN1 to CSN8), but also thirty-six novel potential CSA interactors. Notably, among the novel CSA binding partners, we found two subunits of the TRiC/CCT chaperonin complex (namely CCT3 and CCT8), which is involved in the folding of newly synthesized or unfolded proteins characterized by complex structures, among which WD40 repeat proteins are widely represented. TRiC/CCT is a hetero-oligomeric complex formed by eight CCT subunits (CCT1-CCT8) present in cells either as a 90 kDa oligomer, or as components of micro-complexes, or as monomeric subunits. The complex is essential for enabling the cytoskeletal proteins actin and tubulin to fold to their native state and, in addition to the well-characterized substrate folding mechanism of the TRiC/CCT oligomer, roles for TRiC/CCT subunits as monomeric proteins are emerging (Brackley and Grantham, 2011). The chaperonin is organized as a large cylindrical multimeric complex having a central cavity for binding unfolded or denatured polypeptides. The subunits have a fixed position within the rings (Liou and Willison, 1997). Three domains are present in every single subunit: an equatorial ATP binding domain, an apical and an

intermediate domain. A flexible protrusion located in the apical domain in each subunit acts as a lid and is responsible for closing the central cavity, inside which the substrate is stretched (Kabir et al., 2011). Notably, TRiC/CCT is not up-regulated during heat shock (Horwich et al, 2007), suggesting that the complex does not mediate general refolding of heat-induced off-pathway conformations. It is rather more likely that TRiC/CCT satisfies a very specific folding requirement within the eukaryotic cytosol.

As newly translated polypeptides leak out from the ribosome into the cell, the crowded cell environment increases the possibility that proteins may fail to fold correctly, either as they exit from the ribosome or by later "off-pathway" events resulting in loss of native structure (Brackley and Grantham, 2011). In addition, proteins may misfold or unfold in response to certain stresses, such as changes in the cellular environment due to aging or temperature fluctuations, genetic mutations, or exposure to amino acid analogues. Non-native protein conformations may lead to protein aggregation, a potentially dangerous threat to the cell survival often associated with disease. For this reason a intracellular increase in the burden of misfolded or unfolded proteins is normally counterbalanced by quality control machineries, including chaperones, which act as modulators of protein homeostasis by promoting their folding or degradation (Broadley and Hartl, 2009). Unchecked protein aggregation and misfolding are recognized as the root cause of a vast collection of diseases named "protein misfolding" or "protein conformational" diseases (Chiti and Dobson, 2006). These diseases, which include amyotrophic lateral sclerosis (ALS), Alzheimer's, Parkinson's, Huntington's and other polyglutamine diseases, arise when certain proteins adopt non-native conformations that endow them with a tendency to aggregate and form intra- and/or extra-cellular deposits (Broadley and Hartl, 2009). The TRiC/CCT complex has been extensively implicated in neurodegenerative diseases. In this context, polyQ-expanded huntingtin has been identified as a TRiC/CCT substrate (Behrends at al., 2006, Tam et al., 2006, Kitamura et al., 2006). Several studies showed that TRiC/CCT remodel the morphology of huntingtin aggregates, reducing cell death (Behrends at al., 2006, Kitamura et al., 2006). Moreover, overexpression of CCT1 was effective in inhibiting huntingtin aggregation and increasing viability (Tam et al., 2006). Knockdown of the CCT6 subunit, which impairs the function of the TRiC/CCT complex as a whole, increases huntingtin aggregation and toxicity (Spiess et al., 2004, Kitamura at al., 2006). Interestingly, these results argue that TRiC/CCT as a fully assembled complex exerts neuroprotective effects by modulating huntingtin aggregation.

Relevant of note, TRiC/CCT is also required in the folding process of the telomerase cofactor TCAB1, a seven-WD40-containing protein that controls trafficking of telomerase and small Cajal bodies RNAs (scaRNAs). Mutations in the TCAB1 gene are responsible for the disease dyskeratosis congenita (DKC), a stem cell disease

characterized by symptoms that sometimes are reminiscent of CS clinical manifestations. DKC patient present abnormal skin pigmentation, nail dystrophy, progressive bone marrow failure, hair loss and or/graying, osteoporosis and learning difficulties. Pre- or post-natal growth retardation can also occur but, differently from CS, they may show predisposition to malignancies (Kirwan and Dokal, 2008). Hoyeraal-Hreidarsson syndrome (HHS) refers to a clinically severe variant of DKC characterized by multisystem involvement and early onset in utero. Patients with HHS show intrauterine growth retardation, microcephaly, delayed development, cerebellar hypoplasia and bone marrow failure resulting in immunodeficiency. Death often occurs in childhood (reviewed by Walne et al., 2013). Depletion of TRiC/CCT causes loss of TCAB1 protein, mislocalization of telomerase, scaRNAs to nucleoli and failure of telomerase elongation (Freund et al., 2014).

The archetypal obligate TRiC/CCT substrates are actin and tubulin (Gao et al, 1992). Until recently, only a limited number of proteins had been identified as TRiC/CCT substrates, among which there is a number of cell cycle-related proteins. In particular, Cdc20 and Cdh1 rely upon TRiC/CCT to achieve their native conformations. Cdc20 and Cdh1 are both WD repeat proteins, a class of proteins that have been shown to commonly use TRiC/CCT for their folding requirements (Camasses et al, 2003). Indeed, the propeller-shaped β-sheet structures of WD repeat proteins would fit within the dimensions of the TRiC/CCT cavity (Craig, 2003). We therefore decided to investigate whether the TRiC/CCT complex might have a role in the stability of the WD repeat protein CSA. Indeed, taking advantage of the CS3BE-wtCSA$^{Flag\text{-}HA}$ cell line, we found a physical interaction between CSA and the CCT3/CCT8 subunits of the TRiC/CCT complex (Figure 22 and 23). In addition, we observed that their interaction increases in response to UV-induced cell stress, likely reflecting the augmented CSA cellular necessity to promptly repair UV-induced lesions. On the contrary, treatment of CS3BE-wtCSA$^{Flag\text{-}HA}$ cells with the oxidative stress-inducing agents potassium bromate ($KBrO_3$) and menadione (MD) did not alter the interaction of wtCSA$^{Flag\text{-}HA}$ with the TRiC/CCT complex.

Relevant of note, we demonstrated that the presence of amino acid changes in CSA protein strengthen the interaction with both CCT3 and CCT8 subunits. It is tempting to speculate that a more stable interaction between the TRiC/CCT complex and the mutated forms of CSA$^{Flag\text{-}HA}$ may reflect the prolonged attempt to proper fold the mutated polypeptide.

Nevertheless, we found that that the CCT3 and CCT8 subcellular distribution is not affected neither by the presence of CSA pathological alterations (Figure 29 and 30), nor by the treatment with stressing agents such as UV light, $KBrO_3$ or MD (Figure 28).

Aiming to gain further knowledge about CSA/TRiC interaction, we performed CSA functional assay in primary dermal fibroblasts from a healthy donor following *CCT3* or *CCT8* knockdown. We demonstrated that the silencing of *CCT3* caused a

reduction in the TC-NER activity, as evaluated by recovery of RNA synthesis (RRS) after UV irradiation (Figure 32). This finding demonstrates the relevance of CCT3 in the CSA-dependent signaling pathway. On the contrary, *CCT8* knockdown did not impair TC-NER. It might be postulated that CCT3 has a prominent role in the stability of the TRiC/CCT complex and therefore in the folding of the newly synthesized CSA protein. Upon *CCT3* silencing the folding requirement of CSA is unattended, as reflected by the decreased cellular capacity to remove UV-induced damage.

The availability of primary dermal fibroblasts from CS patients has been instrumental to elucidate the multiple roles of the CS proteins, but also to investigate the molecular defects at the basis of the CS clinical symptoms. In the second part of this work, we investigated the case of an Italian patient (CS11/9_PV) presenting the clinical symptoms of the severe form of CS (COFS), cellular features typical of TC-NER alterations, such as reduced survival and decreased RRS levels, but normal unscheduled DNA synthesis (UDS). Complementation assay revealed TC-NER alteration recovery after cell fusion with CS-A but not CS-B cells. However, no inactivating mutation was found in neither *CSB* nor *CSA*. Prof. Tomoo Ogi (Research Institute of Environmental Medicine, Nagoya University, Japan) performed the whole exome sequencing (WES) analysis in primary dermal fibroblasts and/or lymphoblastoid cells from all the CS11/9_PV family members, identifying potentially pathogenic mutations in three genes, to which we refer as *CS11/9_A*, *CS11/9_B* and *CS11/9_C*.
To discriminate which of the candidate genes may be causative of the CS clinical features in CS11/9_PV patient, we looked for putative interactions with the CSA protein and for an involvement in TC-NER activity. The lack of specific antibodies against CSB did not allow the investigation of a possible interaction with this protein. Interestingly, both CS11/9_A and CS11/9_C interacted with CSA, whereas only the knockdown of *CS11/9_A* reduced the ability of the cell to recover RNA synthesis after the UV-induced DNA damage (Figure 41). Notably, the RRS reduction upon *CS11/9_A* knockdown in C3PV cells is similar to the RRS reduction observed in primary dermal fibroblasts from the CS11/9_PV patient. Altogether, these findings are suggestive of a possible involvement of *CS11/9_A* gene in CS etiopathogenesis. Further analyses are required to fully demonstrate this issue.

In conclusion, our investigations are providing new insights on the molecular alterations underlying the complex CS phenotype and on their relevance in the pathogenesis of the wide range of clinical symptoms that characterize the disease.

7. References

Aamann MD, Sorensen MM, Hvitby C, Berquist BR, Muftuoglu M, Tian J, de Souza-Pinto NC, Scheibye-Knudsen M, Wilson DM 3rd, Stevnsner T, Bohr VA. Cockayne syndrome group B protein promotes mitochondrial DNA stability by supporting the DNA repair association with the mitochondrial membrane. FASEB. 2010; 24:2334-46.

Amalnath D, Mailankody S. Teaching NeuroImages: Cockayne syndrome with extensive intracranial calcification. Neurology. 2015; 84(18):e137.

Anindya R, Aygün O, Svejstrup JQ. Damage-induced ubiquitylation of human RNA polymerase II by the ubiquitin ligase Nedd4, but not Cockayne syndrome proteins or BRCA1. Mol Cell. 2007; 28:386-97.

Anindya R, Mari PO, Kristensen U, Kool H, Giglia-Mari G, Mullenders LH, FousteriM, Vermeulen W, Egly JM, Svejstrup JQ. A ubiquitin-binding domain in Cockayne syndrome B required for transcription-coupled nucleotide excision repair. Mol Cell. 2010; 38:637-48.

Balaban RS, Nemoto S, Finkel T. Mitochondria, oxidants, and aging. Cell. 2005; 120:483–495.

Banerjee D, Mandal SM, Das A, Hegde ML, Das S, Bhakat KK, Boldogh I, Sarkar PS, Mitra S, Hazra TK. Preferential repair of oxidized base damage in the transcribed genes of mammalian cells. J Biol Chem. 2011; 286, 6006–16.

Batenburg NL, Mitchell TR, Leach DM, Rainbow AJ, Zhu XD. Cockayne Syndrome group B protein interacts with TRF2 and regulates telomere length and stability. Nucleic Acids Res. 2012; 40:9661-74.

Beerens N, Hoeijmakers JH, Kanaar R, Vermeulen W, Wyman C. The CSB protein actively wraps DNA. J Biol Chem. 2005; 280:4722-9.

Behrends C, Langer CA, Boteva R, Bottcher UM, Stemp MJ, Schaffar G, Rao BV, Giese A, Kretzschmar H, Siegers K, Hartl FU. Chaperonin TRiC promotes the assembly of polyQ expansion proteins into nontoxic oligomers. Mol Cell. 2006; 23:887- 97.

Bertola DR, Cao H, Albano LM, Oliveira DP, Kok F, Marques-Dias MJ, Kim CA, Hegele RA. Cockayne syndrome type A: novel mutations in eight typical patients. J Hum Genet. 2006; 51:701-5.

Brackley KI, Grantham J. Subunits of the chaperonin CCT interact with F-actin and influence cell shape and cytoskeletal assembly. Exp Cell Res. 2010; 316(4):543-53.

Bradsher J, Auriol J, Proietti de Santis L, Iben S, Vonesch JL, Grummt I, Egly JM. CSB is a component of RNA pol I transcription. Mol Cell. 2002; 10:819-29

Broadley SA, Hartl FU. The role of molecular chaperones in human misfolding diseases. FEBS Lett. 2009; 583(16):2647-53.

Brooks PJ. The case for 8,5'-cyclopurine-2'-deoxynucleosides as endogenous DNA lesions that cause neurodegeneration in xeroderma pigmentosum. Neuroscience. 2007; 145:1407-17.

Camasses A, Bogdanova A, Shevchenko A, Zachariae W. The CCT chaperonin promotes activation of the anaphase-promoting complex through the generation of functional Cdc20. Mol Cell. 2003; 12:87-100.

Chiti F, Dobson CM. Protein misfolding, functional amyloid, and human disease. Annu Rev Biochem. 2006; 75, 333–66.

Christiansen M, Stevnsner T,Modin C,Martensen PM, Brosh Jr RM, Bohr VA. Functional consequences of mutations in the conserved SF2 motifs and post-translational phosphorylation of the CSB protein. Nucleic Acids Res. 2003; 31:963-73.

Citterio E, Van Den Boom V, Schnitzler G, Kanaar R, Bonte E, Kingston RE, Hoeijmakers JH, Vermeulen W. ATP-dependent chromatin remodeling by the Cockayne syndrome B DNA repair-transcription-coupling factor. Mol Cell Biol. 2000; 20:7643-53.

D'Errico M, Pascucci B, Iorio E, Van Houten B, Dogliotti E. The role of CSA and CSB protein in the oxidative stress response. Mech Ageing Dev. 2013; 134(5-6):261-9.

Fischer ES, Scrima A, Böhm K, Matsumoto S, Lingaraju GM, Faty M, Yasuda T, Cavadini S, Wakasugi M, Hanaoka F, Iwai S, Gut H, Sugasawa K, Thomä

NH. The molecular basis of CRL4DDB2/CSA ubiquitin ligase architecture, targeting, and activation. Cell. 2011; 147:1024-39.

Fousteri M, Vermeulen W, van Zeeland AA, Mullenders LH. Cockayne syndrome A and B proteins differentially regulate recruitment of chromatin remodeling and repair factors to stalled RNA polymerase II in vivo. Mol Cell. 2006; 23:471-82.

Freund A, Zhong FL, Venteicher AS, Meng Z, Veenstra TD, Frydman J, Artandi SE. Proteostatic control of telomerase function through TRiC-mediatedfolding of TCAB1. Cell. 2014; 159(6):1389-403.

Fukui H, Moraes CT. The mitochondrial impairment, oxidative stress and neurodegeneration connection: reality or just an attractive hypothesis? Trends Neurosci. 2008; 31, 251–6.

Gao Y, Thomas JO, Chow RL, Lee GH, Cowan NJ. A cytoplasmic chaperonin that catalyzes beta-actin folding. Cell. 1992; 69:1043-50.

García-Otín AL, Guillou F. Mammalian genome targeting using site-specific recombinases. Front Biosci. 2006; 1;11:1108-36.

Graham JM Jr, Anyane-Yeboa K, Raams A, Appeldoorn E, Kleijer WJ, Garritsen VH, Busch D, Edersheim TG, Jaspers NG. Cerebro-oculo-facio-skeletal syndrome with a nucleotide excision-repair defect and a mutated XPD gene, with prenatal diagnosis in a triplet pregnancy. Am J Hum Genet. 2001; 69(2):291-300.

Groisman R, Kuraoka I, Chevallier O, Gaye N, Magnaldo T, Tanaka K, Kisselev AF, Harel-Bellan A, Nakatani Y. CSA-dependent degradation of CSB by the ubiquitinproteasome pathway establishes a link between complementation factors of the Cockayne syndrome. Genes Dev. 2006; 20:1429-34.

Hanawalt PC, Spivak G. Transcription-coupled DNA repair: two decades of progress and surprises. Nat Rev Mol Cell Biol. 2008; 9:958-70.

Hartl, FU, Hayer-Hartl M. Molecular chaperones in the cytosol: from nascent chain to folded protein. Science. 2002; 295, 1852–1858.

Henning KA, Li L, Iyer N, McDaniel LD, Reagan MS, Legerski R, Schultz RA, Stefanini M, Lehmann AR, Mayne LV, Friedberg EC. The Cockayne syndrome

group A gene encodes a WD repeat protein that interacts with CSB protein and a subunit of RNA polymerase II TFIIH. Cell. 1995; 82:555-64.

Horibata K, Iwamoto Y, Kuraoka I, Jaspers NG, Kurimasa A, Oshimura M, Ichihashi M, Tanaka K. Complete absence of Cockayne syndrome group B gene product gives rise to UV-sensitive syndrome but not Cockayne syndrome. Proc Natl Acad Sci USA 2004; 101:15410–5.

Horwich AL, Fenton WA, Chapman E, Farr GW. Two families of chaperonin: physiology and mechanism. Annu Rev Cell Dev Biol. 2007; 23:115-45.

Imam SZ, Indig FE, Cheng WH, Saxena SP, Stevnsner T, Kufe D, Bohr VA. Cockayne syndrome protein B interacts with and is phosphorylated by c-Abl tyrosine kinase. Nucleic Acids Res. 2007; 35:4941-51.

Iyama T, Lee SY, Berquist BR, Gileadi O, Bohr VA, Seidman MM, McHugh PJ, Wilson DM 3rd. CSB interacts with SNM1A and promotes DNA interstrand crosslink processing. Nucleic Acids Res. 2015; 43:247-58.

Jung Y, Lippard SJ. RNA polymerase II blockage by cisplatin-damaged DNA. Stability and polyubiquitylation of stalled polymerase. J Biol Chem. 2006; 281:1361-70.

Kabir MA, Uddin W, Narayanan A, Reddy PK, Jairajpuri MA, Sherman F, Ahmad Z. Functional Subunits of Eukaryotic Chaperonin CCT/TRiC in Protein Folding. J Amino Acids. 2011:843206.

Kamenisch Y, Berneburg M. Mitochondrial CSA and CSB: protein interactions and protection from ageing associated DNA mutations. Mech Ageing Dev. 2013; 134:270-4.

Kamenisch Y, Fousteri M, Knoch J, von Thaler AK, Fehrenbacher B, Kato H, Becker T, Dollé ME, Kuiper R, Majora M, Schaller M, van der Horst GT, van Steeg H,Röcken M, Rapaport D, Krutmann J, Mullenders LH, Berneburg M. Proteins of nucleotide and base excision repair pathways interact in mitochondria to protect from loss of subcutaneous fat, a hallmark of aging. J Exp Med. 2010; 207:379-90.

Kamiuchi S, Saijo M, Citterio E, de Jager M, Hoeijmakers JH, Tanaka K. Translocation of Cockayne syndrome group A protein to the nuclear matrix:possible

relevance to transcription-coupled DNA repair. Proc Natl Acad Sci U S A. 2002; 99:201-6.

Karikkineth AC, Scheibye-Knudsen M, Fivenson E, Croteau DL, Bohr VA. Cockayne syndrome: Clinical features, model systems and pathways. Ageing Res Rev. 2016; 6. pii: S1568-1637(16)30177-5.

Kelley MR, Georgiadis MM, Fishel ML. APE1/Ref-1 role in redox signaling: translational applications of targeting the redox function of the DNA repair/ redox protein APE1/Ref-1. Curr Mol Pharmacol. 2012; 5:36–53.

Khobta A, Epe B. Repair of oxidatively generated DNA damage in Cockayne syndrome. Mech Ageing Dev. 2013; 134(5-6):253-60.

Kirwan M and Dokal I. Dyskeratosis congenita: a genetic disorder of many faces. Clin Genet. 2008; 73: 103-12.

Kitamura A, Kubota H, Pack CG, Matsumoto G, Hirayama S, Takahashi Y, Kimura H, Kinjo M, Morimoto RI, Nagata K. Cytosolic chaperonin prevents polyglutamine toxicity with altering the aggregation state. Nat Cell Biol. 2006; 8:1163-70.

Kleijer WJ, Laugel V, Berneburg M, Nardo T, Fawcett H, Gratchev A. Incidence of DNA repair deficiency disorders in western Europe: xeroderma pigmentosum, cockayne syndrome and trichothiodystrophy. DNA Repair. 2008; 7:744-50.

Klungland A, Bjelland S. Oxidative damage to purines in DNA: role of mammalian Ogg1. DNA Repair (Amst) 2007; 6:481–8.

Koch S, Garcia Gonzalez O, Assfalg R, Schelling A, Schäfer P, Scharffetter-Kochanek K, Iben S. Cockayne syndrome protein A is a transcription factor of RNA polymerase I and stimulates ribosomal biogenesis and growth. Cell Cycle. 2014; 13:2029-37.

Komatsu A, Suzuki S, Inagaki T, Yamashita K, Hashizume K. A kindred with Cockayne syndrome caused by multiple splicing variants of the CSA gene. Am J Med Genet A. 2004; 128A:67-71.

Koob M, Laugel V, Durand M, Fothergill H, Dalloz C, Sauvanaud F, Dollfus H, Namer IJ, Dietemann JL. Neuroimaging in Cockayne syndrome. AJNR Am J Neuroradiol. 2010; 31:1623-30.

Kuraoka I, Ito S, Wada T, Hayashida M, Lee L, Saijo M, Nakatsu Y, Matsumoto M, Matsunaga T, Handa H, Qin J, Nakatani Y, Tanaka K. Isolation of XAB2 complex involved in pre-mRNA splicing, transcription, and transcription-coupled repair. J Biol Chem. 2008; 283:940-50.

Lake RJ, Geyko A, Hemashettar G, Zhao Y, Fan HY. UV-induced association of the CSB remodeling protein with chromatin requires ATP-dependent relief of Nterminal autorepression. Mol Cell. 2010; 37:235-46.

Lanzafame M, Vaz B, Nardo T, Botta E, Orioli D, Stefanini M. From laboratory tests to functional characterisation of Cockayne syndrome. Mech Ageing Dev. 2013; 134:171-9.

Laugel V, Dalloz C, Durand M, Sauvanaud F, Kristensen U, Vincent MC, Pasquier L,Odent S, Cormier-Daire V, Gener B, Tobias ES, Tolmie JL, Martin-Coignard D, Drouin-Garraud V, Heron D, Journel H, Raffo E, Vigneron J, Lyonnet S, Murday V, Gubser-Mercati D, Funalot B, Brueton L, Sanchez Del Pozo J,Muñoz E, Gennery AR, Salih M, Noruzinia M, Prescott K, Ramos L, Stark Z, Fieggen K, Chabrol B, Sarda P, Edery P, Bloch-Zupan A, Fawcett H, Pham D,Egly JM, Lehmann AR, Sarasin A, Dollfus H. Mutation update for the CSB/ERCC6 and CSA/ERCC8 genes involved in Cockayne syndrome. Hum Mutat. 2010; 31:113-26.

Laugel V. Cockayne syndrome: the expanding clinical and mutational spectrum. Mech Ageing Dev. 2013; 134:161-70.

Le Page F, Schreiber V, Dherin C, De Murcia G, Boiteux S. Poly(ADP-ribose) polymerase-1 (PARP-1) is required in murine cell lines for base excision repair of oxidative DNA damage in the absence of DNA polymerase beta. J Biol Chem. 2003; 278:18471–7.

Li D, Roberts R. WD-repeat proteins: structure characteristics, biological function, and their involvement in human diseases. Cell Mol Life Sci. 2001; 58:2085-97.

Licht CL, Stevnsner T, Bohr VA. Cockayne syndrome group B cellular and biochemical functions. Am J Hum Genet. 2003; 73:1217-39.

Liou AK, Willison KR. Elucidation of the subunit orientation in CCT (chaperonin containing TCP1) from the subunit composition of CCT micro-complexes. EMBO J. 1997; 16:4311-6.

Liou AK, Willison KR. Elucidation of the subunit orientation in CCT (chaperonin
Liu X, Lin CY, Lei M, Yan S, Zhou T, Erikson RL. CCT chaperonin complex is required for the biogenesis of functional Plk1. Mol Cell Biol. 2005; 25:4993-5010.

Marteijn JA, Lans H, Vermeulen W, Hoeijmakers JH. Understanding nucleotide excision repair and its roles in cancer and ageing. Nat Rev Mol Cell Biol. 2014; 15(7):465-81.

Muftuoglu M, de Souza-Pinto NC, Dogan A, Aamann M, Stevnsner T, Rybanska I, Kirkali G, Dizdaroglu M, Bohr VA. Cockayne syndrome group B protein stimulates repair of formamidopyrimidines by NEIL1 DNA glycosylase. J Biol Chem. 2009; 284:9270–9.

Muftuoglu M, Selzer R, Tuo J, Brosh Jr RM, Bohr VA. Phenotypic consequences of mutations in the conserved motifs of the putative helicase domain of the human Cockayne syndrome group B gene. Gene. 2002; 283:27-40.

Muftuoglu M, Sharma S, Thorslund T, Stevnsner T, Soerensen MM, Brosh RM Jr,Bohr VA. Cockayne syndrome group B protein has novel strand annealing and exchange activities. Nucleic Acids Res. 2006; 34:295-304.

Nance MA, Berry SA. Cockayne syndrome: review of 140 cases. Am J Med Genet. 1992; 42:68-84.

Nakazawa Y1, Sasaki K, Mitsutake N, Matsuse M, Shimada M, Nardo T, Takahashi Y, Ohyama K, Ito K, Mishima H, Nomura M, Kinoshita A, Ono S, Takenaka K, Masuyama R, Kudo T, Slor H, Utani A, Tateishi S, Yamashita S, Stefanini M, Lehmann AR, Yoshiura K, Ogi T. Mutations in UVSSA cause UV-sensitive syndrome and impair RNA polymerase IIo processing in transcription-coupled nucleotide-excision repair. Nat Genet. 2012; 44(5):586-92.

Nardo T, Oneda R, Spivak G, Vaz B, Mortier L, Thomas P, Orioli D, Laugel V, Stary A, Hanawalt PC, Sarasin A, Stefanini M. A UV-sensitive syndrome patient with a specific CSA mutation reveals separable roles for CSA in response to UV and oxidative DNA damage. Proc Natl Acad Sci U S A. 2009; 106:6209-14.

Newman JC, Bailey AD, Fan HY, Pavelitz T, Weiner AM. An abundant evolutionarily conserved CSB-PiggyBac fusion protein expressed in Cockayne syndrome. PLoS Genet. 2008; 4:e1000031.

Newman JC, Bailey AD, Weiner AM. Cockayne syndrome group B protein (CSB) plays a general role in chromatin maintenance and remodeling. Proc Natl Acad Sci USA. 2006; 103:9613-8.

Nicolai S, Filippi S, Caputo M, Cipak L, Gregan J, Ammerer G, Frontini M, Willems D, Prantera G, Balajee AS, Proietti-De-Santis L. Identification of Novel Proteins Co-Purifying with Cockayne Syndrome Group B (CSB) Reveals Potential Roles for CSB in RNA Metabolism and Chromatin Dynamics. PLoS One. 2015; 10:e0128558.

Osenbroch PO, Auk-Emblem P, Halsne R, Strand J, Forstrom RJ, van der Pluijm I, Eide L. Accumulation of mitochondrial DNA damage and bioenergetic dysfunction in CSB defective cells. FEBS Journal 2009; 276:2811–21.

Pascucci B, Lemma T, Iorio E, Giovannini S, Vaz B, Iavarone I, Calcagnile A, Narciso L, Degan P, Podo F, Roginskya V, Janjic BM, Van Houten B, Stefanini M, Dogliotti E, D'Errico M. An altered redox balance mediates the hypersensitivity of Cockayne syndrome primary fibroblasts to oxidative stress. Aging Cell. 2012; 11:520-9.

Pascucci B, D'Errico M, Romagnoli A, De Nuccio C, Savino M, Pietraforte D, Lanzafame M, Calcagnile AS, Fortini P, Baccarini S, Orioli D, Degan P, Visentin S, Stefanini M, Isidoro C, Fimia GM, Dogliotti E. Overexpression of parkin rescues the defective mitochondrial phenotype and the increased apoptosis of Cockayne Syndrome A cells. Oncotarget. 2016;5.

Proietti-De-Santis L, Drané P, Egly JM. Cockayne syndrome B protein regulates the transcriptional program after UV irradiation. EMBO J. 2006; 25:1915-23.

Ren Y, Saijo M, Nakatsu Y, Nakai H, Yamaizumi M, Tanaka K. Three novel mutations responsible for Cockayne syndrome group A. Genes Genet Syst. 2003; 78:93-102.

Saijo M, Hirai T, Ogawa A, Kobayashi A, Kamiuchi S, Tanaka K. Functional TFIIH is required for UV-induced translocation of CSA to the nuclear matrix. Mol Cell Biol. 2007; 27:2538-47.

Saijo M. The role of Cockayne syndrome group A (CSA) protein in transcription-coupled nucleotide excision repair. Mech Ageing Dev. 2013; 134:196-201.

Sarker AH, Tsutakawa SE, Kostek S, Ng C, Shin DS, Peris M, Campeau E, Tainer JA, Nogales E, Cooper PK. Recognition of RNA polymerase II and transcription bubbles by XPG, CSB, and TFIIH: insights for transcription-coupled repair and Cockayne Syndrome. Mol Cell. 2005; 20:187-98.

Scheibye-Knudsen M. Neurodegeneration in accelerated aging. Dan Med J. 2016; 63(11).

Scheibye-Knudsen M, Croteau DL, Bohr VA. Mitochondrial deficiency in Cockayne syndrome. Mech Ageing Dev. 2013; 134:275-83.

Shen X, Li L. Mutagenic repair of DNA interstrand crosslinks. Environ Mol Mutagen. 2010; 51:493-9.

Smith TF, Gaitatzes C, Saxena K, Neer EJ. The WD repeat: a common architecture for diverse functions. Trends Biochem Sci. 1999; 24:181-5.

Smith TF. Diversity of WD-repeat proteins. Subcell Biochem. 2008; 48:20-30.

Spiess C, Meyer AS, Reissmann S, Frydman J. Mechanism of the eukaryotic chaperonin: protein folding in the chamber of secrets. Trends Cell Biol. 2004; 14, 598–604.

Spivak G, Hanawalt PC. Host cell reactivation of plasmids containing oxidative DNA lesions is defective in Cockayne syndrome but normal in UV- sensitive syndrome fibroblasts. DNA Repair (Amsterdam) 2006; 5:13–22.

Stefanini M, Fawcett H, Botta E, Nardo T, Lehmann AR. Genetic analysis of twenty-two patients with Cockayne syndrome. Hum Genet. 1996; 97:418-423.

Stefanini M, Kraemer KHK. Xeroderma pigmentosum. 2008; In: Neurocutaneous Diseases. Ruggieri M, Pascual-Castroviejo I, Di Rocco C (eds). Chapter 51: 771-792. ISBN 978-3-211-21396-4 SpringerWienNewYork. Springer-Verlag, New York Wien.

Stefanini M, Orecchia G, Rabbiosi G, Nuzzo F. Altered cellular response to UV irradiation in a patient affected by premature aging. Hum Genet. 1986b; 73:189-192.

Sun X, Majumder P, Shioya H, Wu F, Kumar S, Weichselbaum R, Kharbanda S, Kufe D. Activation of the cytoplasmic c-Abl tyrosine kinase by reactive oxygen species. J Biol Chem. 2000; 275:17237-40.

Svilar D, Goellner EM, Almeida KH, Sobol RW. Base excision repair and lesion-dependent subpathways for repair of oxidative DNA damage. Antioxid Redox Signal. 2011; 14:2491–507.

Tam S, Geller R, Spiess C, Frydman J. The chaperonin TRiC controls polyglutamine aggregation and toxicity through subunit-specific interactions. Nat Cell Biol. 2006; 8:1155-62.

Tam S, Spiess C, Auyeung W, Joachimiak L, Chen B, Poirier MA, Frydman J. The chaperonin TRiC blocks a huntingtin sequence element that promotes the conformational switch to aggregation. Nat Struct Mol Biol. 2009; 16:1279-85.

Thorslund T, von Kobbe C, Harrigan JA, Indig FE, Christiansen M, Stevnsner T, Bohr VA. Cooperation of the Cockayne syndrome group B protein and poly(ADP-ribose) polymerase 1 in the response to oxidative stress. Mol Cell Biol. 2005; 25:7625–36.

Ting TW, Brett MS, Tan ES, Shen Y, Lee SP, Lim EC, Vasanwala RF, Lek N, Thomas T, Lim KW, Tan EC. Cockayne Syndrome due to a maternally-inherited whole gene deletion of ERCC8 and a paternally-inherited ERCC8 exon 4 deletion. Gene. 2015; pii: S0378-1119(15)00906-3.

Troelstra C, van Gool A, de Wit J, Vermeulen W, Bootsma D, Hoeijmakers JH. ERCC6, a member of a subfamily of putative helicases, is involved in Cockayne's syndrome and preferential repair of active genes. Cell. 1992; 71:939-53.

Vélez-Cruz R, Egly JM. Cockayne syndrome group B (CSB) protein: at the crossroads of transcriptional networks. Mech Ageing Dev. 2013; 134:234-42.

Vermeulen W, Fousteri M. Mammalian transcription-coupled excision repair. Cold Spring Harb Perspect Biol. 2013; 5(8):a012625.

Vidal AE, Boiteux S, Hickson ID, Radicella JP. XRCC1 coordinates the initial and late stages of DNA abasic site repair through protein–protein interactions. EMBO J. 2001; 20:6530–9.

Walne AJ, Vulliamy T, Kirwan M, Plagnol V, Dokal I. Constitutional mutations in RTEL1 cause severe dyskeratosis congenita. Am J Hum Genet. 2013; 92: 448-53.

Wang D, Bushnell DA, Huang X, Westover KD, Levitt M, Kornberg RD. Structural basis of transcription: backtracked RNA polymerase II at 3.4 angstrom resolution. Science. 2009; 324:1203-6.

Wang Y, Chakravarty P, Ranes M, Kelly G, Brooks PJ, Neilan E, Stewart A, Schiavo G, Svejstrup JQ. Dysregulation of gene expression as a cause of Cockayne syndrome neurological disease. Proc Natl Acad Sci USA. 2014; 111:14454-9.

Wang Y, Kreisberg JI, Bedolla RG, Mikhailova M, deVere White RW, Ghosh PM. A 90 kDa fragment of filamin A promotes Casodex-induced growth inhibition in Casodex-resistant androgen receptor positive C4-2 prostate cancer cells. Oncogene. 2007; 26:6061-70.

Wong HK, Muftuoglu M, Beck G, Imam SZ, Bohr VA, Wilson DM 3rd. Cockayne syndrome B protein stimulates apurinic endonuclease 1 activity and protects against agents that introduce base excision repair intermediates. Nucleic Acids Res. 2007; 35, 4103–13.

Wood RD. Mammalian nucleotide excision repair proteins and interstrand crosslink repair. Environ Mol Mutagen. 2010; 51:520-6.

Xie W, Ling T, Zhou Y, Feng W, Zhu Q, Stunnenberg HG, Grummt I, Tao W. The chromatin remodeling complex NuRD establishes the poised state of rRNA genes characterized by bivalent histone modifications and altered nucleosome positions. Proc Natl Acad Sci USA. 2012; 109:8161-6.

Xu C, Min J. Structure and function of WD40 domain proteins. Protein Cell. 2011; 2(3):202-14.

Zhou HX, Wang G. Predicted structures of two proteins involved in human diseases. Cell Biochem Biophys. 2001; 35:35-47.